OFFICE OF CIVILIAN RADIOACTIVE WASTE MANAGEMENT
SCIENTIFIC ANALYSIS COVER SHEET

1. QA: QA

Page: 1   Of: 110

2. Scientific Analyses Title	Geochemical Interactions in Failed Co-Disposal Waste Packages for N Reactor and Ft. St. Vrain Spent Fuel and the Melt and Dilute Waste Form	
3. DI (including Revision Number)	ANL-EBS-PA-000007 REV 00	

4. Total Attachments	5. Attachment Numbers - Number of pages in each	
1	I-3	

	Print Name	Signature	Date
6. Originator	Sara E. Arthur	SIGNATURE ON FILE	7/24/02
7. Checker	Paul Domski	SIGNATURE ON FILE	7/24/02
8. QER	Dan Tunney	SIGNATURE ON FILE	7/29/2002
9. Responsible Manager/Lead	James Duguid	SIGNATURE ON FILE	7/31/2002
10. Responsible Manager	Jerry McNeish	SIGNATURE ON FILE	8·13·02

11. Remarks

Technical Contact/Department: TSPA

Revision History

12. Revision/ICN No.	13. Description of Revision/Change
REV 00	Initial Issue

CONTENTS

FIGURES

TABLES

1. PURPOSE

The objective of this scientific analysis is to calculate the long-term geochemical behavior in a failed co-disposal waste package (WP) containing U. S. Department of Energy (DOE) spent nuclear fuel (SNF) and high level waste (HLW) glass. This analysis was prepared according to a Technical Work Plan (BSC 2002). Specifically the scope of these calculations is to determine:

- The geochemical characteristics of the fluids inside the WP after breach, including the corrosion/dissolution of the initial WP configuration;

- The transport of radionuclides of concern to performance assessment out of the degraded WP by infiltrating water; and

- The range of parameter variation for additional laboratory and numerical evaluations.

This analysis is limited to three SNF groups, uranium (U)/thorium (Th) carbide SNF (Group 5), U metal SNF (Group 7), and aluminum(Al)-based fuels (Group 9). Group 5 is represented by Ft. St. Vrain (FSV) U/Th carbide SNF, Group 7 is represented by N-Reactor U metal SNF, and Group 9 is represented by the Melt and Dilute (M&D) waste form developed from Al-based SNF. The DOE (2001a, Appendix A) describes all of these fuels. Table 1 shows the groups of DOE SNF, the representative SNF for each group, and the metric tons of heavy metal (MTHM) of SNF in each group.

Table 1. SNF Type, Typical Fuels, Amount, and Percentage in Each SNF Group[a]

Group	SNF Type	Typical Fuel	Total (MTHM)	Percent (of total)
1	Classified	Naval	65	2.60
2	Pu/U alloy	Enrico Fermi Reactor (FERMI) core 1 & 2	9.111	0.37
3	Pu/U carbide	Fast Flux Test Facility (FFTF) Test Fuel Assembly	0.110	0.00
4	Pu/U oxide and Pu oxide	Fast Flux Test Facility (FFTF) Driver Fuel Assembly	12.418	0.50
5	Th/U carbide	Ft. St. Vrain	26.276	1.05
6	Th/U oxide	Shippingport LWBR	50.352	2.02
7	U metal	N Reactor	2,127.235	85.23
8	U oxide	Three Mile Island core debris	178.145	7.14
9	Al based SNF	Foreign Research Reactor pin cluster	20.940	0.84
10	Unknown	Miscellaneous	4.540	0.18
11	U-Zirconium hydride	Training Research Isotope General Atomic (TRIGA)	1.618	0.06
TOTAL			2,495.745	100.00

Source: [a]DOE 2001a, Attached electronic file.

2. QUALITY ASSURANCE

The Quality Assurance (QA) program applies to the development of this analysis. As required by AP-2.21Q, *Quality Determinations and Planning for Scientific, Engineering, and Regulatory Compliance Activities*, this work activity was evaluated and the activity evaluation (BSC 2002, Addendum A) determined that the Office of Civilian Radioactive Waste Management QA program is applicable to the preparation of this document.

Regarding this document, the control of the electronic management of data is in accordance with the controls specified in the TWP (BSC 2002, Addendum B). The methods used include the currently effective work processes and procedures, which were determined to be adequate for this activity.

3.   USE OF SOFTWARE

The computer software used in this analysis is EQ3/6 (EQ3/6, V. 7.2b, CSCI: UCRL-MA-110662) (CRWMS M&O 1998) and version 7.2bLV of EQ6 (EQ6 V. 7.2bLV CSCI: 10075.7.2bLV-00) (CRWMS M&O 1999d) as developed under software activity plan 10075-SAP-7.2bLV-00.   The software (EQ3/6) was used to calculate the interaction between HLW glass and DOE SNF in a failed co-disposal WP. The software used in this analysis was obtained and implemented under AP-SI.1Q, *Software Management* and was only used within the range of validation. The following information on the software used in this analysis report was obtained from the Software Configuration Secretary (SCS).

The software was obtained from the Software Configuration Manager in accordance with the appropriate procedures and was only used within the qualified range. The EQ6 simulations were executed on the following machine using the Microsoft Windows 98 operating system:

- A Dell Latitude laptop Pentium III equipped with a Pentium 650 MHz processor, Framatome ANP DE&S #91BW7 in Albuquerque, New Mexico

The EQ3NR and EQPT simulations were executed on the following machine using the Microsoft Windows 95 operating system:

- A Dell Optiplex GX300 Bechtel SAIC Company #117728 in Las Vegas, Nevada

The EQ3/6 software package originated in the mid-1970s at Northwestern University (Wolery 1992a). Since 1978 Lawrence Livermore National Laboratory (LLNL) has been responsible for maintenance of the software package. The software has most recently been maintained under the sponsorship of the Civilian Radioactive Waste Management Program of the U.S. Department of Energy. The major components of the software package include: (1) EQ3NR (a speciation-solubility code); (2) EQ6 (a reaction path code that simulates water/rock interaction or fluid mixing in either a pure reaction progress mode or a time mode); (3) EQPT (a data file preprocessor); and (4) EQLIB (a supporting software library; and several supporting thermodynamic data files). The software is based on the concepts of the thermodynamic equilibrium, thermodynamic disequilibrium, and reaction kinetics. The supporting data files contain both standard state and activity coefficient-related data. The thermodynamic data file used in this analysis supports the use of the Davies or B-dot equations for the activity coefficients. EQPT takes a formatted data file (a data0 file) and writes an unformatted equivalent called a data1 file, that is actually the form read by EQ3NR and EQ6. The EQ3NR is used for analyzing groundwater chemistry data, and calculating solubility limits. The EQ3NR is also required to initialize an EQ6 calculation through the EQ3NR "pick up" file.

EQ6 simulates the consequences of chemical reactions of an aqueous solution with a set of reactants. EQ6 does not calculate the generation of colloids from the reactions between the aqueous solution and a set of reactants. EQ6 does model fluid mixing and the consequences of changes in temperature on chemistry. This code operates both in a pure reaction progress frame and in a time frame. In a time frame calculation, the user specifies rate laws for the progress of the irreversible reactions. Otherwise, only relative rates are specified. Both EQ3NR and EQ6 use a hybrid Newton-Raphson technique to make thermodynamic calculations. This is supported by a set of algorithms that create and optimize starting values. EQ6 uses an ordinary differential

equation integration algorithm to solve rate equations in the time mode. EQ6 version 7.2bLV, as distributed by LLNL does not contain the SCFT mode. To add this mode, it is necessary to change the EQ6 source code, and recompile the source. However, by using a variant of the "special reactant" type built into EQ6, it is possible to add the functionality of the SCFT mode in a very simple and straightforward manner. This mode was added to EQ6 per Software Change Request LSCR198 (CRWMS M&O 1999c), and the Software Qualification Report for Media Number 30084-M04-001.

The most relevant EQ6 input and output files for this analysis are described below and are contained in the output associated with this analysis (DTN: MO0201SPAGIN07.001):

- EQ6 input files (extensions = 6i) which are described in more detail in Section 6.2.
- Tab-delimited text output files (extension = txt). These contain total aqueous moles of elements (*.elem_aqu.txt), total moles of specific minerals (*.min_info.txt), total moles of elements in minerals, aqueous phase, and remaining special reactants (*.elem_tot.txt), and the total moles of elements in minerals alone (*.elem_min.txt)
- EQ6 text data file used for the calculations named data0.trc, which is described in more detail in Section 4.1.2.8.

Microsoft Excel 97 SR-2 spreadsheets are used for arithmetical manipulations and the graphical and tabular representation of the results of the geochemical calculations (Sections 4 and 6). No macros or subroutines were used for this analysis. Microsoft Excel 97 SR-2 is an exempt software application in accordance with AP-SI.1Q, *Software Management*, Section 2.1.1.

4. INPUTS

4.1 DATA AND PARAMETERS

4.1.1 WP Description

This analysis uses the same WP and drip shield geometry as the TSPA-SR (CRWMS M&O 2000b, Section 3.4; see Figure 1), i.e., a Titanium (Ti) Grade 7 drip shield, an outer shell consisting of an exterior corrosion resistant barrier (constructed of Alloy 22) and an inner structural barrier (constructed of 316NG). The WP and drip shield together form the primary component of the Engineered Barrier System (EBS) (Figure 1). The current approach (CRWMS M&O 2000b, Section 3.4) considers several degradation (i.e. corrosion) scenarios that may eventually cause a breach of the drip shield or WP to occur (see Assumption 5.1). Waste package and drip shield degradation is described in detail in the *Waste Package Degradation Process Model Report* (CRWMS M&O 2000c).

Material nomenclature used throughout this Analysis includes:

- SB-575 N06022, the high-nickel alloy used in the corrosion resistant barrier, referred to as Alloy 22

- SA-240 S31603, 316 low carbon stainless steel, referred to as 316L

- SA-240 S31603, 316 nuclear grade stainless steel, referred to as 316NG

- SA-240 S30403, 304 low carbon stainless steel, referred to as 304L

- SA-516, low carbon steel, referred to as A516.

Figure 2 illustrates the WP design and Figure 1 shows more detail of the outer barrier and the inner stainless steel structural-component. It is convenient to consider the WP as consisting of several structural components, specifically:

- A two-centimeter thick Alloy-22 outer wall to resist corrosion

- A five-centimeter thick stainless steel (316NG) inner wall, to provide structural integrity

- The "outer web", a carbon steel (A516) structure designed to hold the HLW glass-pour canisters (GPCs) in place

- Five GPCs, which are the stainless steel (304L) containers that hold the solidified HLW glass

- The DOE SNF canister (sometimes called the "18 inch canister") composed of 316L.

Waste Package Inner
Barrier (Stainless Steel)

Waste Package Outer Lid
(Alloy 22)

Waste Package Middle Lid
(Alloy 22)

Drip Shield
(Titanium Grade 7)

abq0063G033.ai

Waste Package
(Outer Barrier: 2 cm Alloy 22,
Inner Barrier: 5 cm stainless steel)
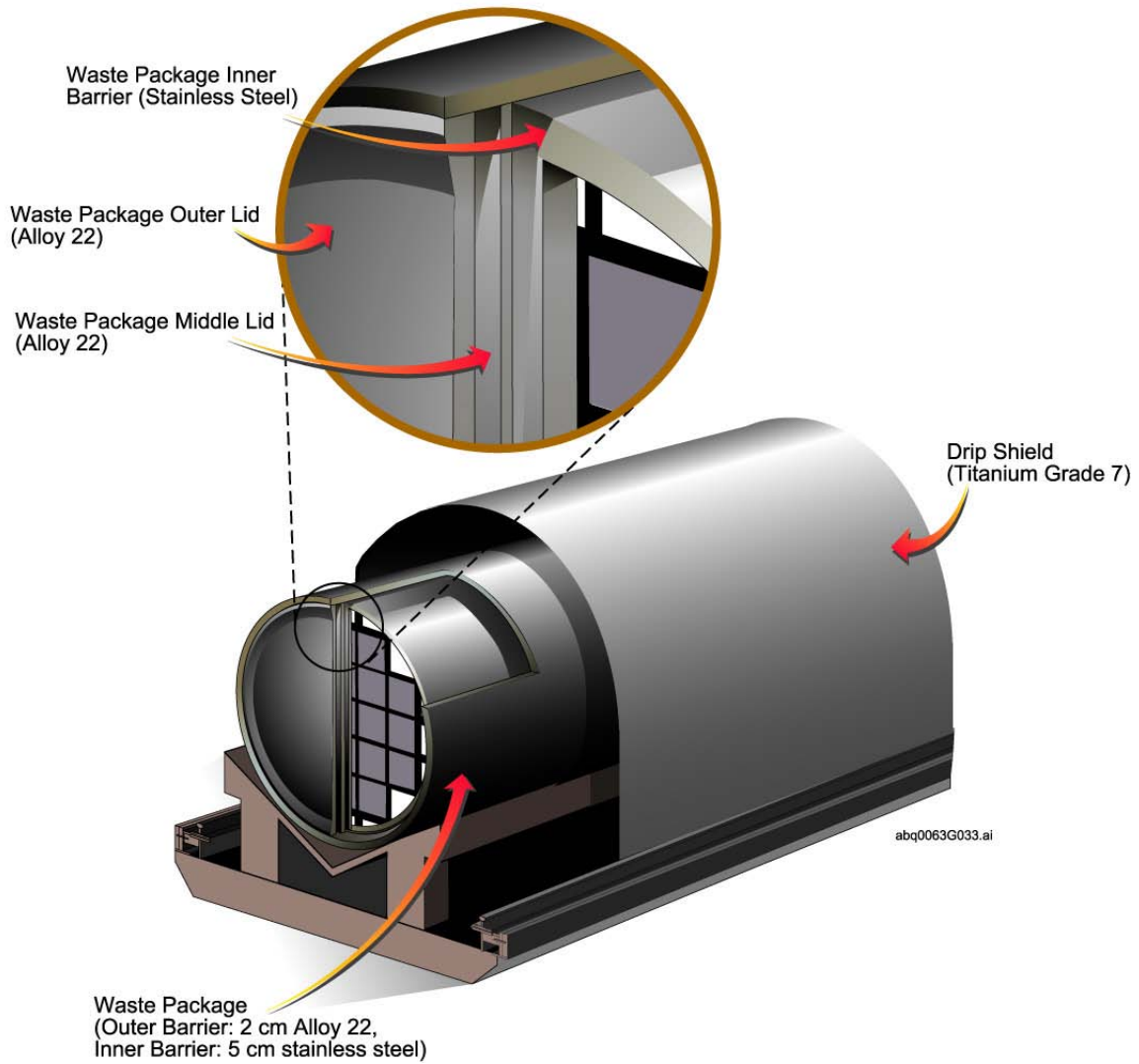
CRWMS M&O 2000b, Figure 3.4-1

Figure 1. Schematic Diagram of the Drip Shield and the WP

5-DHLW Short Waste Package Assembly Configuration
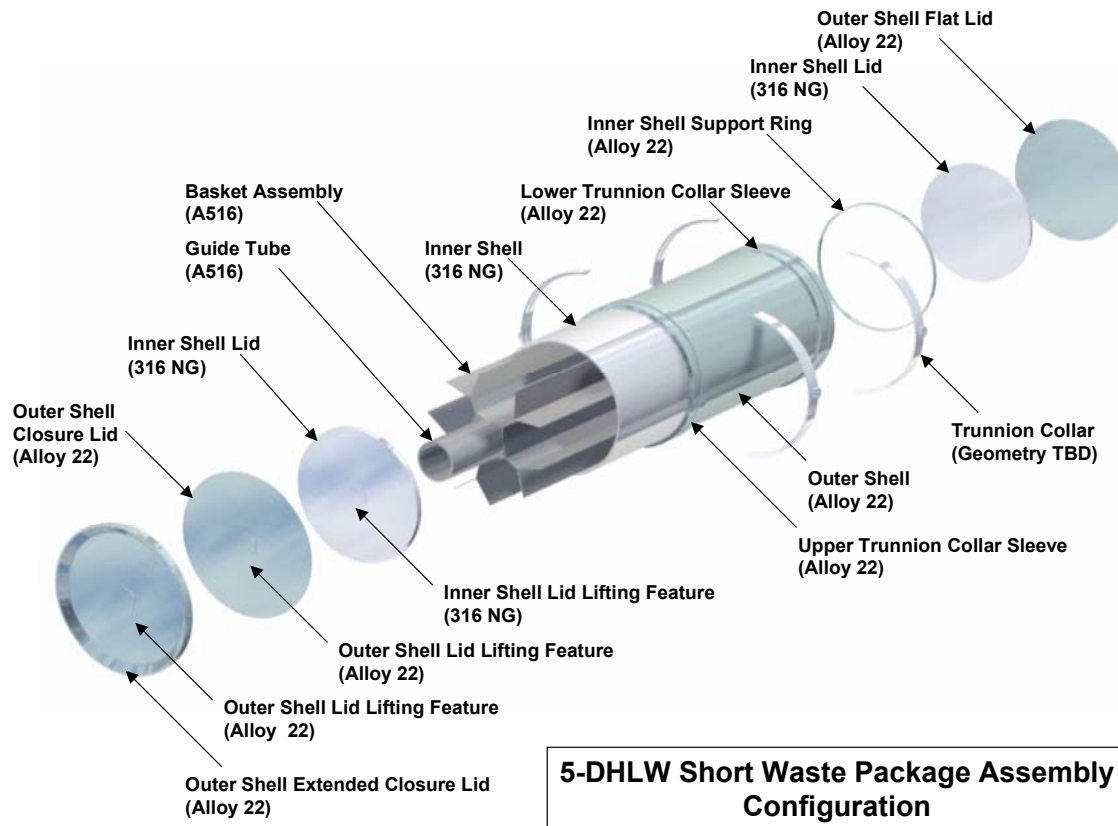
CRWMS M&O 2000a, Figure 6

Figure 2. Co-Disposal WP Containing One Canister of SNF and Five Canisters of HLW

For the N Reactor SNF, a different canister design has been proposed, the multi-canister overpack or MCO (DOE 2000b, Section 4). As a result, the structural components within the N Reactor SNF WPs will be as follows:

- A two-centimeter thick Alloy-22 outer wall to resist corrosion

- A five-centimeter thick stainless steel (316NG) inner wall, to provide structural integrity

- Two, perpendicular, carbon steel (A516) plates which intersect to form 4 vertical compartments separating the two GPCs and the two MCOs (DOE 2001a, Appendix A Section A-1.7) or four MCOs (DOE 2001a, Attached electronic file "WastePack Rev1.doc") inside the WP

- Two (DOE 2001a, Appendix A Section A-1.7) or four (DOE 2001a, Attached electronic file "WastePack Rev1.doc") MCO stands constructed of A516 carbon steel

- Two (or zero) GPCs, the 304L containers of the solidified HLW glass

- Two (DOE 2001a, Appendix A Section A-1.7) or four (DOE 2001a, Attached electronic file "WastePack Rev1.doc") MCOs constructed of 304L stainless steel.

The contents of the DOE SNF canister for FSV SNF and the M&D waste form and the contents of the MCOs for N Reactor SNF WPs are described in the following three sections.

4.1.1.1 DOE Canister Contents for FSV SNF

As described by Taylor (2001, Section 2.1.2) the FSV DOE SNF (Group 5) consists of fuel kernels composed of a Th carbide (ThC_2) or Th/U carbide (($Th/U)C_2$) core surrounded by four protective coatings of silicon carbide (SiC) and pyrolytic carbon (C). These fuel kernels were bound together with a matrix consisting of graphite filler and carbonized coal tar pitch, or petroleum-derived pitch, and then extruded into compacts (rods) by hot injection. Up to a maximum number of 3130 fuel compacts were loaded into a large hexagonal graphite prism to form a fuel element. The maximum loading configuration of FSV fuel in the DOE SNF canister includes five elements stacked vertically (Taylor 2001, Section 2.1.1). The FSV DOE canister thus contains the following components:

- A516 carbon steel impact plates;

- The hexagonal graphite blocks (assumed to be inert—see Assumption 5.12) of the fuel elements.

- The FSV SNF compacts composed of C, SiC, ThC_2, and $(Th/U)C_2$.

Surface areas and moles of the WP components were calculated from their geometry (see Assumption 5.2) by methods the same as BSC (2001a, Section 5.1 and Attachment III). These are reduced to a format suitable for EQ6 input in a Microsoft Excel workbook, "FSVR2.xls" for two different loading options. One loading option considers the maximum loading case of fresh FSV fuel in 5 elements. For the second loading option, the workbook "Rn Fix 05.xls" sheet "DOE_SNF99 (Cat. 5)" (output DTN: MO0201SPAGIN07.001) was used for the average composition and mass of FSV in the DOE SNF inventory (DOE 2001a, Attached Electronic File) which was equivalent to about 4 FSV fuel elements per WP. Both of these workbooks may be found in the electronic media associated with this Analysis (output DTN: MO0201SPAGIN07.001).

4.1.1.2 Multi-Canister Overpack (MCO) Contents for N Reactor SNF

As described by the DOE (2000b, Section 3), the N Reactor (Group 7) DOE SNF elements consist of Mark IV (0.947 wt% ^{235}U) or Mark IA (0.947 or 1.25 wt% ^{235}U for inner or outer rods, respectively) concentric U-metal rods co-extruded with Zircaloy-2 cladding. Because of the extremely slow corrosion rate of Zircaloy, the SNF rod cladding is considered inert in this analysis, similar to the Alloy-22 corrosion resistant barrier (see Assumption 5.6). However, the cladding is conservatively assumed to be breached exposing all of the SNF surface area to corrosion (see Assumption 5.7). This assumption is not as conservative for N Reactor SNF since underwater storage of the fuel has resulted in the breach or partial degradation of over half of the fuel assemblies (DOE 2000b, Appendix C, Section 3). The maximum SNF loading configuration includes five baskets with 54 Mark IA fuel elements, or six baskets with 48 Mark IA fuel elements, stacked vertically inside each MCO (DOE 2000b, Section 3). The N Reactor MCOs thus contain the following components:

- Baskets, constructed of 304 L stainless steel, five containing 54 Mark IA fuel elements each, or six containing 48 Mark IA fuel elements each

- Aluminum (Al 1100) spacers which hold the fuel elements in place

- The N Reactor (U-metal) Mark IA or Mark IV SNF elements.

Surface areas and moles of the WP components were calculated from their geometry (see Assumption 5.2) by the same methods as CRWMS M&O (2001a, Attachment III). These are reduced to a format suitable for EQ6 input in an Excel workbook for different loading options. Workbook "Nreactor2.xls" sheet "Mols_rct" was used for the loading case of two MCOs, each containing five 304L baskets (each with 54 fresh Mark IA fuel elements, ~9609 kg) which is similar to some of the internal criticality cases in CRWMS M&O (2001a, Attachment III). Workbook "Nreactor2.xls" sheet "Mols_rct" was also used for the case of an average loading of N Reactor SNF in 2 MCOs. Workbook "Nreactor2.xls" sheet "Mols_rct 4" was used for the case of an average loading of N Reactor SNF in 4 MCOs. Workbook "Rn Fix 05.xls", sheet "DOE_SNF99 (Cat. 7)" (output DTN: MO0201SPAGIN07.001) was used for calculating the average composition and mass (~17694 kg) of N Reactor SNF in the DOE SNF inventory (DOE 2001a, Attached Electronic File) with 4 MCOs per WP. Workbook "Rn Fix 05.xls", sheet "DOE_SNF99 (Cat. 7)(2)" (output DTN: MO0201SPAGIN07.001) was used for calculating the average composition and mass (~8847 kg) of N Reactor SNF in the DOE SNF inventory (DOE 2001a, Attached Electronic File) with 2 MCOs per WP. Both of these workbooks may be found in the electronic media associated with this Analysis (output DTN: MO0201SPAGIN07.001).

4.1.1.3 DOE Canister Contents for the Melt and Dilute Waste Form

As described by BSC (2001c, Section 3.2) the M&D waste form (Group 9) consists of U-Al-gadolinium (Gd) ingots. The DOE SNF canister will contain from three to six M&D ingots. The reactive components of the M&D WP inside the SNF canister are:

- A516 carbon steel impact plates

- The M&D waste form material consisting of U-Al-Gd ingots with a 1 mm thick, A516 carbon steel coating (see Assumption 5.13).

This Analysis considers cases similar to geometry case 2 in the criticality calculations (BSC 2001b, Tables 3 and 11). Surface areas and moles of the WP components were calculated from their geometry (see Assumption 5.2) by methods the same as BSC (2001b, Attachment I). These are reduced to a format suitable for EQ6 input in Excel workbooks for different loading options. Workbook "Melt Dilute Parameter Matrix2.xls" sheet "Geometry Cases" was used for the case of a maximum loading of 5 M&D ingots with a 1 mm A516 carbon steel coating. Workbook "Rn Fix 05.xls", sheet "DOE_SNF99 (Cat. 9)" (output DTN: MO0201SPAGIN07.001) was used for calculating the average composition and mass of M&D per WP based on the DOE SNF inventory (DOE 2001a, Attached Electronic File) which was equivalent to about 1 M&D ingot. Note that the M&D waste form is the only fuel group addressed in this analysis that is proposed for disposal in a short WP (approximately 3.8 m long), with a short DOE Canister and short GPCs. The FSV SNF and N Reactor SNF are to be disposed of in a long WP (approximately 5.4 m long).

4.1.2   Calculation Inputs

4.1.2.1 Steel Compositions and Corrosion Rates

Table 2 provides a summary of the compositions of the principal steel alloys used in the calculations. Table 3 provides low and high degradation rates for the steels. In all tables in this document, the number of digits reported does not necessarily reflect the accuracy or precision of the calculation. In most tables, three to four digits after the decimal place have been retained, to prevent round-off errors in subsequent calculations.

Table 2. Steel Compositions

Element	A516 Carbon Steel		304L Stainless Steel		316L Stainless Steel		316NG Stainless Steel	
	Weight %[a]	Moles of element per 100-gram mole of reactant	Weight %[b]	Moles of element per 100-gram mole of reactant	Weight %[c]	Moles of element per 100-gram mole of reactant	Weight %[c]	Moles of element per 100-gram mole of reactant
C	0.28	0.0233	0.03	0.0025	0.03	0.0025	0.02[d]	0.0017
Mn	1.045	0.0190	2	0.0364	2	0.0364	2	0.0364
P	0.035	0.0011	0.045	0.0015	0.045	0.0015	0.045	0.0015
S	0.035	0.0011	0.03	0.0009	0.03	0.0009	0.03	0.0009
Si	0.29	0.0103	0.75	0.0267	1	0.0356	1	0.0356
Cr	NA		19	0.3654	17	0.3269	17	0.3269
Ni	NA		10	0.1704	12	0.2045	12	0.2045
Mo	NA		NA	NA	2.5	0.0261	2.5	0.0261
N	NA		0.10	0.0071	0.1	0.0071	0.08[d]	0.0057
Fe	98.315	1.7605	68.045	1.2185	65.295	1.1692	65.325	1.1698
Total	100.000		100.000		100.000		100.000	

Sources: [a] ASTM A 516/A 516M-90 (1991, p. 321, Table 1)
[b] ASTM A 240/A 240M-94b (1994, p. 2, Table 1)
[c] ASTM A 276-91a (1991, p. 2, Table 1)
[d] ASM International (1987, p. 931)

Table 3. Steel Degradation Rates and Rate Constants

	A516 Carbon Steel	304L Stainless Steel	316L Stainless Steel	316NG Stainless Steel
Molecular Weight (g/mole)	100.00[a]	100.00[a]	100.00[a]	100.00[a]
Density (g/cm^3)	7.85[b]	7.94[c]	7.98[c]	7.98[c]
Low Rate (μm/year)	72.271364[d]	0.1[e]	0.1[e]	0.1[e]
Low Rate Constant[g] (mole/cm^2·s)	1.79776E-11	2.516E-14	2.5287E-14	2.5287E-14
High Rate (μm/year)	Same as above	34.405015[f]	1.9996307[f]	1.9996307[f]
High Rate Constant[g] (mole/cm^2·s)	Same as above	8.65642E-12	5.05648E-13	5.05648E-13

NOTES: [a]The molecular weight of all WP components was set to 100 grams to simplify inputs to EQ6.
[b]ASTM A 20/A20M-95a (1995, p. 21)
[c]ASTM G 1-90 (1990, p. 7, Table XI)
[d]Derived from values on pp. 2.2-78 to 2.2-80 in McCright, R.D. (1998), in workbook "A516_rate.xls" sheets
 "Prob" and "Prob_Chart" (output DTN: MO0201SPAGIN07.001). Rate constants were calculated in
 workbook "Nreactor2.xls" sheet "Rates" (output DTN: MO0201SPAGIN07.001).
[e]CRWMS M&O (1997, pp. 11-13)
[f]Rate constants were calculated in workbook "Nreactor2.xls" sheet "Rates" (output DTN:
 MO0201SPAGIN07.001) using Eq. 3-14 ($y = b_0 + b_1x$) where y is the cumulative probability or percentile,
 and x is the log of the corrosion rate (CRWMS M&O 2000c). Parameters are taken from the 50th percentile
 values in Figure 3-15 (CRWMS M&O 2000c).
[g]This rate constant (and all the rate constants in the following tables) must be multiplied by the normalized
 surface area (sk in the EQ6 input file) in cm^2 of each WP component to calculate the actual degradation
 rate in 100-g moles/s of that component.

4.1.2.2 Al Alloy Composition and Dissolution Rates

The N Reactor WPs include Al alloy as part of their contents. The composition, density, and degradation rates of the Al alloy used in this analysis are presented in Table 4.

Table 4. Elemental Composition, Degradation Rate Constant, and
Density of Al Alloy (Al 1100) Spacers in N Reactor WP

Element	Al Alloy (Al 1100) Weight%[b]	Moles of element per 100-gram mole of reactant
Al	99.00	3.669E+00
Cu	0.05	7.868E-04
Si	0.45	1.602E-02
Fe	0.50	8.953E-03
Total	100	
Molecular Weight[a]	100	(g/mole)
Density[c]	2.71	(g/cm^3)
Low Rate[d]	2.96392911	(μm/year)
Low Rate Constant[d]	2.53587E-13	(mole/cm^2·s)
High Rate[e]	29.6392911	(μm/year)
High Rate Constant[e]	2.53587E-12	(mole/cm^2·s)

NOTES: [a]The molecular weight of all WP components was set to 100 grams to simplify inputs to EQ6.
[b]Based on Al 1100 composition in ASTM B 209-96 (1996, p. 7, Table 1)
[c]ASTM G 1-90 (1990, p. 7, Table XI)
[d]Derived from values on p. 603 in Hollingsworth and Hunsicker (1987) in workbook "Nreactor2.xls" sheet "Rates" (output DTN: MO0201SPAGIN07.001)
[e]The high rate was taken to be 10 times the low rate.

4.1.2.3 HLW Glass Composition and Dissolution Rates

Table 5 gives the simplified molar composition of the HLW glass used in the calculations, which is derived from that given by CRWMS M&O (1999a, Attachment I; see Assumption 5.15). Several minor changes were made to the basic composition to increase the efficiency of the calculations, to decrease the EQ6 run time and to allow use of a pH dependent rate law. The simplified glass composition was included in the EQ6 data0.trc database (see Section 4.1.2.8) as a mineral named 'SRL_Bulk'. These simplifications were necessary because the amounts of any element in the SRL_Bulk composition had to exceed 0.0001 moles/100g of glass. Some elements in the HLW glass were removed or merged with chemically similar elements (e.g., Li was merged with Na in the glass composition; see Table 5). Shorter half-life Pu isotopes were "pre-decayed" to longer half-life U isotopes (see Assumption 5.5): ^{240}Pu was combined with ^{236}U; and ^{238}Pu was combined with ^{234}U. Since Neptunium (^{237}Np) and Pu (^{239}Pu and ^{242}Pu) made up less than 1.1% of the total actinide content of the HLW glass, they were added to a second glass mineral reactant, 'HLW_Trace2', described in the next paragraph.

The inventory abstraction of the HLW glass (BSC 2001k, Table I-7) indicates that the HLW glass will, on average, include trace amounts of [129]I and ^{99}Tc, as well as the small amounts of Np and Pu mentioned above. The trace radionuclides found in HLW glass were also included in the database as an I, Np, Pu and Tc oxide mineral named 'HLW_Trace2'. Calculations to convert the HLW glass inventory values for [129]I, [237]Np, [239]Pu, [242]Pu and ^{99}Tc to a format suitable for input to EQ6 are found in sheet "Composition4" of workbook "HLW_glass_rev4.xls" (output DTN: MO0201SPAGIN07.001). The following adjustments (see Assumption 5.5) were made to the radionuclide inventory from BSC 2001k (Table I-7): [241]Am was assumed to decay completely to [237]Np; and [243]Am was assumed to decay completely to [239]Pu.

Both SRL_Bulk and HLW_Trace2 were used as reactants for the EQ6 runs that included HLW glass in this analysis. The moles and surface area of SRL_Bulk were multiplied by a factor equal to the molar ratio of Pu in 100 g of HLW glass to Pu in 100g of HLW_Trace2 (1.8248E-04; sheet "Composition4" of workbook "HLW_glass_rev4.xls" in output DTN: MO0201SPAGIN07.001) to calculate the moles and surface area of HLW_Trace2 used in the EQ6 input files.

The glass dissolution rate law is the pH-dependent rate law of BSC (2001f, Section 6.2.3.3, Equations 7 and 8):

for pH < 7.1 (BSC 2001f, Section 6.2.3.3, Equation 7)

$$\log_{10} \text{rate} = (14.0 \pm 0.5) + (-0.6 \pm 0.1) \bullet \text{pH} + \log_{10}(\exp((-80 \pm 10) \text{ kJ/mol}/(RT))),$$

and for pH $\geq$ 7.1 (BSC 2001f, Section 6.2.3.3, Equation 8)

$$\log_{10} \text{rate} = (6.9 \pm 0.5) + (0.4 \pm 0.1) \bullet \text{pH} + \log_{10}(\exp((-80 \pm 10) \text{ kJ/mol}/(RT))).$$

This rate, in grams/m^2·day, is converted to a format suitable for input to EQ6 in sheet "Rates", workbook "HLW_glass_rev4.xls" (output DTN: MO0201SPAGIN07.001). The first rate mechanism (described with k_1) in Table 5 is dominant at pH values $\geq$ 7.1, while the second rate mechanism (described with k_2) is dominant at pH values below 7.1. The low rate constants (those derived for degradation at 25°C) and the high glass degradation rate constants (those derived for 50°C) are given in Table 5.

Table 5. Simplified HLW Glass Composition, Density, and Degradation Rates

Element	Moles/100-g mole SRL_Bulk[a]	Moles/100-g mole HLW_Trace2[b]
O	2.7042	1.0309
U	0.0077	NA
Ba	0.0011	NA
Al	0.0863	NA
S	0.0040	NA
Ca	0.0162	NA
P	0.0005	NA
Cr	Merged with Al (overwhelmed by steel Cr; Cr_2O_3 similar to Al_2O_3)	NA
Ni	Merged with Fe	NA
Pb	Merged with Ba (both form insoluble $CrO_4^=$ compounds in EQ6 runs)	NA
Si	0.7767	NA
Ti	Merged with Si (TiO_2 similar to SiO_2)	NA
B	0.2913	NA
Li	Merged with Na	NA
F	0.0017	NA
Cu	Merged with Fe	NA
Fe	0.1723	NA
K	0.0751	NA
Mg	0.0333	NA
Mn	Merged with Fe	NA
Na	0.5769	NA
Cl	Removed (overwhelmed by Cl in in-dripping water)	NA
Ag	Removed 0.05 weight percent	NA
Zn	Removed 0.06 weight percent	NA
Th	Removed<0.2 weight percent	NA
Cs	Removed<0.05 weight percent	NA
I	Added to HLW_Trace2	0.0065
Np	Added to HLW_Trace2 (~0.1% of actinides)	0.0095
Pu	^{238}Pu and ^{240}Pu merged with U ^{239}Pu and ^{242}Pu added to HLW_Trace2 (Pu ~1% of actinides)	0.2834
Tc	Added to HLW_Trace2	0.1281
Density (g/cm^3)[d]	2.85	2.85
Total Degradation Rate Constant[c] = $k_1[H+]^{-0.4} + k_2[H+]^{0.6}$ (mole/cm^2·s)		
Low Rate Constant (k_1)	8.85753E-19	(liter/cm^2·s)
High Rate Constant (k_1)	1.07560E-17	(liter/cm^2·s)
Low Rate Constant (k_2)	1.11510E-11	(liter/cm^2·s)
High Rate Constant (k_2)	1.35411E-10	(liter/cm^2·s)

Sources: [a]CRWMS M&O (1999a, Attachment I), reduced in output DTN: MO0201SPAGIN07.001, workbook "HLW_glass_rev4.xls", sheet "Composition4".
[b]BSC (2001k, Table I-7) reduced in output DTN: MO0201SPAGIN07.001, workbook "HLW_glass_rev4.xls", sheet "Composition4".
[c]BSC (2001f, Section 6.2.3.3, Equations 7 and 8) reduced in output DTN: MO0201SPAGIN07.001, workbook "HLW_glass_rev4.xls", sheet "Rates".
[d]Stout and Leider (1991, Table 6.4).

4.1.2.4 Water Composition and Drip Rates

It was assumed that the water composition entering the WP is J-13 well water (see Assumption 5.8). This composition is reproduced in Table 6 (DTN: MO0006J13WTRCM.000). Low concentrations (1.0E-16 molal) of elements present in WP components, but not present in J-13

water were added to the J-13 well water composition to facilitate execution of EQ6 (see Assumption 5.8). The elements added for all three fuels were Al, B, Ba, Cr, Fe, I, Mn, Mo, Ni, Np, P, Pu, Tc and U. Thorium was only added during runs for FSV SNF, Gd was only added during runs for the M&D waste form and Cu was only added to runs for N Reactor SNF. EQ6 requires that a tangible amount of each element in a reaction path calculation be present in the aqueous phase at the start of a calculation (1.0E-16 molal).

Table 6. Major Element Chemistry for J-13 Well Water

Element	Concentration (mol/kg)[a]
Ca	3.24E-04
Mg	8.27E-05
Na	1.99E-03
K	1.29E-04
Cl	2.01E-04
S	1.92E-04
F	1.15E-04
C	2.49E-03
Si	1.02E-03
N	1.42E-04

NOTE: [a]All concentrations expressed as mol/kg. pH and Eh are not reported because they are independently calculated within EQ3NR, based on the gas fugacities (see Assumption 5.3).

Source: DTN: MO0006J13WTRCM.000 (see preceding text)

The assumption is made (see Assumption 5.10) that the drip rate onto a WP is the same as the rate at which water flows through the WP. The drip rate is taken from a correlation between percolation flux and drip rate, also called mean seep flow rate (CRWMS M&O 2000b, Figure 3.2-15). Specifically, values of 0.015 and 0.15 m^3/year were used for most cases, corresponding to percolation fluxes of about 20 mm/year and 80 mm/year. The value of 20 mm/year corresponds to approximately double the high infiltration rate for the present-day climate and 80 mm/year corresponds to about double the high infiltration rate for the glacial-transition climate (CRWMS M&O 2000b, Table 3.2-2). Table 3.2-2 of CRWMS M&O 2000b gives values of net infiltration rate at the surface, rather than percolation flux; however, they are equal at the potential repository level because flow is essentially vertical from the surface to the repository horizon (CRWMS M&O 2000b, Section 3.2.3.4, p. 3-33). For a few runs, the range of allowed drip rates included an upper value of 0.5 m^3/yr, which represents about 100 mm/year percolation flux.

4.1.2.5 FSV SNF Compositions and Dissolution Rates

The DOE SNF heavy metal inventory for SNF Group 5 (DOE 2001a, Attached electronic file; output DTN: MO0201SPAGIN07.001, workbook "Rn Fix 05.xls") indicates that the average mass of heavy metal per WP is equivalent to approximately 4 FSV fuel elements. A more conservative loading from a criticality perspective is to assume a full load (five fuel elements) of fresh fuel (ThC$_2$ or (Th/U)C$_2$ core surrounded by four protective coatings of SiC and pyrolytic C, BSC 2001a, Table 5-4). Table 7 summarizes the assumed (see Assumption 5.14) characteristics of the inventory average and fresh FSV fuel. It is expected that the breach of the WP will not

occur until about 10,000 years after emplacement (CRWMS M&O 2000b, Section 4.1.2), and most of the analysis will involve times greater than 10,000 years post-emplacement. Thus the inventory average fuel composition used in EQ6 has been altered to pre-decay some of the shorter-lived isotopes (see Assumption 5.5), as described for the HLW glass in Section 4.1.2.3.

Table 7. FSV Th/U Carbide SNF Composition and Degradation Rates

Element	Moles per 100-gram mole Inventory Ave. FSV SNF[a]	Moles per 100-gram mole Fresh FSV Fuel[b]
I	5.83513E-05	NA
Tc	2.82383E-04	NA
Np	6.64687E-05	NA
Th	1.27283E-01	1.10709E-01
U	7.10224E-03	1.50419E-02
Pu	1.20732E-05	2.57947E-05
C	5.20344E+00	5.39585E+00
Si	2.22427E-01	2.12264E-01
Average Molecular Weight (g/mole)	100	100
Density (g/cm^3)	1.9972[a]	2.2191[b]
Best Estimate Rate Constant[c]	6.00000E-16	(100-g-mole/cm^2·s)
Conservative Rate Constant[c]	2.77778E-10	(100-g-mole/cm^2·s)

NOTES: [a]DOE (2001a, Attached Electronic file) reduced in workbook "Rn Fix 05.xls", sheet "DOE_SNF99 (Cat.5)" (output DTN: MO0201SPAGIN07.001).
[b]BSC (2001a, Table 5-4 and Attachment III). This idealized fuel composition contains beginning of life (BOL) levels of U, end of life (EOL) levels of Th and Pu based on Taylor (2001, Tables 2-4 and 2-7), but no Np, Tc or I isotopes.
[c]BSC (2001g, Section 6.3.5) and DOE (2001a, Section 6.5) converted to EQ6 input in BSC (2001a, Table 5-4 and Attachment III).

4.1.2.6 N Reactor SNF Compositions and Dissolution Rates

Workbook "Rn Fix 05.xls", sheet "DOE_SNF99 (Cat. 7)" (output DTN: MO0201SPAGIN07.001) was used for calculating the average composition and mass (~17694 kg) of N Reactor SNF in the DOE SNF inventory (DOE 2001a, Attached Electronic File) with 4 MCOs per WP (used for Case 0 only). Workbook "Rn Fix 05.xls", sheet "DOE_SNF99 (Cat. 7)(2)" (output DTN: MO0201SPAGIN07.001) was used for calculating the average composition and mass (8847 kg) of N Reactor SNF in the DOE SNF inventory (DOE 2001a, Attached Electronic File) with 2 MCOs per WP. A more conservative loading, from a criticality perspective, is the case of two MCOs, each containing five 304L baskets (each with 54 fresh Mark IA fuel elements, ~9609 kg, used for Case 1 only), which is similar to some of the internal criticality cases in CRWMS M&O (2001a, Attachment III). Table 8 summarizes the characteristics of the inventory average (see Assumption 5.14) and fresh Mark IA N Reactor (U-metal) fuel. It is reasoned that the breach of the WP will not occur until about 10,000 years after emplacement (CRWMS M&O 2000b, Section 4.1.2) and most of the analysis will involve times greater than 10,000 years post-emplacement. Thus the inventory average N Reactor SNF

composition used in EQ6 has been altered to pre-decay some of the shorter-lived isotopes (see Assumption 5.5), as described for the HLW glass in Section 4.1.2.3.

The best estimate dissolution rate is 5 times and the conservative rate is 25 times the constant U-metal rate of DOE (2000a, Equation 2-39) as recommended by the BSC (2001g, Section 6.3.7):

$$k_1 = 5.03 \cdot 10^9 \exp\left[\frac{-66.4 \pm 2.0 \text{kJ/mol}}{RT}\right] \text{mg U/cm}^2/\text{h} \qquad \text{(DOE 2000a, Equation 2-39)}$$

These rates are reduced to suitable units for EQ6 input in workbook "Nreactor2.xls", sheet "Rates" (output DTN: MO0201SPAGIN07.001) as presented in Table 8.

Table 8. N Reactor (U-metal) SNF Composition and Degradation Rates

Element	Moles per 100-gram mole Inventory Average N Reactor SNF[a]	Moles per 100-gram mole Fresh N Reactor Mark IA Fuel [b]
I	1.57253E-05	NA
Tc	9.91955E-05	NA
Np	5.56772E-05	NA
Pu	7.48895E-04	NA
U	4.19271E-01	4.20147E-01
Molecular Weight (g/mole)	100	100
Fuel Density (g/cm^3)	17.145[a]	18.82[c]
Best Estimate Rate Constant[d]	1.60301E-10	(100g-mole/cm^2·s)
Conservative Rate Constant[d]	8.01505E-10	(100g-mole/cm^2·s)

NOTES: [a]DOE (2001a, Attached Electronic File) reduced in workbook "Rn Fix 05.xls",
sheet "DOE_SNF99 (Cat. 7)" (output DTN: MO0201SPAGIN07.001).
[b]This idealized fresh fuel includes no Pu, Np, Tc or I isotopes (CRWMS M&O
2001a, Table 2 and Attachment III).
[c]CRWMS M&O (2001a, Table 4 and Attachment III)
[d]DOE (2000a, Equation 2-39) as suggested by BSC (2001g, Section 6.3.7)
reduced in workbook "Nreactor2.xls", sheet "Rates" (output DTN:
MO0201SPAGIN07.001).

4.1.2.7 M&D Waste Form Compositions and Dissolution Rates

The Statement of Work (BSC 2001c, Section 3.2) indicates that the M&D WP will contain 3 to 6 M&D ingots. The geometry (see Assumption 5.2) and composition of the M&D ingots may vary within the range of parameters given by BSC (2001c, Section 3.2) as described in Assumption 5.13. This Analysis considers cases similar to geometry case 2 in the criticality calculations (BSC 2001b, Tables 3 and 11). The expected loading scenario assumes (see Assumptions 5.14) the average composition of one M&D ingot taken from the DOE SNF inventory for SNF Group 9 (DOE 2001a, Attached electronic file) and reduced to a form usable by EQ6 in workbook "Rn Fix 05.xls", sheet "DOE_SNF99 (Cat. 9)" (output DTN: MO0201SPAGIN07.001). A more conservative loading from a criticality perspective is to model a WP with 5 M&D ingots (BSC

2001b, Tables 3 and 11). Table 9 summarizes the characteristics and degradation rates of the inventory average M&D ingot composition and the M&D ingot composition used for geometry case 2 in BSC 2001b (Tables 3 and 11). It is reasoned that the breach of the WP will not occur until about 10,000 years after emplacement (CRWMS M&O 2000b, Section 4.1.2), and most of the calculation will involve times greater than 10,000 years post-emplacement. Thus, the inventory average fuel composition used in EQ6 has been altered to pre-decay some of the shorter-lived isotopes (see Assumption 5.5), as described for the HLW glass in Section 4.1.2.3. The best estimate M&D ingot degradation rate is equal to 0.22 mgU/m^2·d as recommended by the BSC (2001g, Section 6.3.9 and Table 1b) and the high rate (2×10^{-3} inches/year or about 75 mgU/m^2·d), is recommended by the BSC (2001c, Section 3.2). These rates were converted to EQ6 rate constants in workbook "Melt Dilute Parameter Matrix2.xls", sheet "Degradation Rates" (output DTN: MO0201SPAGIN07.001).

Table 9. Melt and Dilute Waste Form Composition and Degradation Rates

Element	Moles per 100-gram mole of Inventory Average M&D[a]	Moles per 100-gram mole of M&D[b]
I	3.49914E-05	NA
Tc	2.65378E-04	NA
Np	2.82598E-05	NA
Pu	1.26752E-04	NA
U	7.61830E-02	7.66479E-02
Gd	3.20160E-03	3.17965E-03
Al	3.01471E+00	3.01317E+00
Molecular Weight (g/mole)	100	100
Fuel Density (g/cm^3)	3[c]	3[c]
Best Estimate Rate Constant (100g-mole/cm^2·s)[d]	1.408E-14	1.399E-14
Conservative Rate Constant (100g-mole/cm^2·s)[e]	4.83E-12	4.83E-12

NOTES: [a]DOE (2001a, Attached Electronic File), reduced in workbook "Rn Fix 05.xls", sheet "DOE_SNF99 (Cat. 9)" (output DTN: MO0201SPAGIN07.001).
[b]BSC 2001b (Table 3) as adapted for EQ6 input in workbook "Melt Dilute Parameter Matrix2.xls", sheet "Geometry Cases" (output DTN: MO0201SPAGIN07.001). This composition includes no Pu, Np, Tc or I isotopes.
[c]BSC (2001c, Section 3.2).
[d]BSC (2001g, Section 6.3.9 and Table 1b), as adapted to EQ6 input format in workbook "Melt Dilute Parameter Matrix2.xls", sheet "Degradation Rates".(output DTN: MO0201SPAGIN07.001).
[e]BSC (2001c, Section 3.2) as adapted to EQ6 input format in workbook "Melt Dilute Parameter Matrix2.xls", sheet "Degradation Rates".(output DTN: MO0201SPAGIN07.001).

4.1.2.8 Thermodynamic databases

The thermodynamic database used for the EQ3/6 calculations, data0.trc, is a slightly altered version (see Assumption 5.16) of the data0.ymp.R0 (DTN MO0009THRMODYN.001) which contains 25°C data (see Assumption 5.11). The changes include:

- Addition of the reactants, SRL_Bulk and HLW_Trace2, to represent HLW glass (see Table 5). A pH-dependent kinetic rate law controls the dissolution of these minerals and they are sufficiently soluble that they can not precipitate during the EQ6 runs in this analysis.

- A series of chromium (Cr)- and molybdenum (Mo)-rich minerals were added to the database including Cr-ferrihydrite ($Fe_4(CrO_4)(OH)_{10}$), Cr-ettringite ($Ca_6Al_{12}(CrO_4)_3(OH)_{12}{:}26H_2O$), $Fe_2(MoO_4)_3$ (ferrimolybdate) and the aqueous species $CaCrO_{4(aq)}$ (BSC 2001d, Assumption 5.2, Sections 5 and 6).

- A solid phase, $GdOHCO_3$, was added to the database. The log K was assumed to be the same as the log K for $NdOHCO_3$ in data0.ymp.R0 since Gd and neodymium (Nd) are both lanthanides and are chemically similar.

- The log K of $GdHPO_4+$ was found to be incorrect in the database and was changed from the value of 185 to –5.7 to match the value given in Spahiu and Bruno (1995), the source listed in the database for that reaction.

4.1.2.9 Atomic Weights

Atomic weights of the elements and radionuclide isotopes used in the Excel workbooks (output DTN: MO0201SPAGIN07.001) were taken from Audi and Wapstra (1995) and Parrington et. al. (1996, p. 50). These references have been used as a source for this information throughout the Yucca Mountain Site Characterization project (CRWMS M&O 2001a, Section 5.1.1.5; BSC 2001a, Section 5.1.6; BSC 2001b, Section 5.1.6) and are appropriate as a source for atomic weights in this analysis.

4.1.2.10 Specific Activities

Specific activities, in Curies/gram, for the radionuclide isotopes of I, Np, Pu, Tc and U in the DOE SNF inventory used in Excel workbook "Rn Fix 05.xls" (output DTN: MO0201SPAGIN07.001) were taken from the BSC (2001k, Table I-6). These specific activities have been used to calculate the HLW glass radionuclide inventory in BSC 2001k (Table I-7) which has been used as a source for this information throughout the Yucca Mountain Site Characterization project (see Assumption 5.15). Therefore BSC 2001k (Table I-6) is an appropriate source for the specific activities used in this analysis.

4.2   CRITERIA

There are no criteria applicable to this analysis. These calculations are not intended to address compliance to regulations or specific acceptance criteria in Issue Resolution Status Reports for Key Technical Issues. Those criteria will be addressed in the TSPA-SR itself (CRWMS M&O 2000b, Section 1.3).

4.3   CODES AND STANDARDS

There are no codes and standards associated with this analysis.

5. ASSUMPTIONS

This section identifies assumptions in upstream documentation or inputs that are essential for this analysis. The discussion of each assumption includes four elements: (1) a statement of the assumption; (2) the rationale for the assumption; (3) a statement on the need for further confirmation, if any, of the assumption (i.e., the "to be verified" (TBV) status); and (4) a statement where the assumption is used within the analysis.

5.1   WP CORROSION BARRIER AND DRIP SHIELD

Assumption: For the geochemical calculations in this analysis, it is assumed that the drip shield and corrosion resistant barrier remain intact except for openings near their upper surface that allow dripping groundwater to enter the WP. It is also assumed that the water may exit the WP from these openings.

Rationale: This assumption is conservative because the slow rate of corrosion of Ti Grade 7 and Alloy 22 (Estill 1998), as compared to internal components of the WP (DOE SNF, HLW, and steels), allows water to pool inside the WP. If the Alloy 22 were allowed to react there would be no reservoir to contain water and chemical reaction of water with the spent fuel inside the WP would be minimized.

Confirmation Status: Due to the reasonable conservatism that this assumption would lead to greater dissolution of internal WP components, it does not require further confirmation.

Use within the Analysis: This assumption applies to Section 4.1.1.

5.2   WP GEOMETRY

Assumption: It is assumed that the WP component properties, i.e., masses, volumes and surface areas, are represented to a degree that closely approximates their true properties.

Rationale: The WP geometry(s) are based on previous calculations of FSV SNF (BSC 2001a), N-Reactor SNF (CRWMS M&O 2001a, Attachment III), and the M&D waste form (BSC 2001b). These prior calculations make some minor abstractions of the geometry of the co-disposal WP. The calculation of WP geometry, mass, volume and surface area of WP components, are intended to obtain the greatest accuracy in the representation of the WP. Where adequate information is unavailable to choose between competing models of WP geometry, the choice that should logically lead to the greatest conservatism is always selected. For example, when choosing the geometric properties of a WP component that is known to generate protons, i.e., decrease pH, when it dissolves, and thus increase dissolution of SNF, the choice is always based on maximizing SNF dissolution.

Confirmation Status: Since the WP component geometry is chosen for greatest accuracy, increased degradation of WP components and more rapid release of radionuclides this assumption does not require verification.

Use within the Analysis: This assumption applies to Sections 4.1.1.1, 4.1.1.2, 4.1.1.3, and 4.1.2.7.

5.3   DISSOLVED GASES

Assumption: It is assumed that gases in solution in the WP remain in equilibrium with the ambient atmosphere outside the WP, and the latter will be characterized by specific partial pressures (fugacities) of CO_2 and O_2 of, respectively, $10^{-3.0}$ and $10^{-0.7}$ atm (DOE 1998, pp. 3-67 and 3-69 to 3-72).

Rationale: This assumption is justified because the O_2 partial pressure is equivalent to that in the atmosphere. The CO_2 pressure is somewhat higher than atmospheric and was chosen to reflect the observation that the rock gas composition in boreholes in the unsaturated zone at Yucca Mountain has higher than atmospheric CO_2 levels (Yang et al. 1996, Table 7). The gas phase equilibrium at the repository horizon is expected to be similar to that prevailing in the open atmosphere. Furthermore, the large relative volume of the exterior gas reservoir compared to the relatively small volume of the WP interior also supports equilibrium between the atmosphere and WP interior.

Confirmation Status: This analysis evaluates the impact of reduced O_2 partial pressure, the results of which are discussed in Sections 6.3.7, 6.4.7, and 6.5.7. Previous calculations (CRWMS M&O 1999b, Section 5.3.2) examine the sensitivity of CO_2 partial pressure on in-package chemistry and demonstrate that changing CO_2 fugacity has a negligible effect on the outcome of the simulation. Therefore, no further confirmation is required.

Use within the Analysis: This assumption applies to Sections 4.1.2.4, 5.4, 6.2, 6.3.7, 6.4.7 and 6.5.7.

5.4   PRECIPITATED SOLIDS

Assumption: It was assumed that the suppression of minerals or solids not expected to form under the conditions inside a WP or that changing the iron oxide assemblage in the WP degradation products by suppressing hematite and goethite would not adversely affect the results of this analysis and would more realistically represent the chemistry of the WP solution and the elemental composition of the degradation products.

Rationale: Minerals may precipitate and dissolve instantaneously to maintain equilibrium with the surrounding solution. Instantaneously, in the context of the calculations, means over time scales shorter than those over which water is to react with WP components (in other words, hundreds of years or less). The choice of which minerals will precipitate is determined internally to EQ6 via consideration of the thermodynamics of the chemical system. Additionally, the analyst may prevent certain minerals from precipitating based on the analyst's knowledge of a phase's mode of occurrence and the relative kinetics of formation. For example, amorphous silica is more soluble than quartz at low temperatures, hence quartz reaches saturation first; however, quartz formation is not observed in low temperature aqueous systems. Therefore, the analyst would "suppress" quartz formation for a low-temperature simulation. Several minerals known to precipitate only in high temperature and/or pressure environments were not allowed to form during the simulations in this analysis. A listing of all of the minerals suppressed for each EQ6 run can be found in the corresponding EQ6 input file (*.6i files found in the output DTN: MO0201SPAGIN07.001).

Radionuclide bearing phases were not suppressed with the following exceptions. Plutonium oxide (PuO_2) was suppressed, in part, to be consistent with a previous calculation (BSC 2001e, Sections 5 and 6). The solubilities of solid Pu(IV) oxide/hydroxide scatter within several orders of magnitude because of the difficulties of establishing equilibrium of Pu(IV), polymerization and disproportionation reactions and the strong sorption capacities of Pu^{4+} (Runde 1999).

Experimental Pu solution concentrations during PuO_2 or PWR SNF degradation have been shown to be between the solubility of PuO_2 and that of a more soluble phase, $Pu(OH)_4$ (or $PuO_2 \cdot 2H_2O$) (Rai and Ryan 1982; Wilson and Bruton 1989, Section 3.1 and Table 3). So, by suppressing formation of PuO_2, we are increasing the amount of soluble Pu to a more realistic or somewhat conservative level. Thorianite (ThO_2) was suppressed for the runs considering degradation of FSV SNF since it is found only in igneous rocks and it would, therefore, not be expected to form under the temperature and pressure conditions in the WP (BSC 2001a, Section 5.2.1). In addition, a U mineral, soddyite ($(UO_2)_2SiO_4 \cdot 2H_2O$), was also suppressed in all of the EQ6 runs in order to be consistent with a previous calculation (BSC 2001e, Sections 5 and 6). Suppression of soddyite had no effect on the results of this analysis, since this mineral is fairly soluble under the conditions simulated and it would not have precipitated in any of the EQ6 runs even if its formation had not been suppressed.

Also, thermodynamically more stable hematite and goethite were suppressed for most of the EQ6 runs in this analysis to allow the formation of kinetically favored Cr- and Mo-bearing Fe(III) minerals (Cr(VI)-ferrihydrite and $Fe_2(MoO_4)_3$) which were added to the thermodynamic database (see Section 4.1.2.8 and Assumption 5.16; Carlson and Schwertmann 1981). Total suppression of the formation of hematite and goethite is not realistic considering the duration of the time frame of this analysis, until 100,000 after WP breach. Considering the temperature, solution and pH conditions we are simulating in the WP, a mixture of goethite and hematite would, eventually, be the most abundant iron oxides in the corrosion products (Schwertmann and Cornell 1991, Chapters 4, 5 and 10). It is not possible to simulate the formation of such a mixture of iron oxides with EQ6 since only the most thermodynamically stable solid is allowed to form. If hematite is not suppressed it will be the only iron oxide formed in a run. If hematite is suppressed and goethite is not, then goethite will be the only iron oxide that forms during an EQ6 run. However, during WP degradation, mixed Fe(II)-Fe(III) minerals, such as magnetite (Fe_3O_4) and green rusts (Fe hydroxy salts of chloride, sulfate or carbonate) as well as Fe(III) oxides such as maghemite ($\gamma\text{-}Fe_2O_3$) and lepidocrocite ($\gamma\text{-}FeOOH$) may also be the products of steel corrosion in the WP (Schwertmann and Cornell 1991, Introduction and Chapter 1; Furet et al. 1990). Of these minerals, only magnetite is in the current EQ6 database and magnetite will not form during most of our simulations because our assumption about O_2 fugacity (see Assumption 5.3) has the effect of completely oxidizing Fe(0) to Fe(III), as well as Cr(0) to Cr(VI) and Mo(0) to Mo(VI). Minerals such as ferrihydrite ($Fe_5HO_8 \bullet 4H_2O$) and $Fe(OH)_3$, which form during rapid oxidation of Fe(II) and hydrolysis of Fe(III), will probably be present throughout the period of steel degradation in the WP (Schwertmann and Cornell 1991, Chapters 1 and 8). These poorly crystalline iron oxides are unstable with respect to hematite and goethite, but their transformation is significantly inhibited or retarded by their adsorption of anions such as silicate and phosphate, which are common components of the WP solution (Carlson and Schwertmann 1981, Anderson and Benjamin 1985, Cornell et al. 1987). It is common for Cr^{3+} (ionic radius = 0.061 nm, Schwertmann and Cornell 1991, Table 1-2), which is very similar in size to Fe^{3+} (ionic radius = 0.064 nm, Schwertmann and Cornell 1991, Table 1-2) to substitute for Fe(III) in natural iron oxides (Schwertmann and Taylor 1989, pp. 380-382). Chromium-substitution in ferrihydrite also tends to slow its transformation to hematite or goethite (Schwertmann and Cornell 1991, Chapter 5). Since Cr-substituted goethite can be synthesized by aging a Cr-ferrihydrite precipitate (Schwertmann and Cornell 1991, Chapter 5), it is likely that Cr-substituted ferrihydrite or $Fe(OH)_3$ minerals which form during WP degradation will eventually transform to Cr-substituted goethite or hematite. Thermodynamic data for such mixed Fe-Cr minerals are not available in the EQ6 database at this time. The adsorption of

Mo(VI) on Fe oxides, Al oxides and smectites (like nontronites) is pH-dependent, reaching a maximum between pH 4 and 5 and then decreasing with increasing pH with very little adsorption above pH 8 (Goldberg et al. 1996). The adsorption process cannot be modeled with EQ6 at this time, but the ferrimolybdate, $Fe_2(MoO_4)_3$, added to the EQ6 database may also be the product of the reaction of iron oxides with Mo(VI) (Lindsay 2001, Chapter 22; Titley 1963). The total oxidation and release of soluble Cr, and to a lesser extent, Mo cause an unrealistically low pH and high ionic strength to be simulated during WP degradation, especially when high steel degradation rates and low drip rates are used. So, by suppressing hematite and goethite, and allowing the formation of $Fe(OH)_3$, Cr(VI)-ferrihydrite and $Fe_2(MoO_4)_3$ we are more realistically representing the chemistry of the WP solution and elemental composition of the degradation products.

Confirmation Status: Since this assumption results in a more realistic representation of WP corrosion product and WP solution compositions, and realistic or slightly elevated radionuclide release from the WP it is considered reasonable and does not require further verification.

Use within the Analysis: This assumption applies to Sections 5.16, 6.2, 6.3, 6.4 and 6.5.

5.5   SHORT-LIVED ISOTOPES

Assumption: It is assumed that the short-lived isotopes (those with half-lives less than 10,000 years) can be pre-decayed to their longer-lived daughter products and totaled by element for representation in EQ6.

Rationale: This assumption is conservative since the radionuclides of concern to performance assessment are generally the long-lived daughter products. It is also justified since the time to first WP breach is greater than 10,000 years (CRWMS M&O 2000b, Section 4.1.2).

Confirmation Status: Due to the reasonable conservatism of this assumption, in that it does not influence the radionuclides of concern, it does not require further verification.

Use within the Analysis: This assumption applies to Sections 4.1.2.5, 4.1.2.6 and 4.1.2.7.

5.6   INSOLUBLE METALS

Assumption: It is assumed that the drip shield (Ti Grade 7), the outer corrosion resistant barrier fabricated from Alloy 22, and the Zircaloy SNF cladding will have a negligible effect on the chemistry.

Rationale: These metals and alloys corrode very slowly compared to other WP materials and compared to the rate at which soluble corrosion products will be flushed from the WP, and thus would have a negligible effect on the chemistry (Estill 1998, and Hillner et.al. 1998).

Confirmation Status: This assumption does not require further verification because the effects on geochemistry would be small and would not significantly alter the results of these calculations.

Use within the Analysis: This assumption applies to Section 4.1.1.2.

5.7   SNF CLADDING

Assumption: The SNF cladding is initially assumed to be completely breached (allowing 100% of the fuel surface area to be exposed to degradation) to allow for damage that may occur during handling and transportation.

Rationale: This is very conservative in that it would allow the maximum dissolution of SNF and thus the maximum availability of radionuclides for transport from the WP.

Confirmation Status: Due to the increased conservatism of more radionuclides being available for release, this assumption does not require further verification.

Use within the Analysis: This assumption applies to Section 4.1.1.2.

5.8   VOID SPACE AND WATER COMPOSITION

Assumption: It is assumed that: (1) an aqueous solution fills all voids within WPs; (2) the solution that drips into the WP has the major ion composition of J-13 well water as given in DTN: MO0006J13WTRCM.000 for at least 100,000 years, and (3) addition of small amounts (1.0E-16 molal) of trace elements present in the WP to the EQ3NR input file used to calculate J-13 fluid speciation does not affect the nature or extent of the WP degradation pathway that is subsequently calculated using EQ6.

Rationale: The basis for the first part of this assumption is that it provides the maximum degradation rate with the potential for the fastest flushing of the radionuclides from the WP, and is thereby reasonably conservative.

For some of the cases examined in this analysis, the volume of remaining WP components and of corrosion products precipitated in the WP may nearly reach or exceed the volume of the voids in the WP before 100,000 years after WP breach. For the portions of these cases after the time when this occurs, this assumption is no longer reasonable. It is likely that some of the solids formed in the WP would leave the WP as suspended colloids, thus slowing the filling of the WP with corrosion products, but this cannot be modeled by EQ6 and is beyond the scope of this analysis. It is also likely that the rate of reactions within the WP, especially oxidation reactions which are controlled by the availability of $O_2(g)$, would decrease as WP components are separated from the aqueous phase by a thick layer of corrosion products. EQ6 simulations of these conditions have shown that U and Pu release from the WP would be greatly diminished (CRWMS M&O 2000f, Section 6.3).

The basis for the second part of the assumption is that the groundwater composition is controlled largely by transport through the host rock, over pathways of hundreds of meters, and the host rock composition is not expected to change substantially over one million years.

The basis for the third part of the assumption, is that EQ6 requires that a tangible amount of each element in a reaction path calculation be present in the aqueous phase at the start of a calculation (1.0E-16 molal).

Confirmation Status: Because this assumption provides the maximum degradation rate and the fastest flushing of radionuclides from the WP, the most likely major ion groundwater composition and the elemental aqueous composition necessary for EQ6 calculations it is reasonable, conservative and does not require further verification.

Use within the Analysis: This assumption applies to Section 4.1.2.4.

5.9   WATER CIRCULATION

Assumption: For the geochemical calculations (in Sections 4 and 6) it is assumed that the water circulates freely enough within the partially degraded WP that all of the WP components and degraded solid products may react with each other through the aqueous solution medium.
Rationale: The radioactive decay heat retained within the WP is expected to cause convective circulation and mixing of the water inside the WP (CRWMS M&O 1996, Attachment VI). Free circulation of water within the WP is reasonably conservative because it yields a greater opportunity for dissolution and removal of radionuclides from the WP. For some of the cases examined in this analysis, the volume of remaining WP components and of corrosion products precipitated in the WP may nearly reach or exceed the volume of the voids in the WP before 100,000 years after WP breach. For the portions of these cases after the time when this occurs, this assumption is no longer reasonable, since the WP solution would not be able to circulate freely. It is also likely that the rate of reactions within the WP, especially oxidation reactions which are controlled by the availability of $O_2(g)$, would decrease as WP components are separated from the aqueous phase by a thick layer of corrosion products. EQ6 simulations of these conditions have shown that U and Pu release from the WP would be greatly diminished (CRWMS M&O 2000f, Section 6.3).
Confirmation Status: Due to the reasonable conservatism of this assumption, and resulting greater release of radionuclides from the failed WP, it does not require further verification.
Use within the Analysis: This assumption applies to Sections 6.1 and 6.2.

5.10   ENTRY AND EGRESS OF WATER INTO WP

Assumption: It is assumed that the rate of entry of water into, and the rate of egress from, a WP equals the rate at which water drips onto the WP.
Rationale: For most of the time period of interest (i.e., after the WP barriers become largely degraded) it is more reasonable to presume that all of the drips enter the degraded WP than to presume that a significant portion will be diverted around the remains of the WP. This presumption yields the greatest release of radionuclides from the failed WP and is very conservative.
Confirmation Status: Due to this inherent conservatism (greater release of radionuclides) this assumption does not require further verification.
Use within the Analysis: This assumption applies to Sections 4.1.2.4 and 6.1.

5.11   THERMODYNAMIC DATABASE

Assumption: It is assumed that the $25^{o}C$ thermodynamic database data0.ymp.R0 (DTN MO0009THRMODYN.001) for use with the EQ3/6 computer package (EQ3/6, V. 7.2b, CSCI: UCRL-MA-110662) is sufficiently accurate for the purposes of this analysis.
Rationale: All of these data have been carefully scrutinized by many experts over the course of several decades and have been carefully selected for incorporation into the database (Spahiu and Bruno, 1995; Wolery 1992a; Wolery 1992b; Daveler and Wolery 1992; and Wolery and Daveler 1992). These databases are periodically updated and include references internally for the sources of the data. The reader is referred to this documentation, included in the electronic file labeled data0 that accompanies this analysis (see output DTN: MO0201SPAGIN07.001). The calculations represent geochemical reactions that occur at times greater than 10,000 years, which is after the thermal pulse has passed and WP temperatures are at or below, 100°C. The

justification for using 25°C thermodynamic data to model processes that might occur at somewhat higher temperatures is that many of the thermodynamic input parameters are not strongly sensitive to temperature over the range of 25 to 100°C.

Confirmation Status: Due to reasonable conservatism in this assumption and the previous reviews of these data no further verification is necessary.

Use within the Analysis: This assumption applies to Section 4.1.2.8.

5.12 GRAPHITE BLOCK IN FSV SNF ELEMENTS

Assumption: In the EQ6 calculations of the FSVR WPs, it is assumed that the graphite block which holds the fuel compacts in place will essentially be inert, so it was not included in the calculations except for use in calculations of volumes.

Rationale: The rationale for this assumption is that graphite degrades very slowly (Propp 1998). Over the time frame of interest for this analysis, the loss of graphite would be negligible, and thus it is reasonable to consider it to be inert.

Confirmation Status: Due to the small effect this assumption could have on the results of these calculations no further verification of this assumption is required.

Use within the Analysis: This assumption applies to Section 4.1.1.1.

5.13 COMPOSITION OF M&D INGOTS

Assumption: It is assumed that the Melt and Dilute ingot composition is about 18 wt % U [plus inventory average values of iodine (I), neptunium (Np), Pu, and technetium (Tc) (DOE 2001a, Attached electronic file; see Assumption 5.14)] about 0.5 wt% Gd with the balance of the ingot being Al. It is also assumed that the ingot has a 1 mm thick coating of A516 carbon steel.

Rationale: BSC (2001c, Section 3.2) suggests two possible general ingot compositions. The first contains 13.2 ± 5 wt% U, 0.5 wt% Gd, with the balance of the ingot Al. The second is 13.2 ± 5 wt% U, 0.5 wt% Gd, 2.5 wt% hafnium (Hf) and the rest Al. The M&D ingots may also contain up to 2 wt% silicon (Si) and 3 wt% calcium (Ca). The ingot has an optional A516 carbon steel crucible liner (ingot coating) up to 0.5 inches (13 mm) thick.

Sensitivity analyses have shown, however, that the addition of Hf, Si, and Ca to the ingot composition (BSC 2001b, Section 6.2.5), or varying the thickness of the ingot coating (BSC 2001b, Section 6.2.6) have little affect on U, Gd or Hf loss during EQ6 simulations of M&D WP degradation. Therefore, it is reasonable to assume a more limited ingot composition for the purposes of this analysis.

Confirmation status: The lack of influence of these assumptions on U, Gd or Hf losses removes the need for further confirmation.

Use within the Analysis: This assumption applies to Sections 4.1.1.3 and 4.1.2.7.

5.14 RADIONUCLIDE INVENTORIES

Assumption: The radionuclide inventories assumed in the simulations for Group 5 (FSV), Group 7 (N-Reactor), and Group 9 (M&D) DOE SNF are considered appropriate.

Rationale: The radionuclide inventories used in this Analysis are appropriate because they are the most up to date and the best available technical information provided by the DOE (2001a, Attached electronic file). DOE 2001a is the latest version of DOE 1999 (attached electronic file) which has been used as a source for the radionuclide inventory of DOE SNF throughout the Yucca Mountain Site Characterization project (CRWMS M&O 2000d, Sections 2.2 and 3.1;

BSC 2001e, Sections 5.3.6, 6.1.2, 6.2.2, 6.3.2 and Table 5.3-9; BSC 2001h, Tables 5.2-2 and III-1).

Confirmation Status: This assumption is based on the best available technical information consistent with its use throughout the Yucca Mountain Site Characterization project and no further confirmation is required.

Use within the Analysis: This assumption applies to Sections 4.1.2.5, 4.1.2.6, 4.1.2.7, 6.2, 6.3.1, 6.4.1, 6.4.5, and 6.5.1.

5.15   HLW GLASS COMPOSITION

Assumption: The HLW glass composition is assumed to be the same as that produced at Savannah River (CRWMS M&O 1999a, Attachment I) and the radionuclide inventory is assumed to be that of the Savannah River inventory abstraction (BSC 2001k, Table I-7).

Rationale: The references cited above are the most recent and comprehensive sources available to provide this information. CRWMS M&O 1999a has been used as a source for the HLW glass composition throughout the Yucca Mountain Site Characterization project (CRWMS M&O 1999b, Table 5-2; BSC 2001a, Table 5-3; BSC 2001b, Table 5). BSC 2001k (Table I-7) is the latest version of BSC 2001j (Table I-7) and CRWMS M&O 2000e (Table 34) which have been used as sources for the radionuclide inventory in HLW across the Yucca Mountain Site Characterization project (BSC 2001e, Section 5.3.3, Table 5.3.5, Assumption 3.15; BSC 2001h, Section 5.2.2, Table 5.2.3, Assumption 3.2; BSC 2001i, Section 6.4; CRWMS M&O 2001b, Sections 4, 4.1, Table 4.12, Assumption 5.2, Section 6.3.2; DOE 2001b, Section 4.2.6.3.9, Table 4-23)

Confirmation Status: The composition of HLW glass and its radionuclide inventory abstraction are from corroborative technical products that have been used for this information throughout the Yucca Mountain Site Characterization project such that no further confirmation is needed.

Use within the Analysis: This assumption applies to Sections 4.1.2.3 and 4.1.2.10.

5.16   CHANGES TO THE THERMODYNAMIC DATABASE

Assumption: It is assumed that minor changes to the 25°C thermodynamic database data0.ymp.R0 (DTN MO0009THRMODYN.001) for use with EQ3/6 will not compromise the results of the EQ6 simulations.

Rationale: Several reactants, i.e., WP components, were added to the database (See Section 4.1.2.8) to facilitate the use of pH dependent kinetic rate laws. All of these reactants were assigned large solubilities to prevent their formation via precipitation reactions.

A Gd compound, $GdOHCO_3$ was added to the database with an assumed log K value identical to the Nd compound, $NdOHCO_3$, in data0.ymp.R0 (DTN MO0009THRMODYN.001). Since Gd and Nd are both lanthanides, with similar chemical behavior, this assumption is reasonable.

Also, the log K of the soluble species, $GdHPO_4^+$, was found to be incorrect in data0.ymp.R0 (DTN MO0009THRMODYN.001) and was changed from the value of 185 to -5.7 to match the value given in Spahiu and Bruno (1995), the source listed in the database for that reaction.

Additionally, a series of Cr- and Mo-bearing mineral phases were added to the database (BSC 2001d, Assumption 5.2) because the database (data0.ymp.R0 DTN MO0009THRMODYN.001) lacked Cr and Mo phases that were favored to form under the simulated conditions (See Assumption 5.4). Dissolution of Mo- and Cr-rich steel alloys in the EQ6 simulations (Section 6) require mineral phases to function as a sink for excess aqueous Cr and Mo, otherwise the

solution would become unrealistically concentrated with respect to these elements. This is especially true for cases with high steel degradation rates.

Confirmation Status: Due to the necessity of using pH dependent rate laws for the dissolution of WP components, the chemical similarity of Gd and Nd, the corroborative evidence for the correction of the log K value for $GdHPO_4^+$, and the lack of sufficient Cr- and Mo-bearing phases in data0.ymp.R0 (DTN MO0009THRMODYN.001) the assumption of these minor changes in the database will lead to more logical results from the EQ6 simulations, and therefore, they require no further confirmation.

Use within the Analysis: This assumption applies to Sections 4.1.2.8 and 6.2.

6. SCIENTIFIC ANALYSIS DISCUSSION

6.1 APPROACH

The calculations begin with selection of data for compositions, amounts, surface areas, and reaction rates of the various components of the three DOE SNF WPs. These quantities are converted to the form required for input suitable for EQ3/6. Spreadsheets (output DTN: MO0201SPAGIN07.001) detail the reduction of each WP component to input units and format. The final part of the input consists of the composition and inflow rate of J-13 well water entering the WP. The analysis itself involves the following steps:

- Use of the basic EQ3/6 software package described in Section 3 to trace the progress of reactions with evolution of the chemistry, including the estimation of the concentrations remaining in solution and the composition of the precipitated solids. EQ3NR is used to determine a starting fluid composition for the EQ6 calculations; it does not simulate reaction progress.

- Use of SCFT mode in EQ6; in this mode, an increment of aqueous "feed" solution is added continuously to the WP system, and a like volume of the existing solution is removed, simulating a continuously-stirred tank reactor (see Assumptions 5.9 and 5.10). This mode is discussed in Section 3 (LSCR198. CRWMS M&O 1999c).

- Determination of radionuclide aqueous concentrations as a function of time (from the output of EQ6 simulated reaction times up to 100,000 years).

- Determination of the composition and amounts of solids (precipitated minerals or corrosion products) and the amounts of unreacted WP materials.

In this analysis EQ3/6 was used to provide:

- A general overview of the nature of chemical reactions to be expected,

- The degradation and precipitation products likely to result from corrosion of the waste forms, fuels and canisters, and

- An indication of the aqueous concentration of radionuclides versus time.

The details of the spreadsheet manipulations, summary data for material compositions, and degradation/infiltration rates are presented in output DTN: MO0201SPAGIN07.001. The details of the calculation and the nomenclature for each run are described in Section 6.2.

6.2 EQ6 CALCULATIONS AND SCENARIOS REPRESENTED

The EQ6 cases evaluated in this Analysis are selected to explore extreme pH conditions and the geochemical sensitivity to different degradation scenarios represented by eight cases. In general, each case could be classified as a single or multiple-stage run. For a single-stage run all of the WP contents within the Alloy-22 outer shell are exposed to water as soon as the Alloy-22 shell is breached. Thus a single-stage simulation assumes that all the WP contents inside the Alloy-22

shell are exposed to water simultaneously (see Assumption 5.9). In contrast, for a multiple-stage run the WP contents are exposed in a sequence, as the containers within the WP fail. One multiple-stage run of particular interest to criticality is the two-stage run, where the DOE SNF canister is the last WP component to fail. This represents an extreme scenario for the WP chemistry, since it removes all of the HLW glass (and associated glass alkalinity) prior to exposure of the SNF (Sections 6.3.6, 6.4.6, and 6.5.6). This Analysis includes both single and two-stage cases in the modeled scenarios for each fuel.

- Case 0 is a special sensitivity run with a fuel-specific scenario.

- Case 1 is the criticality case with a scenario based on previous internal criticality calculations of FSV SNF (BSC 2001a, Sections 5 and 6), N-Reactor SNF (CRWMS M&O 2001a, Sections 5 and 6), and the M&D waste form (BSC 2001b, Sections 5 and 6).

- Case 2 is the Base Case scenario for each fuel, consisting of a single-stage simulation with low rates of corrosion, dissolution, and average drip rate, with the inventory average compositions and average SNF load (see Assumption 5.14). Case 2 also uses the O_2 and CO_2 fugacities described in Assumption 5.3 and a slightly modified version of the data0.ymp database (see Assumption 5.16 and Section 4.1.2.8). Case 2 thus forms the reference case for comparisons to the remaining cases.

- Case 3 evaluates WP geochemistry for high steel and glass corrosion rates and low drip rates, such as might be found under high temperature conditions.

- Case 4 evaluates the impact of allowing hematite to form under the same conditions as the Base Case (Case2). Since hematite and goethite are thermodynamically more stable than $Fe_2(MoO_4)_3$, $Fe(OH)_3$ or Cr-ferrihydrite, either hematite or goethite will be the only iron oxide that forms during an EQ6 run, unless their precipitation is suppressed (see Assumption 5.4). However, it is likely that solids like $Fe_2(MoO_4)_3$, $Fe(OH)_3$ or Cr-ferrihydrite along with a mixture of iron oxides would form during steel degradation (see Assumption 5.4). For this case, neither hematite nor goethite was suppressed, which is similar to the Base Case runs in a previous calculation (BSC 2001e, Section 6).

The remaining cases (Cases 5, 6 and 7) evaluate the WP geochemistry under conditions that might produce extreme pH and radionuclide loss.

- Case 5 examines the effects of a two-stage simulation (degrading the HLW glass completely before allowing the contents of the DOE SNF canister, or of the MCOs, for N Reactor SNF, to degrade). This type of case may be more realistic than the single stage cases in which all of the WP components are exposed to degradation simultaneously.

- Case 6 evaluates the impact of reducing the O_2 fugacity, such as might occur if corrosion products restrict air circulation in the WP.

- Case 7 examines the case of high rates of corrosion and average drip rates.

Tables 10, 11, and 12 summarize the cases and the associated conditions simulated for the three SNF groups. The "Root File Names" column in these tables provides the root file names used to describe the runs. Several input files, corresponding to separate EQ6 runs, may be grouped into a "Case". The most important run conditions can be inferred from the root file name. Typically, EQ6 input/output file names follow a convention that will tell you approximately the scenario being evaluated. The format is: f#va1234, where:

f = Corresponds to the fuel type: v = FSV, r = N Reactor, m = M&D.

= Corresponds to the Case, with 2 = the base case.

v = Version number (if applicable).

a = The stage of the simulation (if the simulation is broken into sections for numerical stability or to simulate more complex histories).

1 = The steel corrosion rate, 1 = low and 2 = high.

2 = The glass corrosion rate, 1 = low and 2 = high.

3 = The fuel corrosion rate, 1 = best estimate and 2 = conservative. (For the FSV fuel, 2 = 1% of fuel moles and surface area at the conservative rate and 99% of fuel moles and surface area at the best estimate rate, while 3 = the conservative rate.)

4 = The J-13 drip rate, 2 = 2 × maximum current dry climate (~20 mm/yr), 3 = 2 × maximum glacial transition climate (~80 mm/yr), and 4 = ~100 mm/yr.

For example, FSV Case 2 has file names of the form: v21a1113.*, which represents low rates of corrosion and 2 × the maximum glacial transition drip rate.

Table 10. Calculation Cases for FSV SNF (Group 5)

Case and Objective	Root File Name(s)	Metals	Glass[b]	Fuel Loading	Water Flow Rate
Case 0: Base Case With 1% damaged fuel With 4 fuel elements in WP[a]	V02a1113 V02b1113	Low rates: 304/316L: 0.1 μm/yr A516: 72 μm/yr	Low rate	Inventory average in 4 elements 1% Conservative rate (10X U-metal) 99% Best estimate rate (SiC rate)	80 mm/yr (0.15 m^3/yr) l
Case 1: Criticality case[a] With 5 fuel elements in WP	V12a1113 V12b1113	As above	As above	Fresh FSV fuel in 5 elements, high fissile content with no Pu,Np,Tc,I Best estimate rate (SiC rate)	As above
Case 2: Base Case[a] With 4 fuel elements in WP	V22a1113 V22b1113	As above	As above	Inventory average in 4 elements, Best estimate rate (SiC rate)	As above
Case 3: Worst case[a]: High rates, low flow With 4 fuel elements in WP	V36a2232	High rates: 304L: 34 μm/yr 316L: 2.0 μm/yr A516: 72 μm/yr	High rate	Inventory average in 4 elements, Conservative rate (10X U-metal)	20 mm/yr (0.015 m^3/yr)
Case 4: Base Case with hematite and goethite not suppressed With 4 fuel elements in WP	V42a1113	VA best est. rates: 304/316L: 0.1 μm/yr A516: 72 μm/yr	Low rate	Inventory average in 4 elements, Best estimate rate (SiC rate)	80 mm/yr (0.15 m^3/yr) l
Case 5: Base Case as two-stage[a] (DOE Canister contents untouched until HLW glass is degraded) With 4 fuel elements in WP	V52a2204 V52b2204 V52c1012	1st stage: High rates 2nd stage: Low rates	High rate	2nd stage: Inventory average in 4 elements, Best estimate rate (SiC rate)	1st stage: 100 mm/yr (0.5 m^3/yr) 2nd stage: 20 mm/yr 0.015 m^3/yr
Case 6: Base Case[a] With low fO$_2$ With 4 fuel elements in WP	V62a1113 V62b1113	Low rates: 304/316L: 0.1 μm/yr A516: 72 μm/yr	Low rate	Inventory average in 4 elements, Best estimate rate (SiC rate)	80 mm/yr (0.15 m^3/yr) l
Case 7: Base Case[a] + high rates, avg. flow With 4 fuel elements in WP	V72a2233	High rates: 304L: 34 μm/yr 316L: 2.0 μm/yr A516: 72 μm/yr	High rate	Inventory average in 4 elements, Conservative rate (10X U-metal)	As above

NOTES: [a]Suppresses the minerals, hematite, goethite, soddyite, thorianite and PuO$_2$, but includes molybdate and chromate phases.

Table 11. Calculation Cases for N Reactor SNF (Group 7)

Case and Objective	Root File Name(s)	Metals	Glass[b]	Fuel Loading	Water Flow Rate
Case 0: Base Case With 4 MCOs and no GPCs in WP[a]	R02a1013	Low rates: 304/316L: 0.1 μm/yr A516: 72 μm/yr	No HLW glass	Inventory average in 4 MCOs, Best estimate rate (5X U-metal)	80 mm/yr (0.15 m^3/yr) l
Case 1: Criticality case[a]	R12a1113 R12b1113	As above	2 GPCs Low rate	Fresh Mark IA fuel in 2 MCOs, high fissile content with no Pu,Np,Tc,I Best estimate rate (5X U-metal)	As above
Case 2: Base Case[a]	R22a1113	As above	As above	Inventory average in 2 MCOs, Best estimate rate (5X U-metal)	As above
Case 3: Worst case: High rates, low flow[a]	R32a2222 R32b2222 R32c2222	HIgh rates: 304L (34 μm/yr) 316L (2.0 μm/yr); A516 (72 μm/yr)	2 GPCs High rate	Inventory average in 2 MCOs, Conservative rate (25X U-metal)	20 mm/yr (0.015 m^3/yr)
Case 4: Base Case with hematite and goethite not suppressed	R42a1113 R42b1113 R42c1113	Low rates: 304/316L: 0.1 μm/yr A516: 72 μm/yr	2 GPCs Low rate	Inventory average in 2 MCOs, Best estimate rate (5X U-metal)	80 mm/yr (0.15 m^3/yr) l
Case 5: Base Case as two-stage[a] (MCOs untouched until HLW is gone)	R52a2204 R52b2204 R52c2204 R52d2204 R52e1012	1st stage: High rates\n\n2nd stage: Low rates	2 GPCs 1st stage: High rate (until gone)	2nd stage: Inventory average in 2 MCOs, Best estimate rate (5X U-metal)	1st stage: 100 mm/yr (0.5 m^3/yr)\n\n2nd stage: 20 mm/yr 0.015 m^3/yr
Case 6: Base Case[a] + low fO$_2$	R62a1113	Low rates: 304/316L (0.1 μm/yr); A516: (72 μm/yr)	2 GPCs Low rate	Inventory average in 2 MCOs, Best estimate rate (5X U-metal)	80 mm/yr (0.15 m^3/yr) l
Case 7: Base Case[a] + high rates, avg. flow	R72a2223 R72b2223 R72c2223 R72d2223	High rates: 304L: 34 μm/yr 316L: 2.0 μm/yr A516: 72 μm/yr	2 GPCs High rate	Inventory average in 2 MCOs, Conservative rate (25X U-metal)	As above

NOTES: [a]Suppresses the minerals, hematite, goethite, soddyite and PuO$_2$; but includes molybdate and chromate phases.

Table 12. Calculation Cases for M&D Waste Form (Group 9)

Case and Objective	Root File Name(s)	Metals	Glass[b]	Fuel Loading	Water Flow Rate
Case 0: Base Case + Ingot surface area X 10[a]	M01a1113 M01b1113	Low rates: 304/316L: 0.1 μm/yr A516: 72 μm/yr	Low rate	Inventory average in 1 M-D ingot Ingot surface area X 10; Best estimate rate (0.22 mg U/m^2 day)	80 mm/yr (0.15 m^3/yr) l
Case 1: Criticality case[a]	M11a1113	As above	As above	5 M-D ingots, high fissile content with no Pu, Np, Tc, or I; Best estimate rate (0.22 mg U/m^{2}d)	As above
Case 2: Base Case[a]	M21a1113	As above	As above	Inventory average in 1 M-D ingot, Best estimate rate (0.22 mg U/m^{2}d)	As above
Case 3: Worst case: High rates, low flow[a]	M31a2222	High rates: 304L: 34 μm/yr 316L: 2.0 μm/yr A516: 72 μm/yr	High rate	Inventory average in 1 M-D ingot, Conservative rate (2 mils/year)	20 mm/yr (0.015 m^3/yr)
Case 4: Base Case with hematite and goethite not suppressed[b]	M41a1113	Low rates: 304/316L: 0.1 μm/yr A516: 72 μm/yr	Low rate	Inventory average in 1 M-D ingot, Best estimate rate (0.22 mg U/m^{2}d)	80 mm/yr (0.15 m^3/yr) l
Case 5: Base Case as two-stage[a] (DOE Canister untouched until HLW gone)[c]	M51a2204 M51b1012	1st stage: High rates 2nd stage: Low rates	High rate	In 2nd stage: Inventory average in 1 M-D ingot, Best estimate rate (0.22 mg U/m^{2}d)	1st stage: 100 mm/yr (0.5 m^3/yr) 2nd stage: 20 mm/yr 0.015 m^3/yr
Case 6: Base Case[a] + low fO$_2$	M61a1113	Low rates: 304/316L: 0.1 μm/yr A516: 72 μm/yr	Low rate	Inventory average in 1 M-D ingot, Best estimate rate (0.22 mg U/m^{2}d)	80 mm/yr (0.15 m^3/yr) l
Case 7: Base Case[a] + High rates, avg. flow	M71a2223	High rates: 304L: 34 μm/yr 316L: 2.0 μm/yr A516: 72 μm/yr	High rate	Inventory average in 1 M-D ingot, Conservative rate (2 mils/year)	As above

NOTES: [a]Suppresses: hematite, goethite, soddyite and PuO$_2$; includes added chromate and molybdate phases
[b]Suppresses the minerals soddyite and PuO$_2$; but not hematite or goethite which effectively excludes added chromate and molybdate phases.

6.3   FORT SAINT VRAIN SNF

Table 13 presents the summary of results for the FSV SNF calculations, summarized by the pH range, the maximum ionic strength, and the percentages of key radionuclides retained in the WP at the end of the simulation (~100,000 years after WP breach). The complete output tables (aqueous, mineral, and total moles) for all the cases are included in the files associated with this Analysis (output DTN: MO0201SPAGIN07.001).

Table 13. Results Summary for FSV SNF (Group 5)

Case and Objective	EQ6 File Name(*.6i)	Percent of initial moles retained in WP						pH Range		Max. Log Ionic Strength
		U	Pu	Np	I	Tc	Th	Min.	Max.	
Case 0: Base Case with 99% intact and 1% damaged fuel[b]	V02a1113 V02b1113	69.24	69.30	67.09	66.67	68.44	94.38	5.69	8.20	-2.00
Case 1: Criticality case[b]	V12a1113 V12b1113	69.31	69.32	69.32	69.32	69.32	95.33	5.69	8.20	-2.00
Case 2: Base Case[b]	V22a1113 V22b1113	69.25	69.30	67.27	66.88	68.51	94.37	5.69	8.20	-2.00
Case 3: Worst case: High rates, low flow[b]	V36a2232	0.00	0.00	0.00	0.00	0.00	0.00	4.06	9.71	-0.07
Case 4: Base Case sensitivity to hematite formation[a]	V42a1113	90.02	72.58	69.62	69.06	71.44	97.69	5.29	8.15	-1.76
Case 5: Base Case as two-stage[b] (DOE SNF canister unbreached until HLW is gone)	V52a2204 V52b2204 V52c1012	0.69	0.18	20.83	24.72	8.16	99.90	6.45	8.63	-1.90
Case 6: Base Case[b] + low fO$_2$	V62a1113 V62b1113	69.52	76.92	98.77	67.07	68.76	94.53	5.67	8.18	-1.99
Case 7: Base Case[b] + high rates, avg. flow	V72a2233	0.00	0.00	0.00	0.00	0.00	92.60	4.43	9.08	-1.15

NOTES: [a]Suppresses the minerals soddyite, thorianite and PuO$_2$; Cr and Mo phases do not form without hematite and goethite suppression

[b]Suppresses the minerals, hematite, goethite, soddyite, thorianite and PuO$_2$; but includes Cr and Mo phases.

For some of the FSV SNF cases examined in this analysis, the volume of remaining WP components and of corrosion products precipitated in the WP nearly reaches the volume of the WP before 100,000 years after WP breach. Table 14 presents the years after WP breach when the volume of the WP would be at least 2/3 full of solids and also the percentage of the WP volume filled with solids at the end of each FSV SNF case. For the portions of these cases after the time when the WP is about 2/3 full of solids Assumptions 5.8 and 5.9 may no longer be reasonable. On the other hand, the degradation rates of WP components would probably decrease if a thick layer of WP corrosion products separates them from the WP solution (See

discussion in Assumptions 5.8 and 5.9) and this would also slow the production of corrosion products.

Table 14 shows that the WP is not predicted to be totally filled with solids for any of the FSV SNF cases. For the cases with high degradation rates (Cases 3, 5 and 7) the WP is predicted to be nearly full of solids by ~100,000 years after WP breach. For all of the cases except Cases 4 and 6, the WP is predicted to be at least 2/3 full of solids before 100 years after WP breach. In Case 4, the WP volume is only slightly more than 2/3 filled at the end of the run. This is probably due mostly to the formation of hematite in this run instead of the Cr-ferrihydrite and $Fe(OH)_3$ which are allowed to form in all the other cases. The molar volume of hematite is smaller (30.274 cm^3/mole) than that of Cr-ferrihydrite (129 cm^3/mole) or $Fe(OH)_3$ (34.36 cm^3/mole) (file data0.trc in output DTN: MO0201SPAGIN07.001). The lower pH values predicted to occur during Case 4 (Figure 3) may also destabilize some of the corrosion product solids that would otherwise form in the WP. The less rapid filling of the WP during Case 6 is probably due to the instability of some of the corrosion product solids in the slightly reducing environment caused by the lower $O_2(g)$ concentration used throughout this run.

Table 14. WP Volume Summary for FSV SNF (Group 5)

Case	% WP Volume Filled with Solids	Years After WP Breach	% WP Volume Filled with Solids	Years After WP Breach
Case 0	70.5	77	85.3	100010
Case 1	69.4	69	85.3	100010
Case 2	69.3	69	85.3	100010
Case 3	68.5	53	95.4	100050
Case 4	66.0	12261	68.9	100010
Case 5	72.7	74	96.8	100030
Case 6	66.0	3744	79.7	100010
Case 7	65.1	34	96.3	100010

Figures 3 to 9 show the predicted variation of pH and WP solution concentrations of I, Np, Pu, Tc, Th and U during all of the FSV SNF cases. Differences in radionuclide concentrations in the WP solution between the cases are dependent on several variables, some of which are: the degradation rates of the WP components; the J-13 drip rate; the solubilities of solid corrosion products; and the pH of the WP solution. These differences will be discussed on a case by case basis in the following sections.
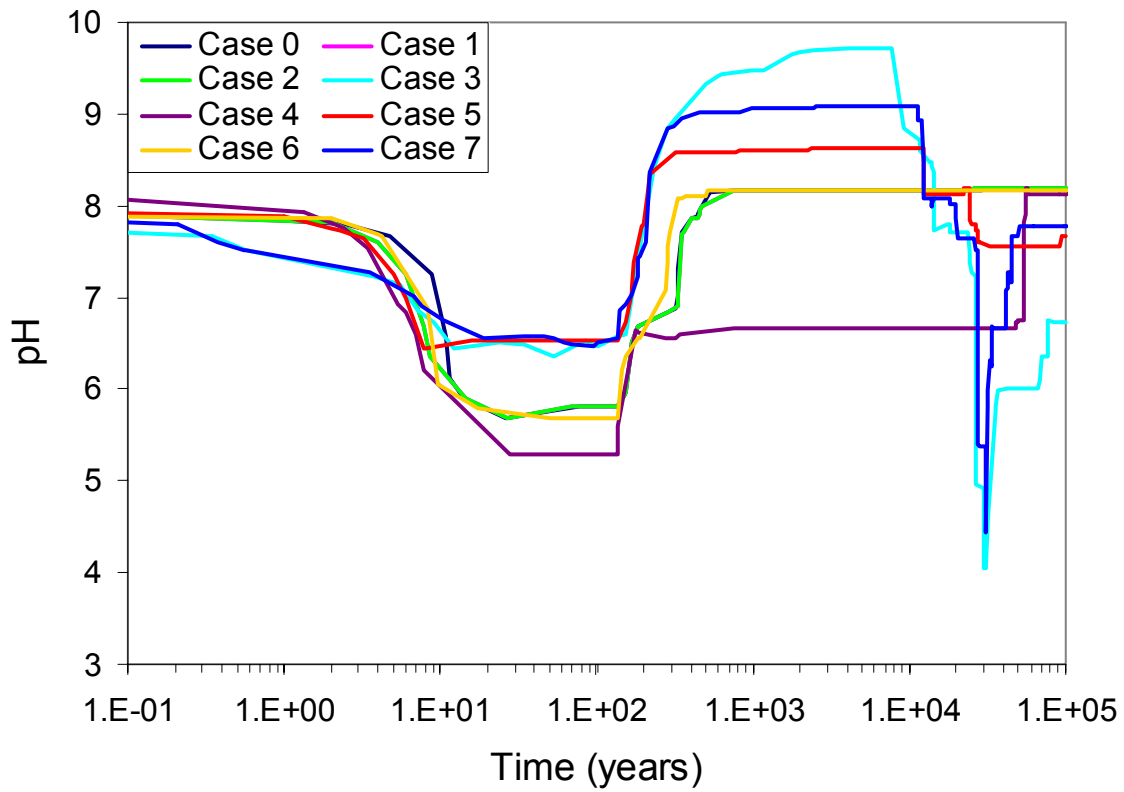
Output DTN: MO0201SPAGIN07.001

Figure 3. pH for FSV SNF Cases
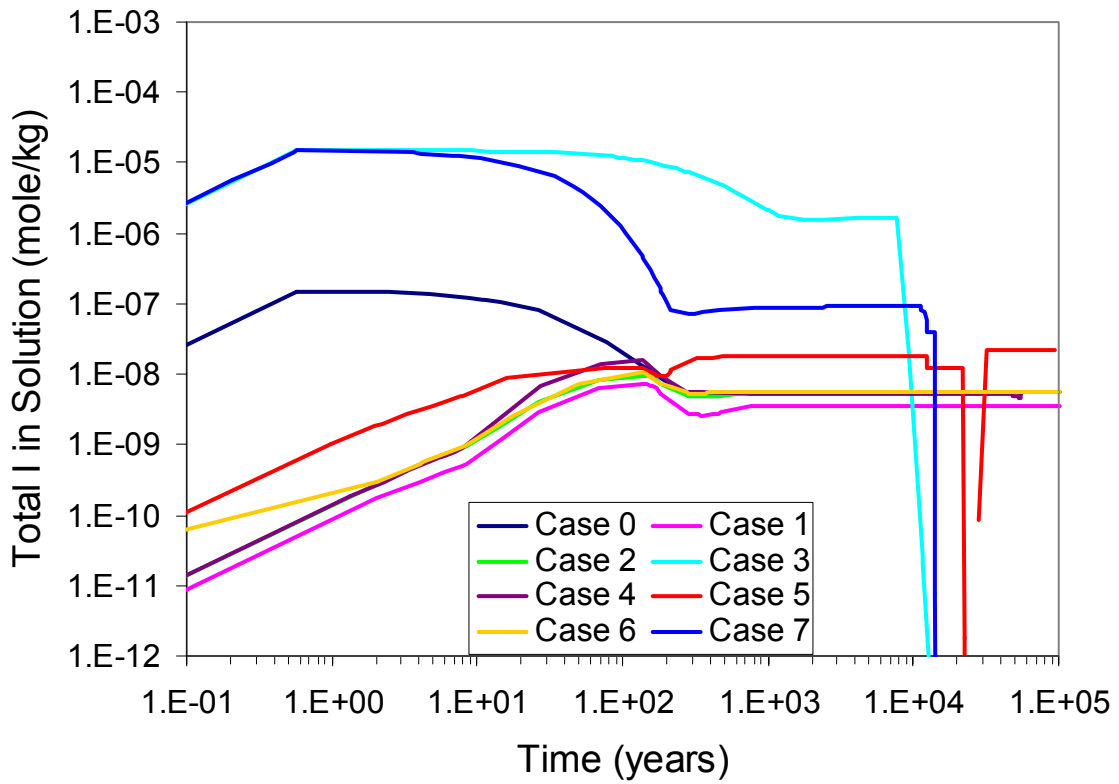
Output DTN: MO0201SPAGIN07.001

Figure 4. Total I in Solution During FSV SNF Cases
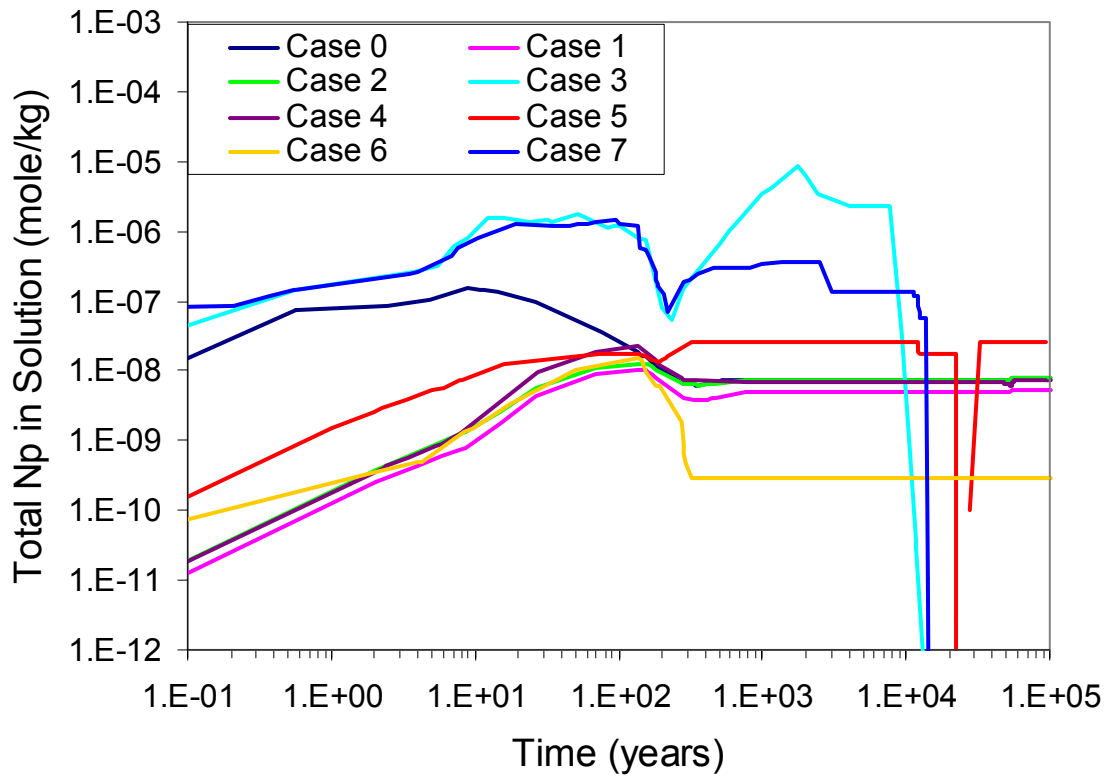
Output DTN: MO0201SPAGIN07.001

Figure 5. Total Np in Solution During FSV SNF Cases
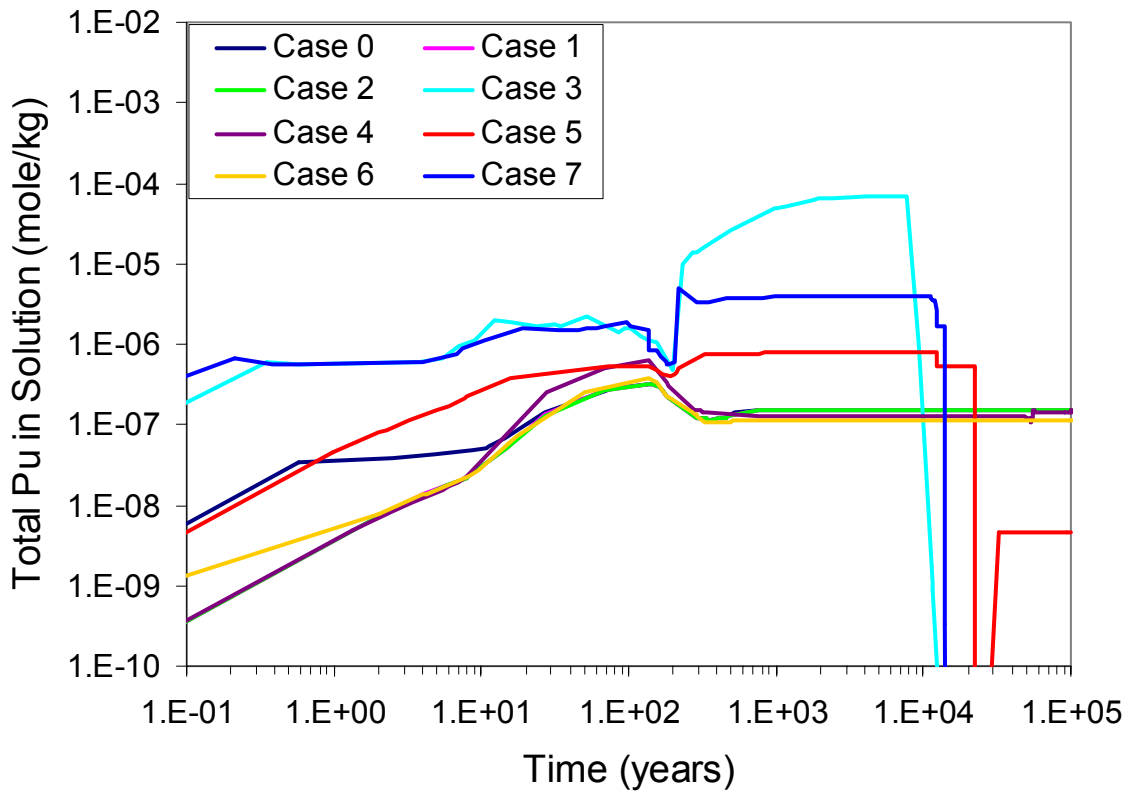
Output DTN: MO0201SPAGIN07.001

Figure 6. Total Pu in Solution During FSV SNF Cases
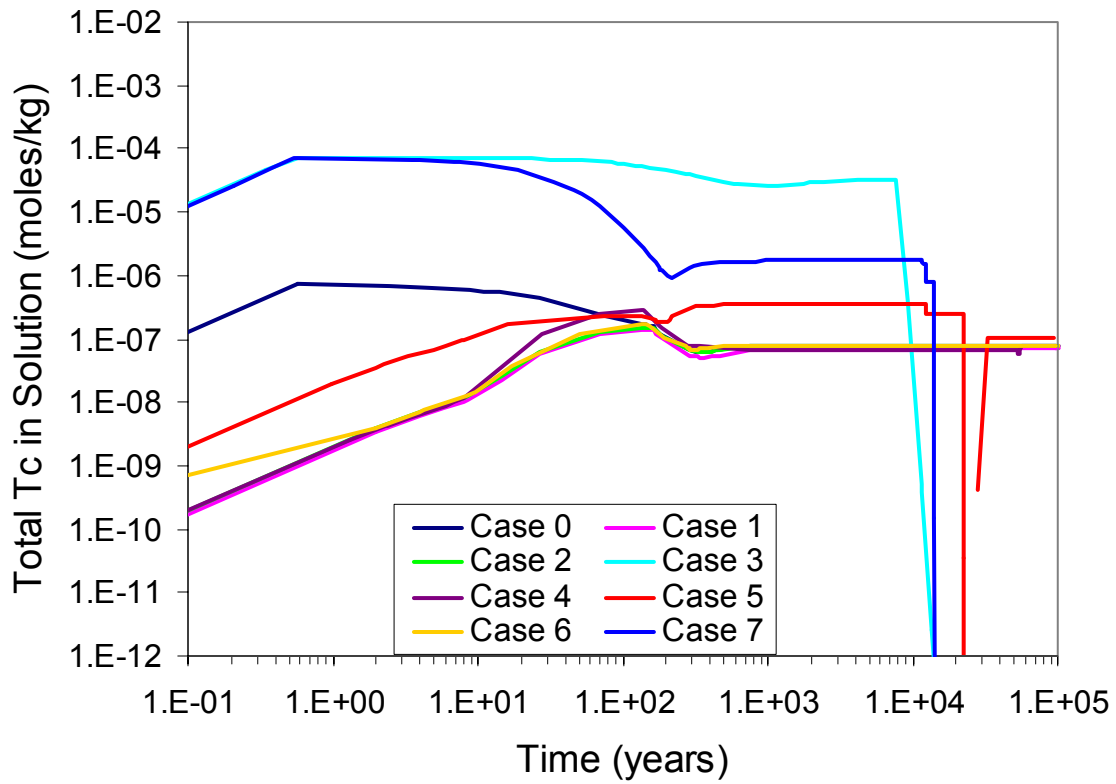
Output DTN: MO0201SPAGIN07.001

Figure 7. Total Tc in Solution During FSV SNF Cases
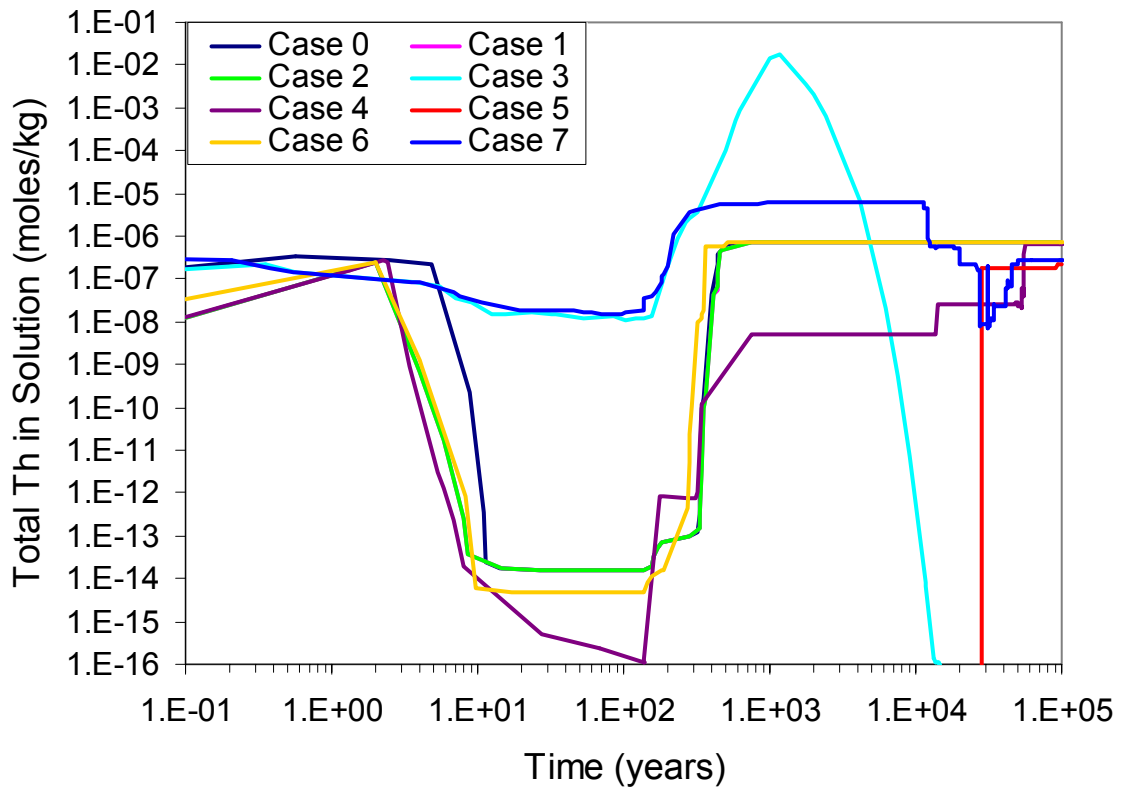
Output DTN: MO0201SPAGIN07.001

Figure 8. Total Th in Solution During FSV SNF Cases
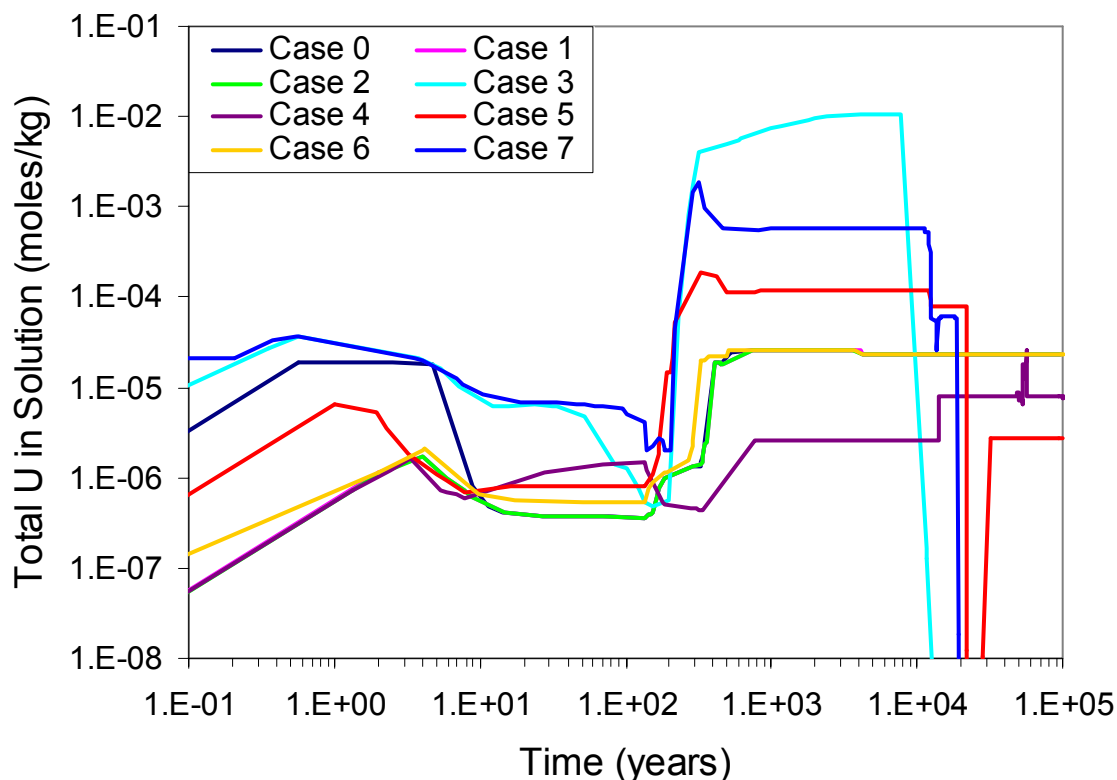
Output DTN: MO0201SPAGIN07.001

Figure 9. Total U in Solution During FSV SNF Cases

6.3.1   Base Case (Case 2)

The Base Case is a single-stage simulation that examines WP chemistry under moderate rates of corrosion and dissolution, with the expected CO_2 and O_2 fugacities and an 80 mm/year infiltration rate. In this case, the DOE SNF is assumed (see Assumption 5.14) to consist of the average composition and mass of FSV in the DOE SNF inventory (DOE 2001a, Attached Electronic File) which was equivalent to about 4 FSV fuel elements per WP.

Figure 10 shows the degradation of WP components and pH versus time from WP breach of the Base Case simulation. The pH response at early times is dominated by the corrosion of the A516 carbon steel, dropping to a minimum of 5.69 and remaining below 6 until the A516 is finally exhausted. After the A516 carbon steel is exhausted, the pH rises and nearly reaches the maximum value of 8.2 at about 1000 years after WP breach.
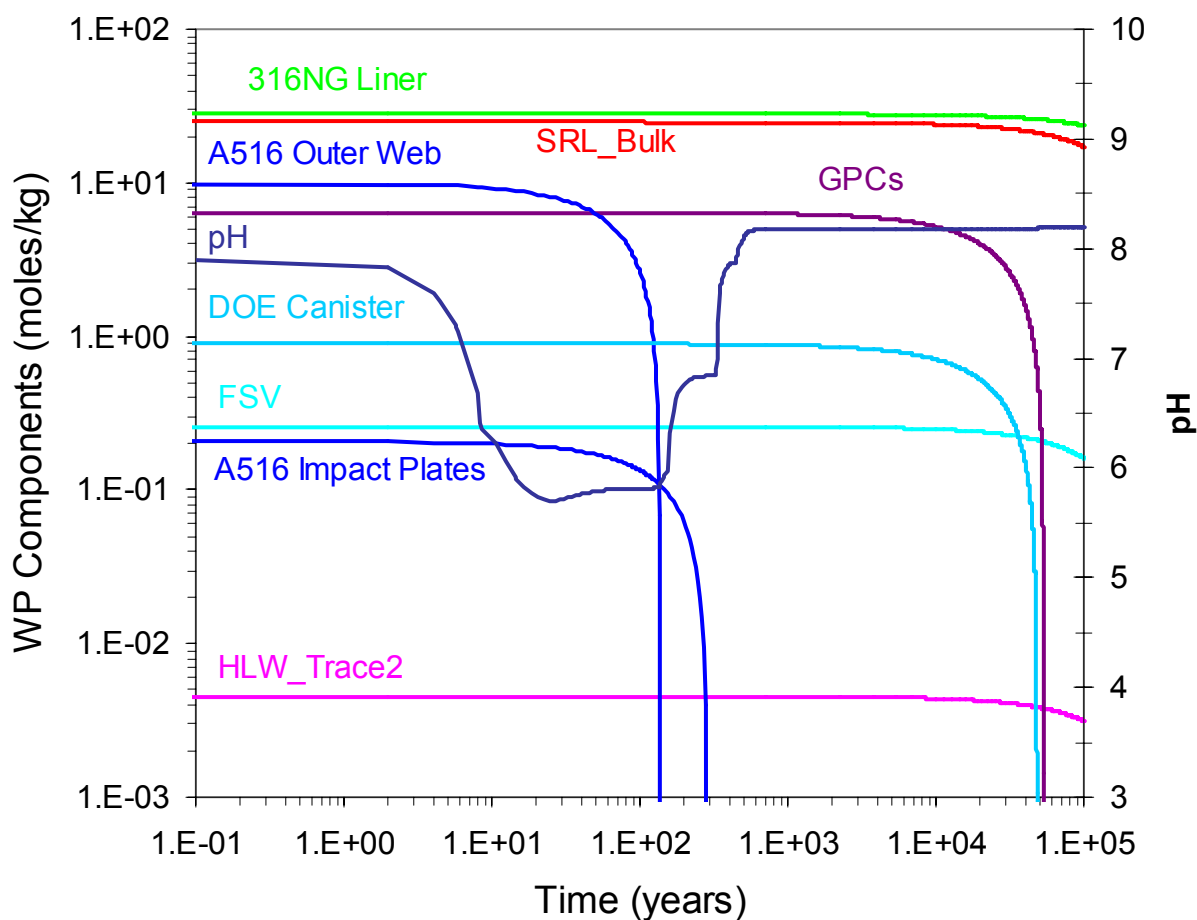
Output DTN: MO0201SPAGIN07.001
Figure 10. WP Components and pH for FSV SNF Case 2

Figure 11 presents the radionuclide minerals precipitating in this simulation, that control the aqueous solubility of the radionuclides of interest (Figures 4 to 9) and pH versus time from WP breach. The most insoluble Pu and Th minerals (Pu oxide and thorianite) were suppressed (see Assumption 5.4). The dominant U minerals are U phosphate $((UO_2)_3(PO_4)_2 \cdot 6H_2O)$ and Na-boltwoodite $(NaUO_2SiO_3OH \cdot 1.5H_2O)$. Thorium solubility is controlled by formation of $Th_{0.75}PO_4$ and amorphous ThO_2. Table 13 shows that 66 to 70% of the I, Np, Pu, Tc and U are retained in the partially degraded HLW glass and SNF with the exception of U which is also retained in precipitated minerals. Nearly all of the Th (94%) is retained in the WP as partially degraded FSV SNF and as precipitated Th minerals.

Note that no I, Np, Pu or Tc minerals form, thus these elements are not solubility limited and their aqueous concentrations are controlled by the degradation rates of the HLW glass and the SNF. The HLW glass rate is pH-dependent, thus the aqueous concentrations of elements found in the HLW vary with pH. This appears to be true for the predicted WP solution concentrations of I, Np, Pu and Tc which all increase during the early period of low pH and then decrease and level off as the pH rises to a plateau at 8.2 (Figures 4 through 7).
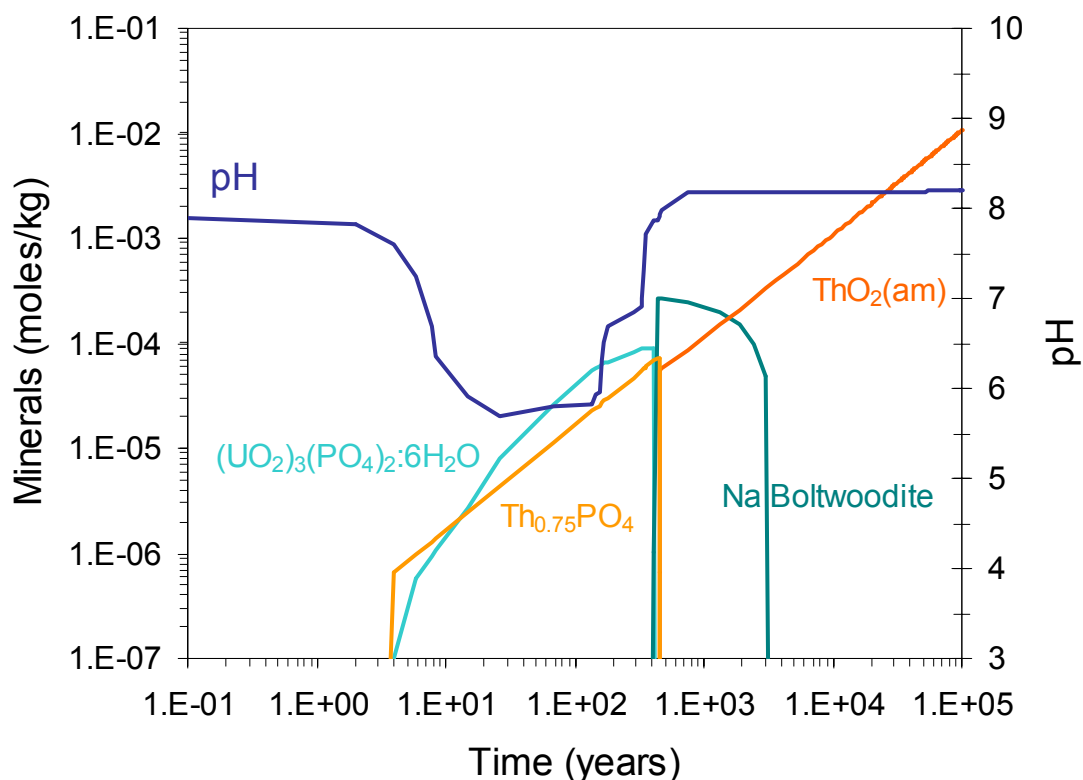
Output DTN: MO0201SPAGIN07.001

Figure 11. Radionuclide Mineral Formation During FSV SNF WP Degradation in Case 2

Figure 12 presents the major non-radionuclide minerals precipitating during this simulation. Information about the minor minerals which formed during Case 2 is available in the "*.min_info.txt" files in the output DTN: MO0201SPAGIN07.001. The major corrosion product sinks of the metals from steel degradation are $Fe(OH)_3$, Cr-ferrihydrite, trevorite ($NiFe_2O_4$), and pyrolusite (MnO_2). Chalcedony is the major sink for Si from HLW glass degradation. The nontronites are Fe-rich smectites which are a corrosion product of both HLW glass and steel degradation.
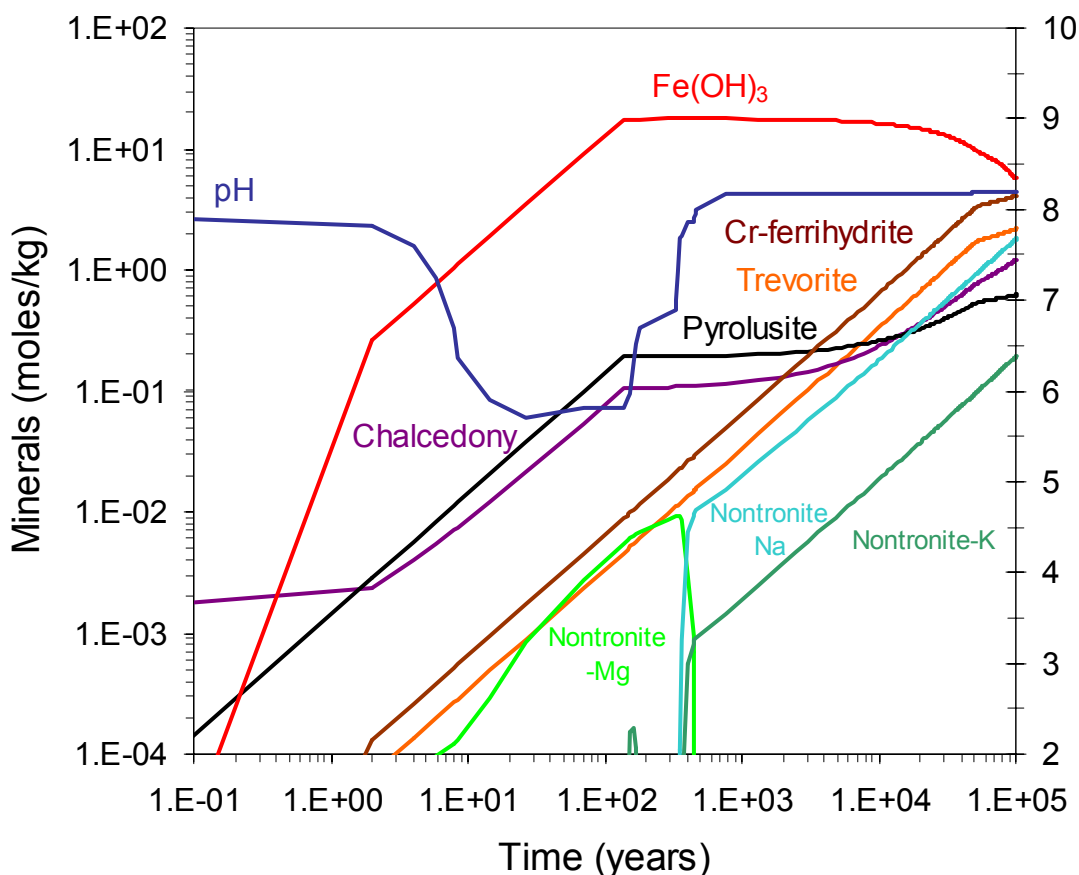
Figure 12. Major Mineral Formation During FSV SNF WP Degradation in Case 2

6.3.2   Effects of High Degradation Rates with Low Flow (Case 3)

The Base Case assumed average rates of steel corrosion, glass dissolution and FSV SNF dissolution. Case 3 evaluates the effects of high rates of dissolution and corrosion combined with a low flow rate (20 mm/year), such as might occur at higher temperatures.   The consequences of using high corrosion and dissolution rates are the most extreme pH values of the FSV simulations, the highest ionic strength, and complete loss of radionuclides from the WP (Table 13).

Figure 13 shows the degradation of FSV WP components and pH versus time for Case 3. The pH response at early times is dominated by the corrosion of the A516 carbon steel and the 304L stainless steel GPCs, dropping to around 6.5 and remaining below 7 until the A516 and 304L are finally exhausted. After these steels are exhausted, the pH rises to the maximum value of 9.7, controlled by the high degradation rate of HLW glass, which is completely exhausted by about 10,000 years after WP breach. After the HLW glass is exhausted, the pH, which is controlled by

the high degradation rate of the 316NG stainless steel liner, drops to a minimum value of 4.06 and then rises to near 7 as the liner is completely degraded.
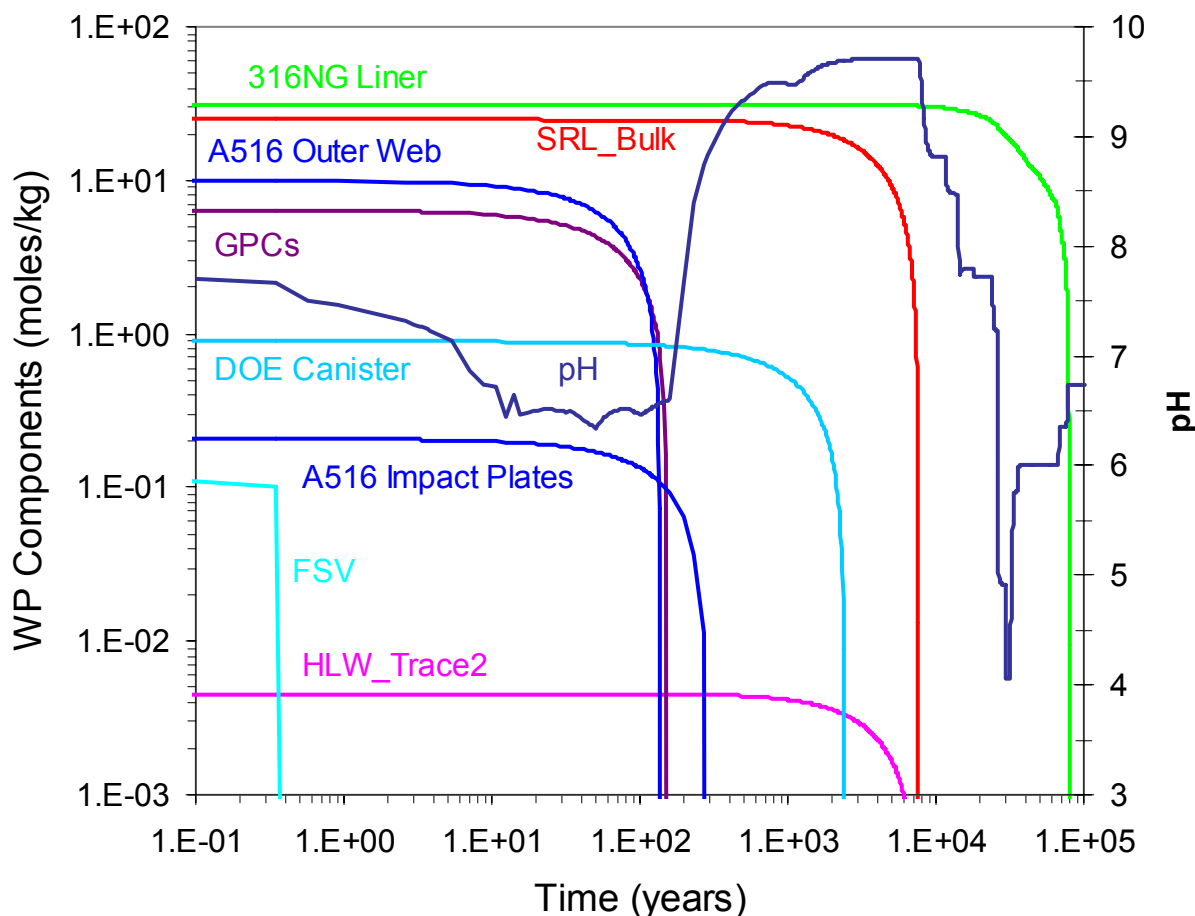
Output DTN: MO0201SPAGIN07.001
Figure 13. WP Components and pH for FSV SNF Case 3

Figure 14 presents the radionuclide minerals precipitating in this simulation, that control the aqueous solubility of the radionuclides of interest (Figures 3 to 9) and pH versus time from WP breach. The most insoluble Pu and Th minerals (Pu oxide and thorianite) were suppressed (see Assumption 5.4). Note that no I or Tc minerals form, thus these elements are not solubility limited and their aqueous concentrations are controlled by the degradation rates of the HLW glass and the SNF. The HLW glass rate is pH-dependent, thus the aqueous concentrations of elements found in the HLW glass vary with pH. Mineral formation occurs at very early times in Case 3 during the rapid degradation of the FSV SNF. The U minerals, which are stable only at early times, are uranyl phosphate hydrate ($(UO_2)_3(PO_4)_2 \cdot 6H_2O$), α-uranophane ($Ca(UO_2SiO_3OH)_2 \cdot 5H_2O$), Na-boltwoodite ($NaUO_2SiO_3OH \cdot 1.5H_2O$) and schoepite ($UO_3 \cdot 2H_2O$). Thorium solubility is controlled by formation of $Th_{0.75}PO_4$ and amorphous ThO_2 until a few thousand years after WP breach. $PuO_2(OH)_2$ formation controls Pu solubility until only a few hundred years after WP breach. $KNpO_2CO_3$ forms later, during the period of highest pH, when

the level of dissolved carbonate is high and while sufficient Np is available from HLW glass dissolution. No radionuclide minerals remain in the WP at late times, so that all of the radionuclides are flushed out of the WP by the end of the simulation.
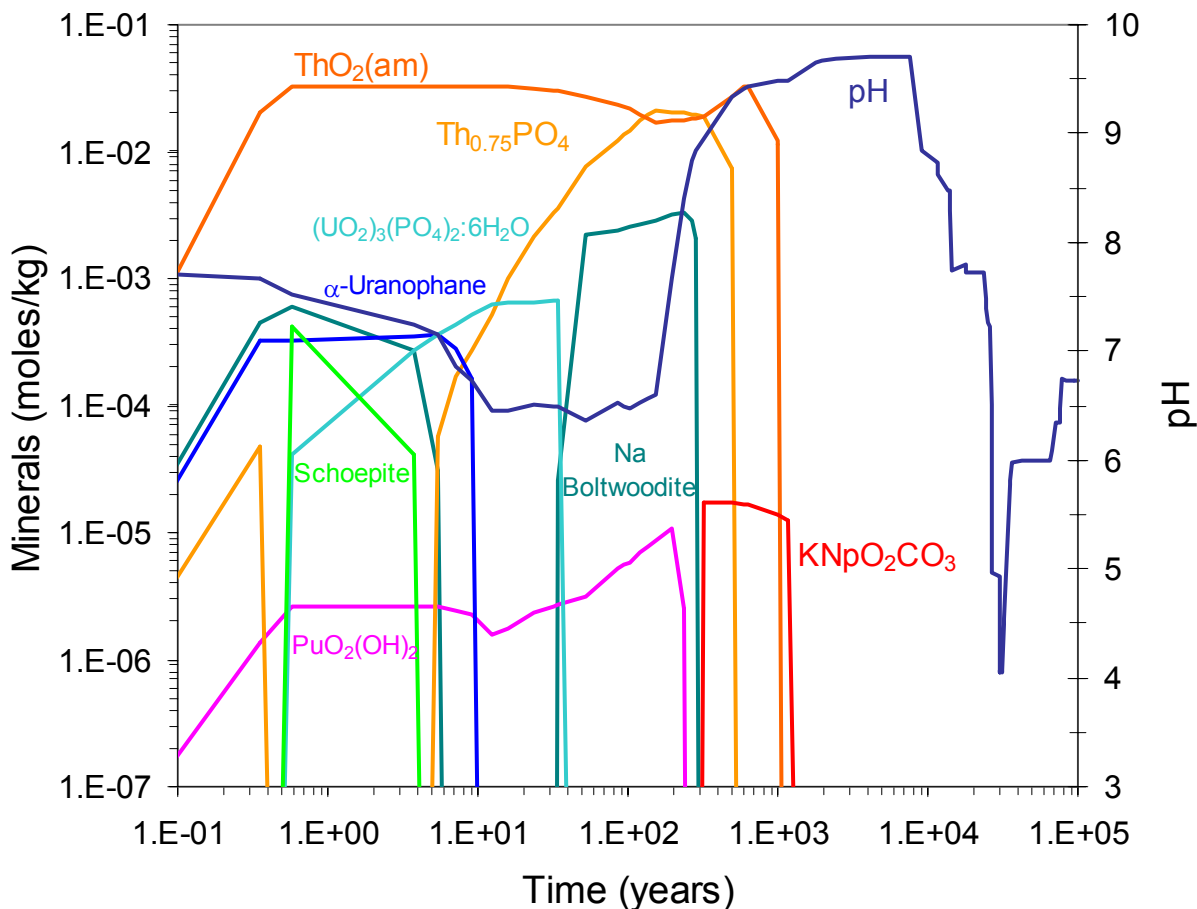
Output DTN: MO0201SPAGIN07.001

Figure 14. Radionuclide Minerals and pH for FSV SNF Case 3

Figure 15 presents the major non-radionuclide minerals precipitating during this simulation. Information about all the minerals which were predicted to form during Case 3 is available in the associated "*.min_info.txt" files in the output DTN: MO0201SPAGIN07.001. The major corrosion product sinks of the metals from steel degradation are $Fe(OH)_3$, Cr-ferrihydrite, trevorite, and pyrolusite. Chalcedony is the major sink for Si from HLW glass degradation. The nontronites are Fe-rich smectites which are a corrosion product of both HLW glass and steel degradation. Chalcedony becomes unstable early in the period of very high pH and dissolves adding to the Si available for nontronite formation. $Fe(OH)_3$ also becomes unstable near the end of the high pH period releasing Fe for increases in Cr-ferrihydrite and trevorite formation. As the pH drops to 4, the nontronites also become unstable for a time and gibbsite formation becomes a sink for Al released in the WP.
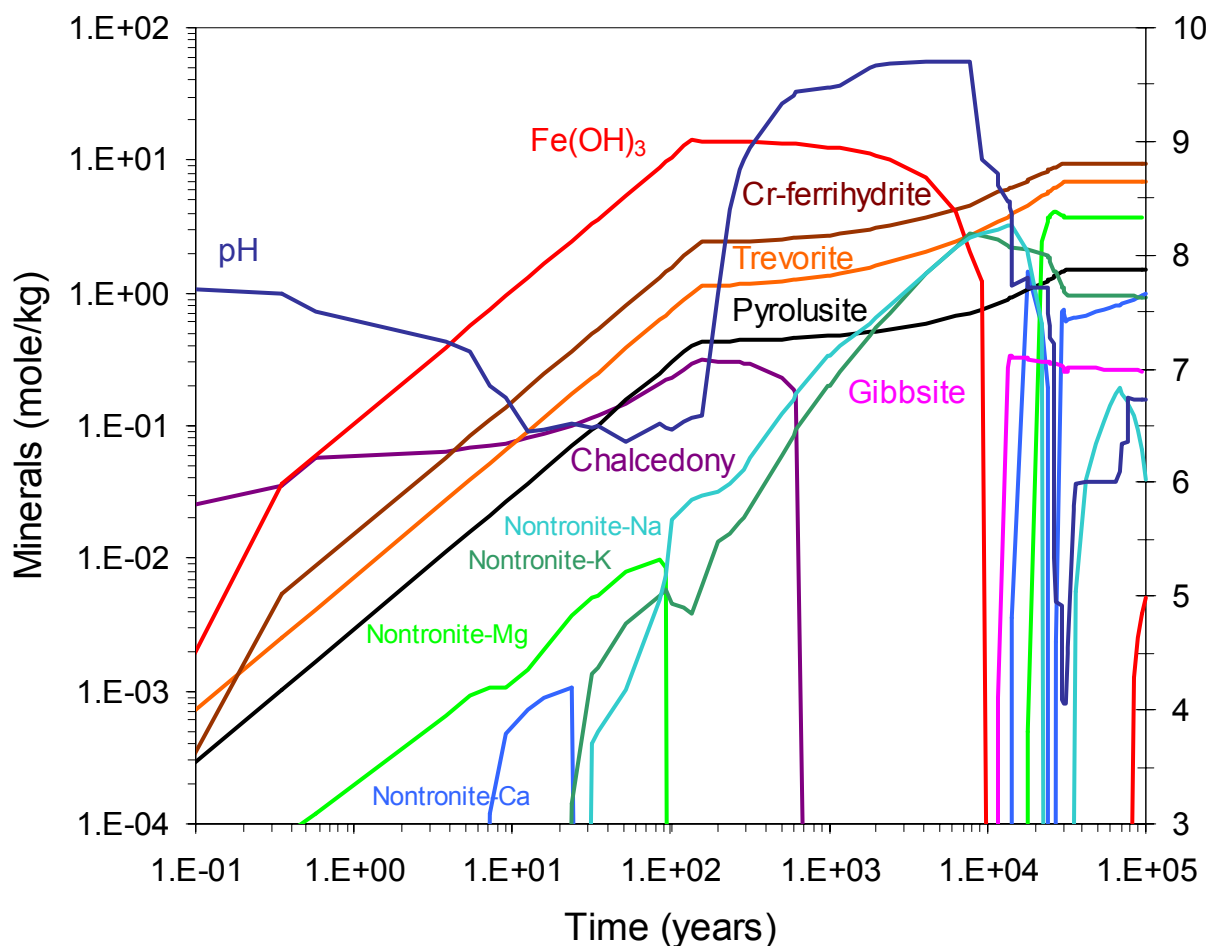
Output DTN: MO0201SPAGIN07.001

Figure 15. Major Minerals and pH for FSV SNF Case 3

6.3.3   Sensitivity to Hematite Formation (Case 4)

This case, Case 4, evaluates the effects of allowing hematite to form under the same conditions as the Base Case (i.e., as in Case 2, with moderate rates of degradation for HLW glass and steels). Table 13 shows that the pH minimum and maximum values are slightly lower than in Case 2, but that the percentages of initial radionuclide moles retained are slightly higher in Case 4. Case 4 also has slightly higher ionic strength. The degradation of WP components should be very similar to Case 2 (Figure 10) except that the slightly lower pH values may increase the rate of HLW glass degradation slightly. Figure 16 shows that the set of major minerals formed are different, with hematite taking the place of the Fe hydroxide ($Fe(OH)_3$), Cr-ferrihydrite and some of the trevorite formed in Case 2. Nontronites also form, but talc forms during Case 4 as an additional sink for Si and Al.
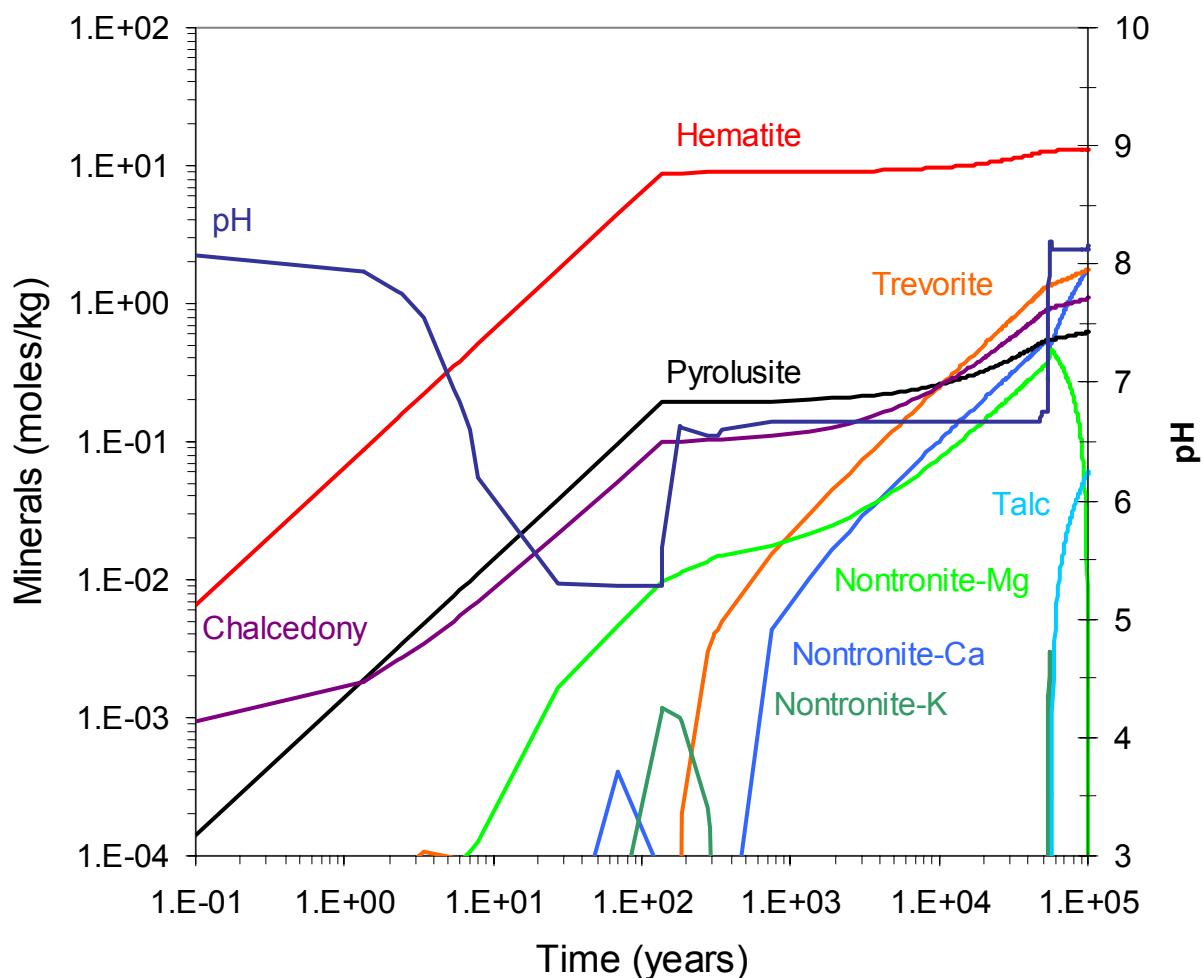
Output DTN: MO0201SPAGIN07.001

Figure 16. Major Minerals and pH for FSV SNF Case 4

Figure 17 presents the radionuclide minerals precipitating in Case 4, that control the aqueous solubility of the radionuclides of interest (Figures 3 to 9) and pH versus time from WP breach. The most insoluble Pu and Th minerals (Pu oxide and thorianite) were suppressed (see Assumption 5.4). Note that no I, Np, Pu or Tc minerals form, thus these elements are not solubility limited and their aqueous concentrations are controlled by the degradation rates of the HLW glass and the SNF. The HLW glass rate is pH-dependent, thus the aqueous concentrations of elements found in the HLW glass vary with pH. The U minerals forming during Case 4 are U phosphate hydrate $((UO_2)_3(PO_4)_2 \cdot 6H_2O)$, α-uranophane $(Ca(UO_2SiO_3OH)_2 \cdot 5H_2O)$, and Na-boltwoodite $(NaUO_2SiO_3OH \cdot 1.5H_2O)$. Thorium solubility is controlled by formation of $Th_{0.75}PO_4$ and amorphous ThO_2. The lower pH during Case 4 compared to Case 2 apparently increases the stability of U phosphate hydrate and $Th_{0.75}PO_4$, while decreasing the stability of amorphous ThO_2 and Na-boltwoodite.
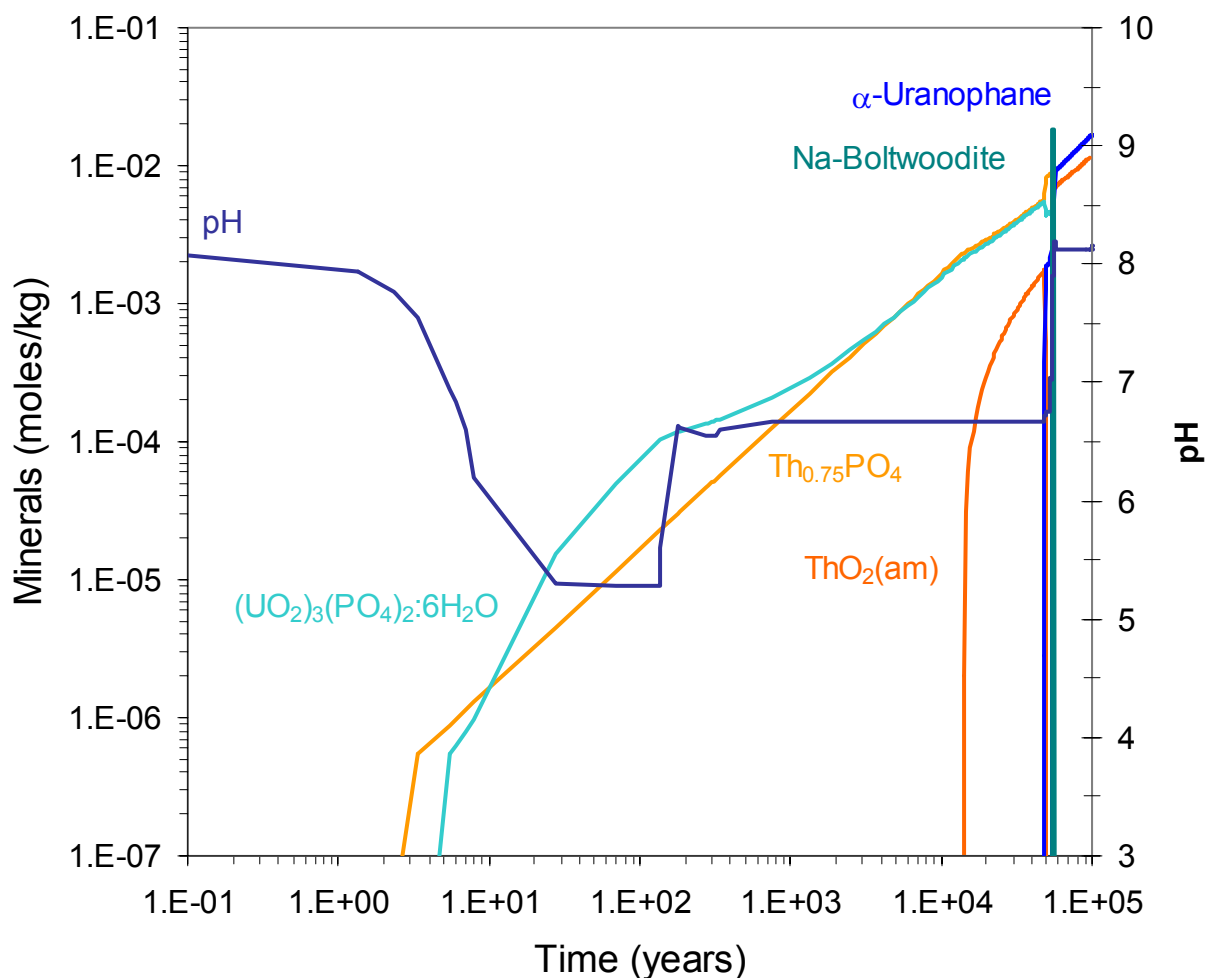
Output DTN: MO0201SPAGIN07.001

Figure 17. Radionuclide Minerals and pH for FSV SNF Case 4

6.3.4   Sensitivity to 1% damaged FSV SNF (Case 0)

This case considers the effect of 1% of the FSV SNF fuel moles and surface area degrading at the conservative rate (10 times U-metal rate) while the remainder of the fuel degrades at the same rate as Case 2. The results for Case 0 are very similar to those of Case 2 (Table 13) and the pH profile of these two cases is nearly identical (Figure 3). Figures 4 through 9 show that the amounts of Pu, U, and Th are higher in the WP solution until 10 years after WP breach for Case 0 than Case 2, while concentrations of I, Np, and Tc are higher than Case 2 during the first 100 years of Case 0. The relatively short duration of these higher radionuclide concentrations in the WP solution is probably the reason for the similarity in results for Case 0 and Case 2. Therefore, the predicted geochemical interactions inside the WP during Case 0 is probably described quite well by Figures 10 through 12 for Case 2.

6.3.5   Internal Criticality Case (Case 1)

This case considers a more conservative loading from a criticality perspective assuming a full load (five FSV elements) of fresh fuel (ThC_2 or $(Th/U)C_2$ core surrounded by four protective coatings of SiC and pyrolytic C, BSC 2001a, Table 5-4). This idealized fuel composition contains BOL levels of U, EOL levels of Th and Pu based on Taylor (2001, Tables 2-4 and 2-7), but no Np, Tc or I isotopes. Case 1 evaluates the in-WP chemistry for a maximum loading of fresh fuel, similar to the internal criticality calculations of BSC (2001a, Sections 5 and 6). Table 13 indicates that this case has the same pH range and maximum ionic strength as the Base Case (Case 2). Figure 3 shows that the pH profiles during Case 1 and Case 2 are nearly identical. The slight increase in SNF mass and the change in SNF composition change the masses and the proportions of radionuclides removed by the J-13 water flowing through the WP. For example, Np, Tc and I are found only in the HLW glass for Case 1 (fresh fuel lacks these radionuclides). Figures 4, 5, and 7 show that the predicted concentrations of I, Np and Tc in the WP solution are slightly less for Case 1 than Case 2, while the levels of Pu (Figure 6) and U (Figure 9) are very similar for the two cases. Since higher concentrations of these elements are available for release from the WP during Case 2, the percentage of Np, Tc and I retained in the WP is greater in Case 1 than during Case 2.

6.3.6   Two-Stage Simulation (Case 5)

Case 5 is a two-stage simulation that allows exposure of the HLW glass, the outer web, and the stainless steel GPC to degradation before the contents of the DOE SNF canister are exposed to J-13 water. Relatively high rates of degradation are used initially to remove all HLW glass before exposing the DOE SNF canister contents. Once the HLW glass is removed, moderate degradation rates are used for the remaining reactants. Table 13 shows that this case results in nearly complete loss of U, Pu, and Tc, 75 to 80% loss of I and Np, and almost complete retention of Th in the WP.

Figure 3 shows that the pH profile for Case 5 is similar to Case 2 at early times, similar to Case 3 during the first period of low pH and then has pH values between Case 2 and Case 3 during late times. The first-stage of Case 5 has a very high J-13 water drip rate (0.5 m^3/year) which prevents the pH (8.63) from rising as high as it does in Case 3 (9.71) which has a very low drip rate (0.015 m^3/year). The second-stage of Case 5 (which begins 28,000 years after WP breach) has the same degradation rates as Case 2, but the same J-13 drip rate as Case 3. The absence of HLW glass and low drip rate in this stage drives the pH lower than in Case 2, while the lower steel degradation rate keeps the pH above that of Case 3.

Since all of the HLW glass is degraded during the first stage of Case 5, all of the U, Pu, Tc, I, and Np in the glass would be lost from the WP unless they are retained in corrosion products. The radionuclide minerals forming during the first stage of Case 5 should be similar to those forming during the first part of Case 3 (Figure 14). Although U and Pu minerals form at early times, they are not stable when pH values rise above 8. The Np mineral, $KNpO_2CO_3$, forms at higher pH when CO_3^{2-} is abundant, but it only persists in the WP if enough Np is available. Figures 4 through 7 and 9 show that the WP solution concentration of each of the radionuclides from HLW glass degradation decreases to negligible values by the end of the first stage of Case 5. During the second stage of Case 5, FSV SNF degradation occurs, probably in a manner

similar to Case 2 (Figure 10), with incomplete fuel degradation by the end of Case 5. The radionuclides retained in the WP are mostly contained in the remaining FSV SNF. Most of the Th released from SNF degradation is probably precipitated as ThO_2(am) and $Th_{0.75}PO_4$, which are stable in the pH range of 8 to 7.5 (Figures 11 and 14) that occurs during the second stage of Case 5 (Figure 3)

6.3.7   Sensitivity to O_2 Fugacity (Case 6)

Case 2 (the Base Case) assumed a fixed value for log O_2 fugacity as –0.7 (see Assumption 5.3). Case 6 evaluates the sensitivity of the simulations to reducing the log O_2 fugacity to -10.0, such as might result from the chemical O_2 demand of steel corroding in a closed environment. Table 13 presents the effects of this change. Figures 4 through 9 show that all of the predicted radionuclide concentrations during the first year of Case 6 are slightly higher than those predicted for Case 2. After that, Th is slightly higher and U slightly lower than in Case 2 for several hundred years. After the early period of low pH, Np concentration is much lower in the WP solution during Case 6 than predicted for Case 2. The change in the O_2 concentration allows NpO_2 to form at late times, retaining the majority of the Np in the WP (*.min_info.txt files for Case 6 in output DTN: MO0201SPAGIN07.001). The change in the O_2 concentration also allows an alternate Pu mineral, $PuO_2 \cdot 2H_2O$, to form during Case 6 (*.min_info.txt files for Case 6 in output DTN: MO0201SPAGIN07.001). This Case is otherwise similar to Case 2.

6.3.8   Effects of High Rates of Degradation with Average Flow (Case 7)

The Base Case assumed low rates of steel corrosion, glass dissolution and SNF dissolution. Case 7 evaluated the effects of high rates of dissolution and corrosion under conditions otherwise similar to the Base Case. The results of Case 7 are similar to Case 3 (which had low drip rates), with a wide range of pH variation, high ionic strength and complete degradation of WP contents. The higher drip rate for Case 7 results in a slightly narrower range of pH variation and a lower maximum ionic strength than those predicted for Case 3 (Figure 3 and Table 13). After the HLW glass and SNF are exhausted, all of the radionuclides, except Th, are flushed out of the WP at slightly later times than for Case 3 (Figures 4 through 9). Amorphous ThO_2 is the only radionuclide mineral remaining in the WP at the end of Case 6. Otherwise, no radionuclide minerals remain in the WP at late times similar to the results for Case 3 (Figure 14).

6.4 N REACTOR SNF

Table 15 presents a summary of the results of the calculations for N Reactor SNF for the pH range, the maximum ionic strength, and the percentages of key radionuclides retained in the WP at the end of the simulation (~100,000 years after WP breach). The complete output tables (aqueous, mineral, and total moles) for all the cases are included in the files associated with this analysis (output DTN: MO0201SPAGIN07.001).

Table 15. Results Summary for N Reactor SNF (Group 7)

Case and Objective	EQ6 File Name(*.6I)	Percent of initial moles retained in WP					pH Range		Max Log Ionic Strength
		U	Pu	Np	I	Tc	Min.	Max.	
Case 0: Base Case With 4 MCOs and no GPCs in WP[a]	R02a1013	99.13	86.85	19.15	0.00	0.00	4.20	8.09	-1.84
Case 1: Criticality case[a]	R12a1113 R12b1113	97.21	76.91	76.91	76.91	76.91	5.68	8.14	-2.25
Case 2: Base Case[a]	R22a1113	96.78	83.84	64.99	3.59	10.20	5.12	8.14	-2.23
Case 3: Worst case: High rates, low flow[a]	R32a2222 R32b2222 R32c2222	99.71	0.00	0.00	0.00	0.00	3.99	8.09	0.11
Case 4: Base Case with hematite and goethite not suppressed	R42a1113 R42b1113 R42c1113	99.29	73.82	1.48	3.48	9.90	5.11	8.09	-2.00
Case 5: Base Case as two-stage[a] (contents of MCOs untouched until HLW is gone)	R52a2204 R52b2204 R52c2204 R52d2204 R52e1012	99.66	94.46	93.07	0.00	0.00	4.72	8.14	-0.40
Case 6: Base Case[a] + low fO$_2$	R62a1113	96.39	96.99	99.85	3.56	10.13	4.99	8.12	-2.25
Case 7: Base Case[a] + high rates, avg. flow	R72a2223 R72b2223 R72c2223 R72d2223	97.83	0.00	0.00	0.00	0.00	4.12	8.09	-0.58

NOTES: [a]Suppresses the minerals soddyite and PuO$_2$.
[b]Suppresses the minerals, hematite, goethite; soddyite and PuO$_2$; but includes chromate phases.

For some of the N Reactor SNF cases examined in this analysis, the volume of remaining WP components and of corrosion products precipitated in the WP nearly reaches or exceeds the volume of the WP before 100,000 years after WP breach. Table 16 presents the years after WP breach when the volume of the WP would be at least 2/3 full of solids and also the percentage of the WP volume filled with solids at the end of each N Reactor SNF case (or at the time when the WP volume would be 100% full of solids). For the portions of these cases after the time when the WP is about 2/3 full of solids Assumptions 5.8 and 5.9 may no longer be reasonable. On the other hand, the degradation rates of WP components would probably decrease if a thick layer of WP corrosion products separates them from the WP solution (See discussion in Assumptions 5.8 and 5.9) and this would slow the production of corrosion products.

Table 16 shows that the WP is predicted to be totally filled or nearly totally filled with solids before or by ~100,000 years after WP breach for all the N Reactor SNF cases except Case 4. For all of the cases except Case 5, the WP is predicted to be at least 2/3 full of solids before 10 years after WP breach. This is the result of the total degradation of N Reactor SNF which is predicted to occur before 10 years after WP breach for all of the cases except Case 5 (Figures 24, 27 and 32). Table 15 shows that almost all of the U from SNF and/or HLW glass degradation is predicted to remain in the WP (as precipitated minerals and solids or remaining HLW glass) until ~100,000 years after WP breach for all of the N Reactor cases. For the cases with high

degradation rates (Cases 3 and 7) the WP is predicted to be totally full of solids by ~2000 years after WP breach. For Case 0, in which about twice as much N Reactor SNF is allowed to degrade in the WP, the WP is predicted to be completely full by about 11 years after WP breach. The WP in Case 1 contains slightly more N Reactor fuel than in the Base Case (Case 2) and is predicted to be completely full of solids earlier (about 76,000 years after WP breach). In Case 4, the WP volume is less than 90% filled at the end of the run. This is probably due mostly to the formation of hematite in this run instead of the Cr-ferrihydrite and $Fe(OH)_3$ which are allowed to form in all the other cases. The molar volume of hematite is smaller (30.274 cm^3/mole) than that of Cr-ferrihydrite (129 cm^3/mole) or $Fe(OH)_3$ (34.36 cm^3/mole) (file data0.trc in output DTN: MO0201SPAGIN07.001). The lower pH values predicted to occur during Case 4 (Figure 3) may also destabilize some of the corrosion product solids that would otherwise form in the WP.

Table 16. WP Volume Summary for N Reactor SNF (Group 7)

Case	% WP Volume Filled with Solids	Years After WP Breach	% WP Volume Filled with Solids	Years After WP Breach
Case 0	65.8	3	99.8	11
Case 1	70.9	9	100.0	75592
Case 2	68.2	6	98.9	100010
Case 3	66.2	1	100.6	2344
Case 4	66.3	6	87.1	100000
Case 5	66.4	155	100.0	23335
Case 6	69.0	7	98.7	100000
Case 7	66.3	1	100.0	2133

Figures 18 to 23 show the predicted variation of pH and WP solution concentrations of I, Np, Pu, Tc, and U during all of the N Reactor SNF cases. Differences in radionuclide concentrations in the WP solution between the cases are dependent on several variables, some of which are: the degradation rates of the WP components; the J-13 drip rate; the solubilities of solid corrosion products; and the pH of the WP solution. These differences will be discussed on a case by case basis in the following sections.
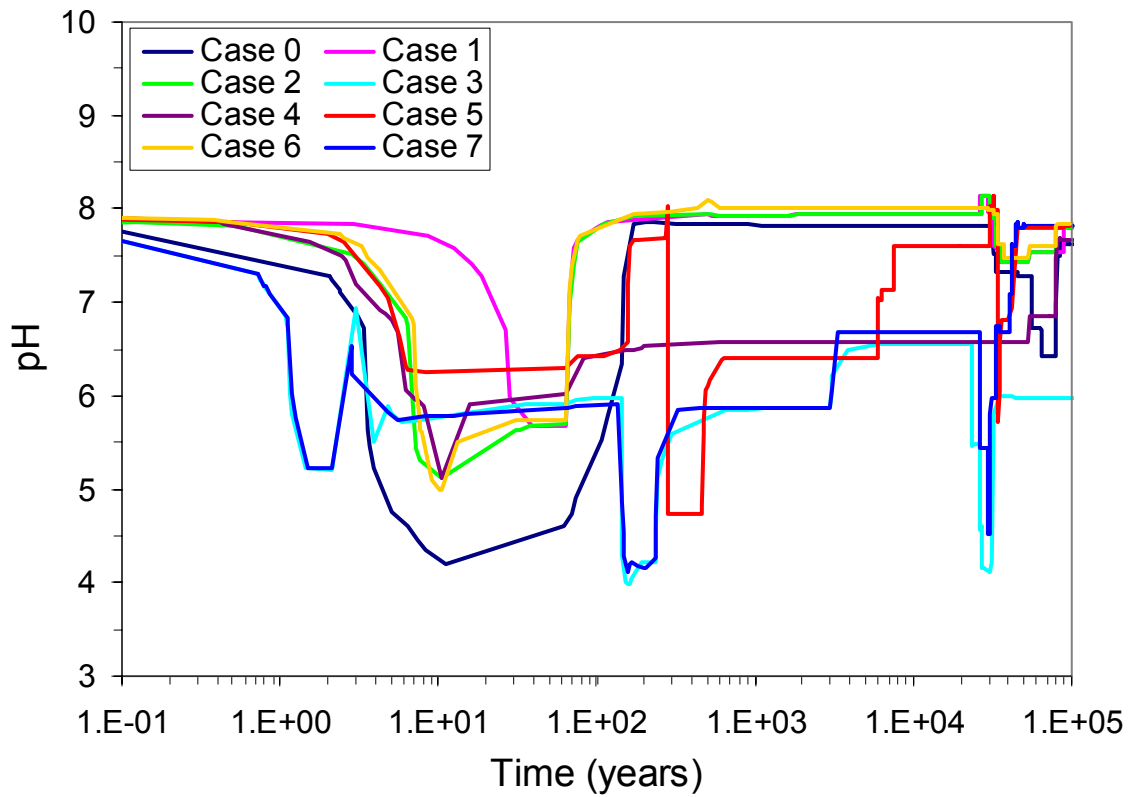
Output DTN: MO0201SPAGIN07.001

Figure 18. pH During N Reactor SNF Cases
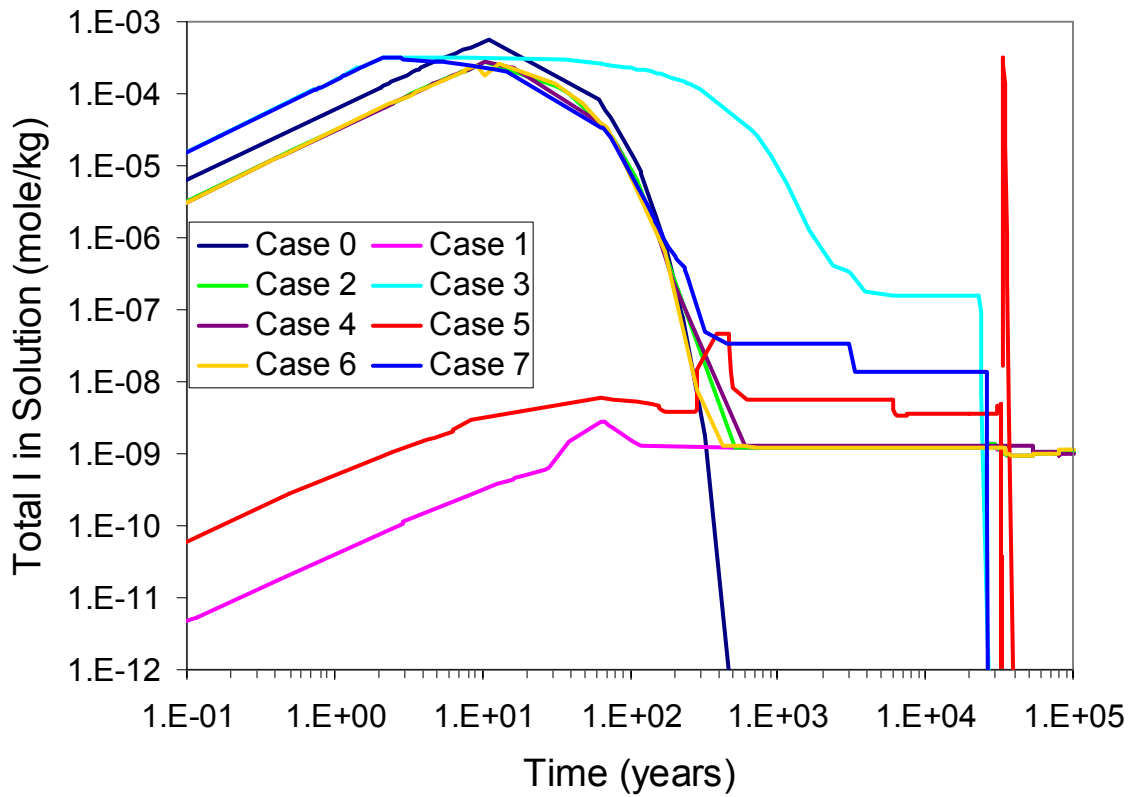
Output DTN: MO0201SPAGIN07.001

Figure 19. Total I in Solution During N Reactor SNF Cases
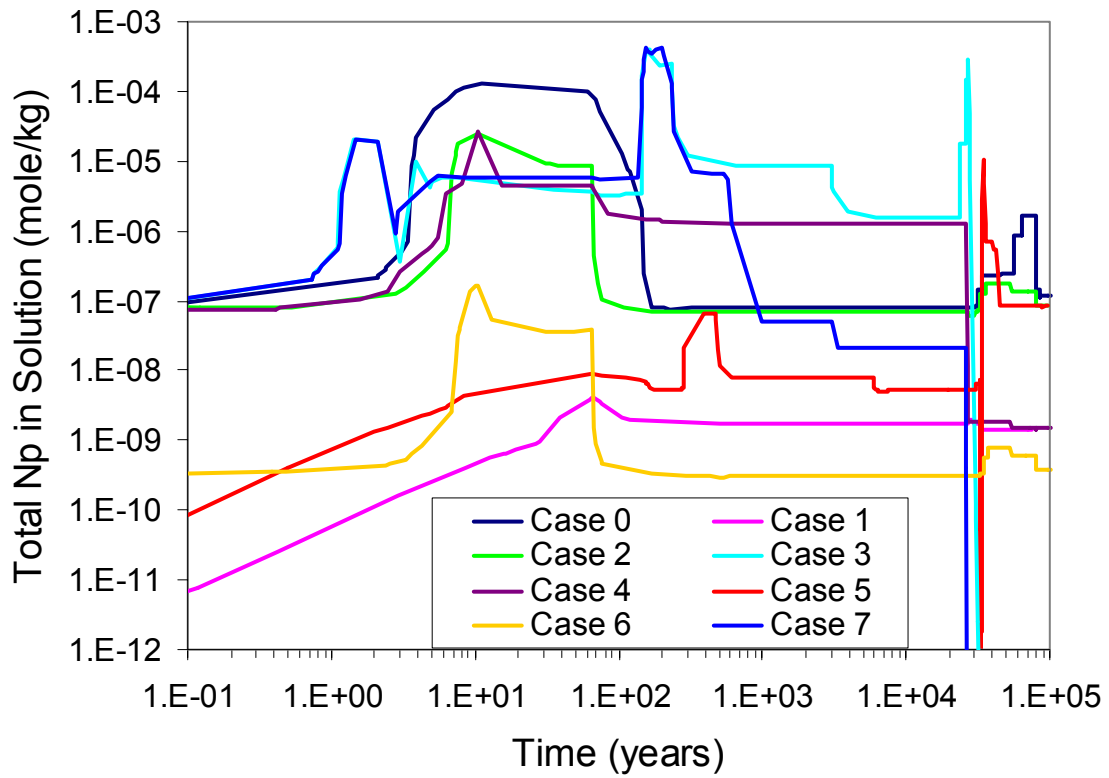
Output DTN: MO0201SPAGIN07.001

Figure 20. Total Np in Solution During N Reactor SNF Cases
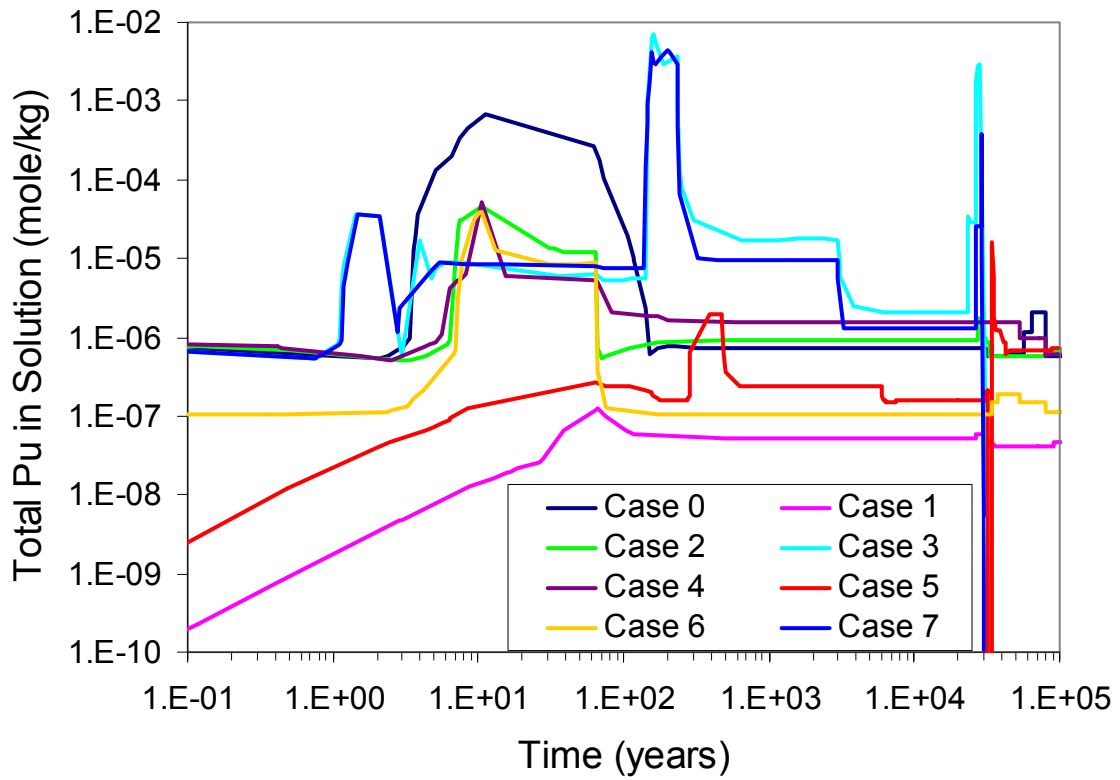
Output DTN: MO0201SPAGIN07.001

Figure 21. Total Pu in Solution During N Reactor SNF Cases
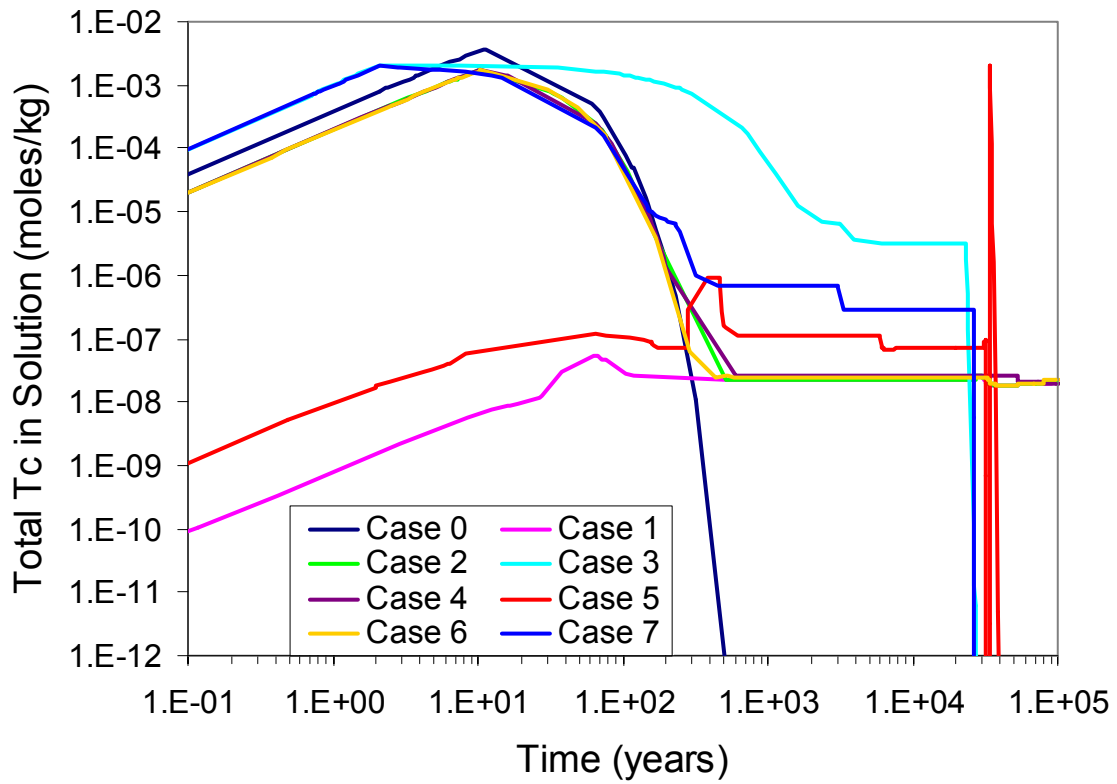
Output DTN: MO0201SPAGIN07.001

Figure 22. Total Tc in Solution During N Reactor SNF Cases
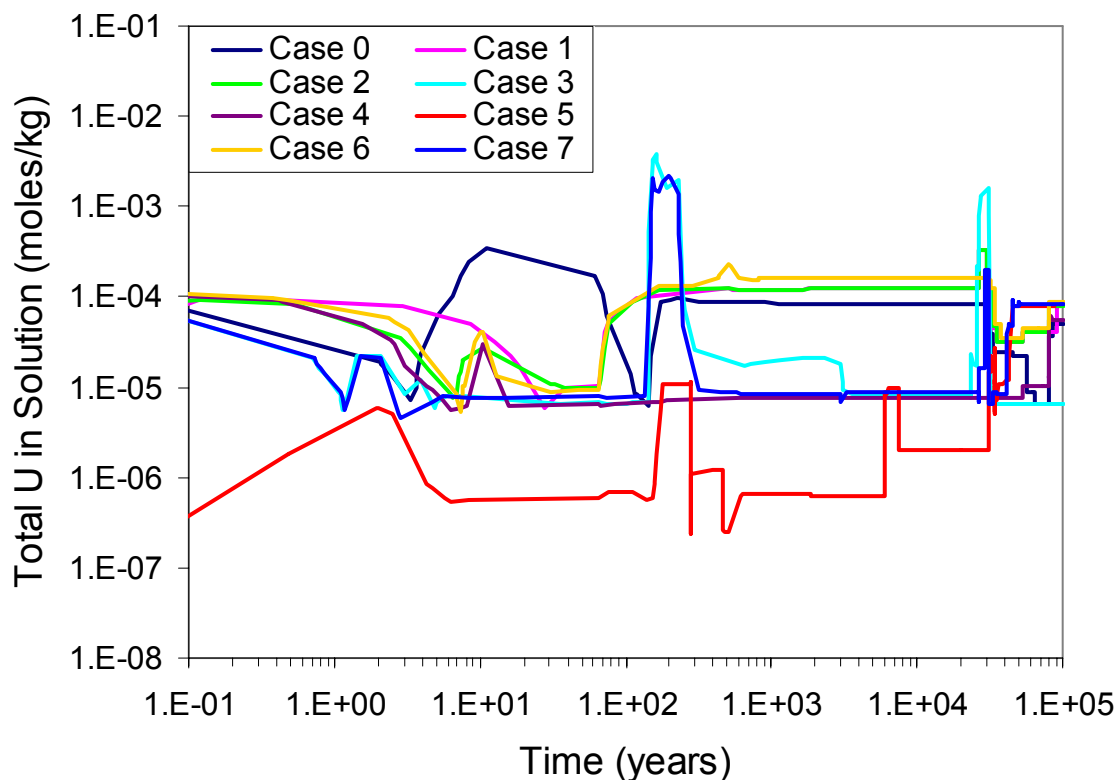
Figure 23. Total U in Solution During N Reactor SNF Cases

6.4.1   Base Case (Case 2)

The Base Case is a single-stage simulation that examines WP chemistry under moderate rates of corrosion and dissolution, with the expected CO_2 and O_2 fugacities and an 80 mm/year infiltration rate. In this case, the SNF is assumed (see Assumption 5.14) to consist of the average composition and mass (~8847 kg) of N Reactor SNF in the DOE SNF inventory (DOE 2001a, Attached Electronic File; modified for EQ6 input in workbook "Rn Fix 05.xls", sheet "DOE_SNF99 (Cat. 7)(2)", output DTN: MO0201SPAGIN07.001) with 2 MCOs per WP. Table 15 shows that most of the U (97 %), Pu (84%) and Np (65%) are retained in the WP during Case 2, while most of the I (96%) and Tc (90%) are lost from the WP.

Figure 24 shows the degradation of WP components and pH versus time from WP breach of the Base Case simulation. The pH response at early times is dominated by the degradation of N Reactor SNF and corrosion of the A516 carbon steel, dropping to a minimum of 5.12 during fuel degradation and remaining below 6 until the A516 is finally exhausted. After the A516 carbon steel is exhausted, the pH rises and reaches a plateau just below 8. The maximum pH value of 8.14 is not reached until about 30,000 years after WP breach.
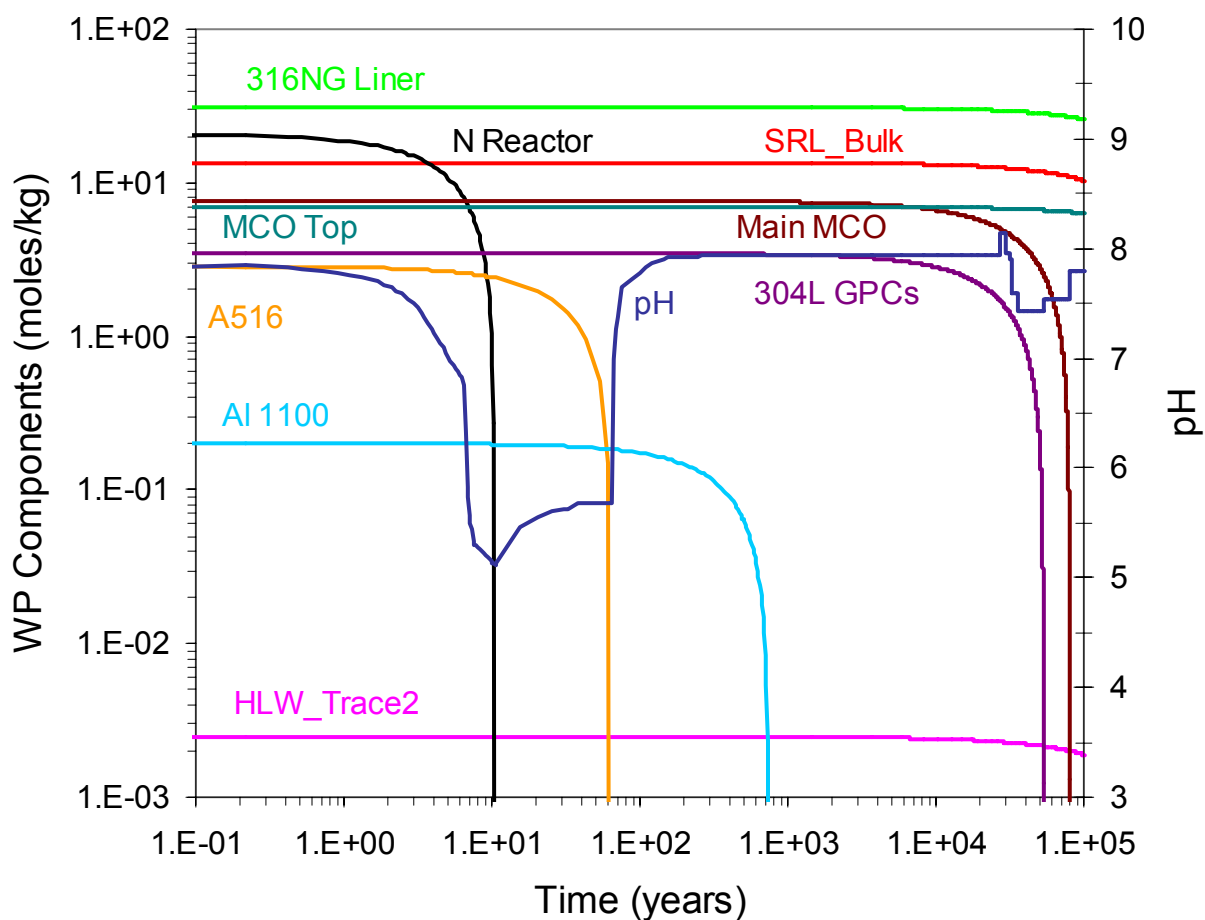
Output DTN: MO0201SPAGIN07.001

Figure 24. WP Components and pH During N Reactor SNF Case 2

Figure 25 presents the radionuclide minerals precipitating in this simulation. The most insoluble Pu mineral (PuO_2) was suppressed (see Assumption 5.4). The dominant U mineral is schoepite ($UO_3 \cdot 2H_2O$), with smaller amounts of uranyl phosphate hydrate ($(UO_2)_3(PO_4)_2 \cdot 6H_2O$), and $CaUO_4$ also forming. Uranium solution concentration is pH dependent during the first 100 years after WP breach and then appears to be controlled by the solubilites of schoepite and $CaUO_4$ (Figures 18 and 23). Plutonium solubility increases during the early period of low pH and then is controlled by formation of $PuO_2(OH)_2$ (Figures 18 and 21). Neptunium solubility also increases during the pH low at early times and then is controlled by formation of NpO_2 (Figures 18 and 20). Since no I or Tc minerals are predicted to form, the WP solution concentrations of these two radionuclides are not solubility limited, but rather are controlled by the pH-dependent degradation rate of the HLW glass and the constant degradation rate of N Reactor SNF (Figures 19 and 22). Since all of the I and Tc in the N Reactor SNF is released into the WP solution at very early times in Case 2, most of the loss of these radionuclides occurs before 1000 years after WP breach (Table 15, Figures 19 and 22).
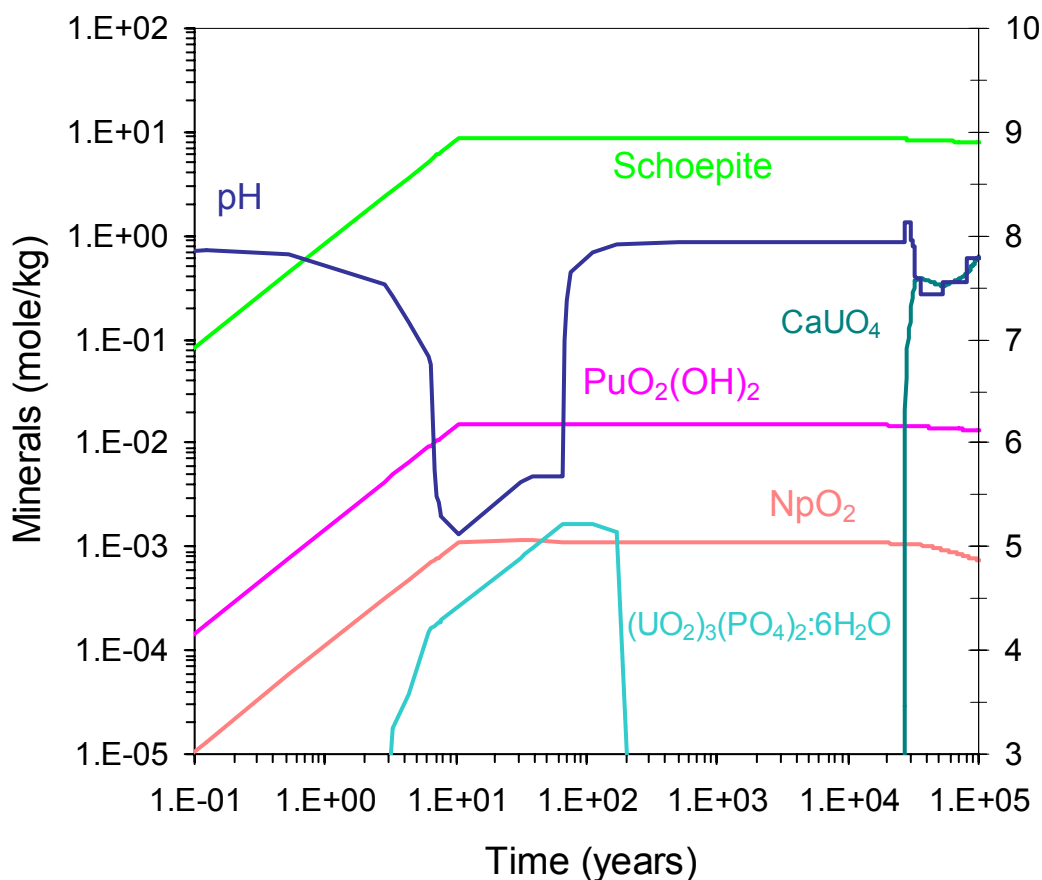
Output DTN: MO0201SPAGIN07.001

Figure 25. Radionuclide Mineral Formation During N Reactor SNF Case 2

Figure 26 presents the results of Case 2, showing the major minerals and pH versus time after WP breach. Information about the minor minerals predicted to form during Case 2 is available in the "*.min_info.txt" files in the output DTN: MO0201SPAGIN07.001. The corrosion products of the steels are the minerals $Fe(OH)_3$, Cr-ferrihydrite, trevorite ($NiFe_2O_4$), pyrolusite (MnO_2), and the Fe-rich smectite, nontronite. The HLW glass also contributes to the formation of nontronite.
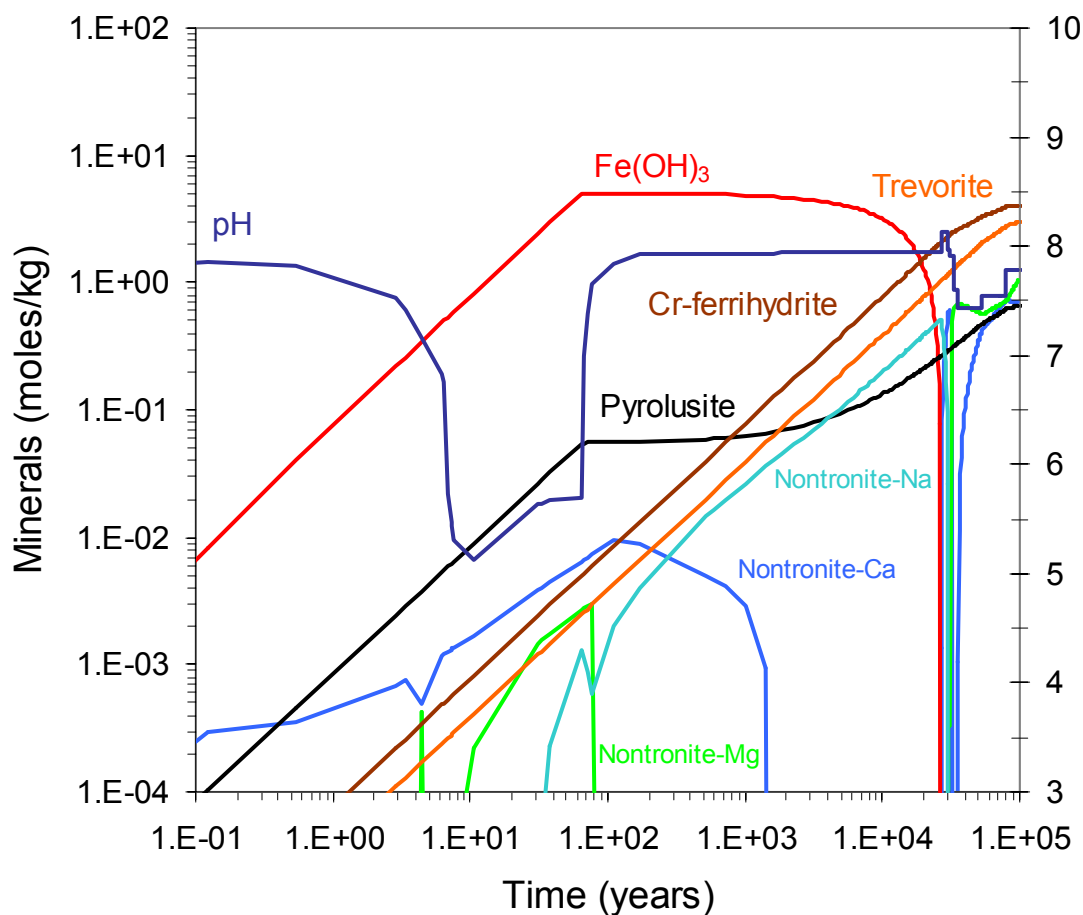
Output DTN: MO0201SPAGIN07.001

Figure 26. Major Mineral Formation During N Reactor SNF Case 2

6.4.2   Effects of High Degradation Rates with Low Flow (Case 3)

The Base Case used average rates of steel corrosion, glass dissolution, and N Reactor SNF dissolution. Case 3 evaluates the effects of high rates of degradation combined with low flow rates, such as might occur at higher temperatures.   The consequences of the rapid glass dissolution and steel corrosion rates is the lowest pH (3.99) and the highest ionic strength of all the N Reactor SNF cases, with complete loss of all of the radionuclides except U from the WP (Table 15).

 shows the degradation of WP components and pH versus time from WP breach during the Case 3 simulation. Minimum pH values are caused by the degradation of N Reactor SNF, and corrosion of the A516 carbon steel and Al 1100, the 304L GPCs and Main MCO, the MCO top and the 316NG liner. There is complete degradation of all WP components by 30,000 years after WP breach.
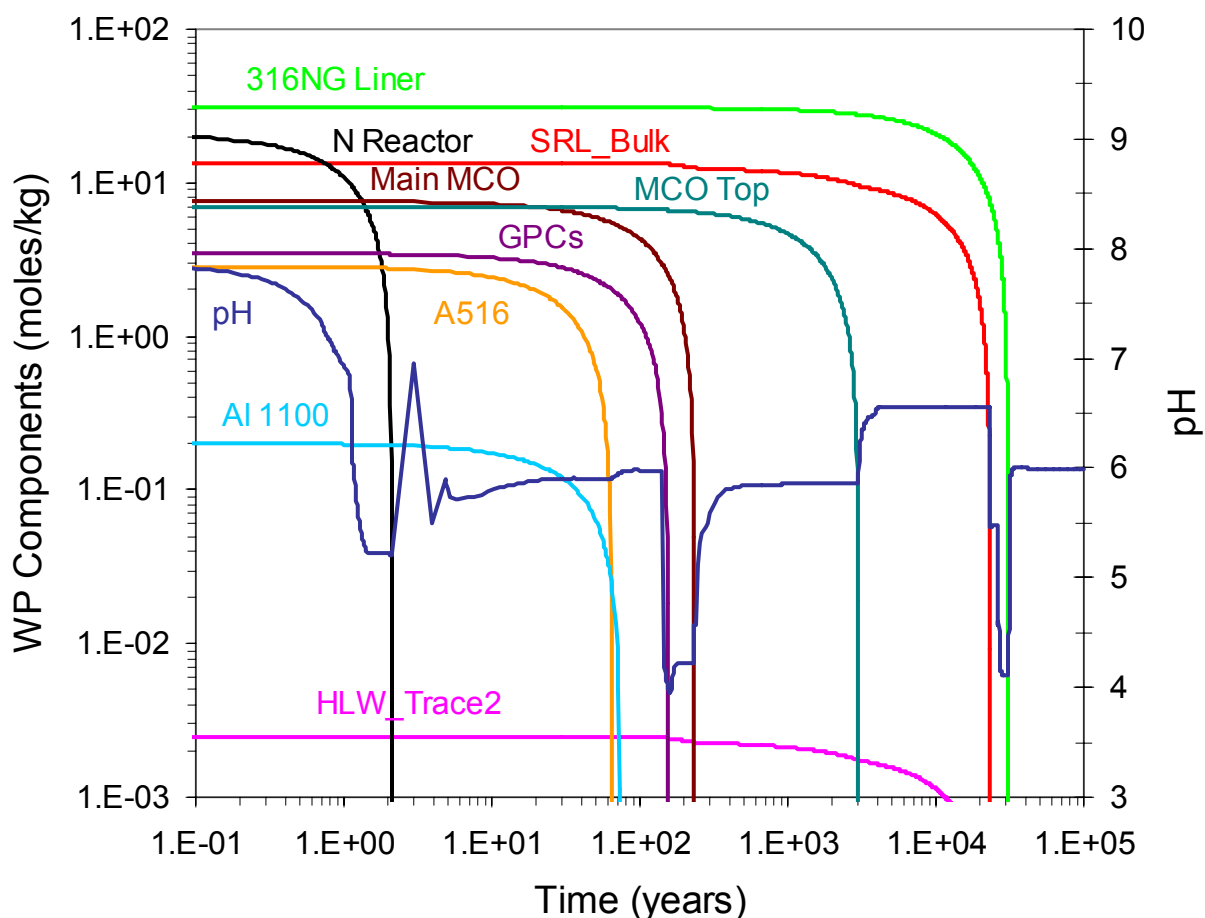
Output DTN: MO0201SPAGIN07.001

Figure 27. WP Components for N Reactor SNF During Case 3

Figure 28 presents the radionuclide minerals precipitating in this simulation. The most insoluble Pu mineral (PuO_2) was suppressed (see Assumption 5.4). The dominant U mineral is schoepite ($UO_3 \cdot 2H_2O$), with smaller amounts of uranyl phosphate hydrate ($(UO_2)_3(PO_4)_2 \cdot 6H_2O$) also forming. Uranium solution concentration is pH dependent, decreasing when pH decreases (Figures 18 and 23). Plutonium solubility increases during periods of low pH and is partially controlled by formation of $PuO_2(OH)_2$ (Figures 18 and 21). Neptunium solubility also increases during the pH lows and is partially controlled by formation of NpO_2 (Figures 18 and 20). $PuO_2(OH)_2$ and NpO_2 are unstable during periods of extremely low pH. They form in the WP during the rapid degradation of N Reactor SNF and remain until complete degradation of the HLW glass occurs removing a second source of Pu and Np and pH drops during degradation of the remaining 316L liner (Figure 27). Since no I or Tc minerals are predicted to form, the WP solution concentrations of these two radionuclides are not solubility limited, but rather are controlled by the pH-dependent degradation rate of the HLW glass and the constant degradation rate of N Reactor SNF (Figures 19 and 22). Since all of the I and Tc in the N Reactor SNF is released into the WP solution at very early times in Case 3, most of the loss of these radionuclides occurs before 1000 years after WP breach and complete loss of I and Tc occurs after complete degradation of the HLW glass occurs (Table 15, Figures 19, 22 and 27).
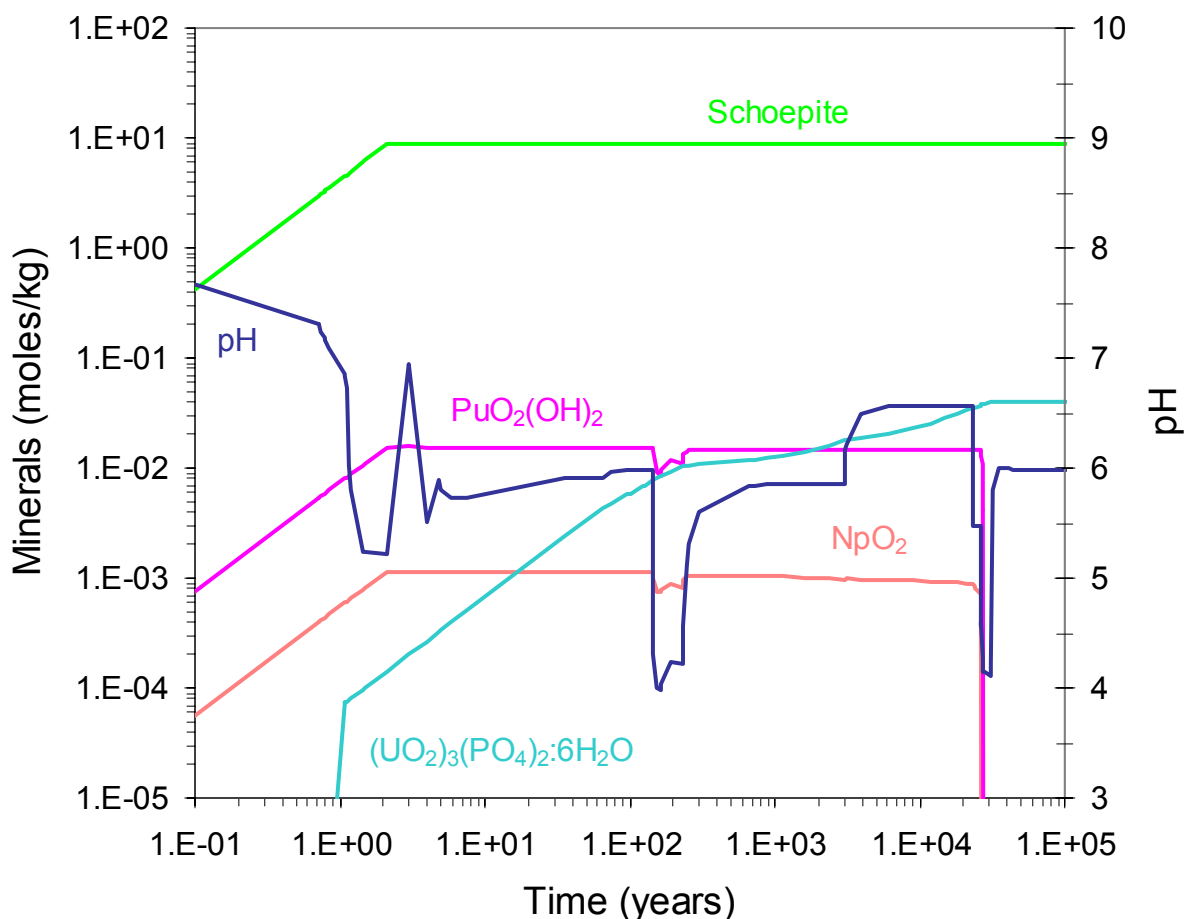
Output DTN: MO0201SPAGIN07.001

Figure 28. Radionuclide Mineral Formation and pH During N Reactor SNF Case 3

Figure 29 presents the results of Case 3, showing the major minerals and pH versus time after WP breach. Information about the minor minerals predicted to form during Case 3 is available in the "*.min_info.txt" files in the output DTN: MO0201SPAGIN07.001. The corrosion products of the steels are the minerals $Fe(OH)_3$, Cr-ferrihydrite, trevorite ($NiFe_2O_4$), pyrolusite (MnO_2), and the Fe-rich smectite, nontronite. The HLW glass also contributes to the formation of nontronite.
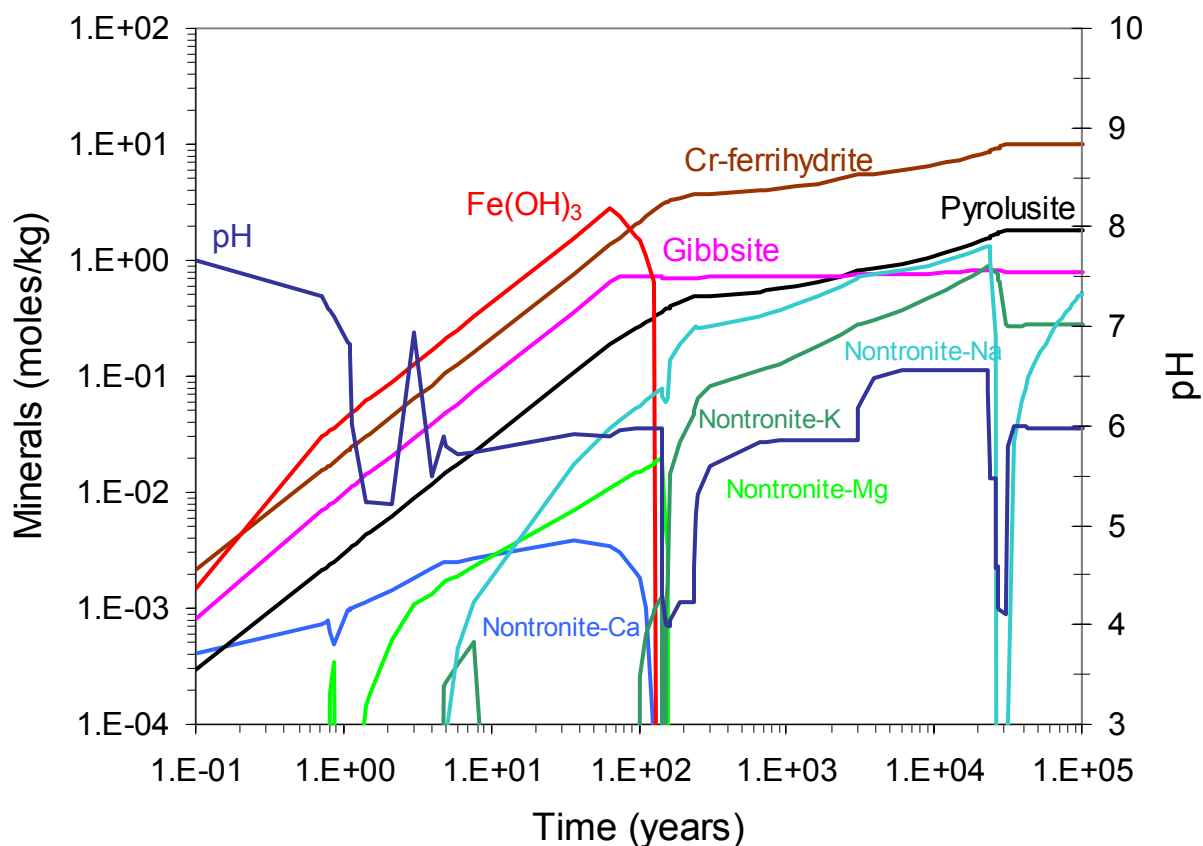
Figure 29. Major Mineral Formation During N Reactor SNF Case 3

6.4.3   Sensitivity to Hematite Formation (Case 4)

The rapid glass dissolution and steel corrosion combined with low flow rates of Case 3 required redefining the data0.ymp database to include a series of Cr-rich minerals and the suppression of hematite and goethite. Case 4 evaluates the effects of not suppressing hematite or goethite under the same conditions as the Base Case (i.e., as in Case 2, with moderate rates of degradation for HLW glass and steels). Table 15 shows that the pH range and maximum ionic strength are similar to the Base Case. The percentage of initial radionuclide mass retained is slightly lower for I and Tc, significantly lower for Np and Pu, but higher for U in Case 4 compared to Case 2 (Table 15). Figure 18 shows that pH during Case 4 is similar to Case 2 until about 100 years after WP breach. After that time, pH during Case 4 is much lower (~6.5) compared to Case 2 (~8) until about 80,000 years after WP breach.

The degradation of WP components should be very similar to Case 2 (Figure 24) except that the overall lower pH values may increase the rate of HLW glass degradation slightly. Figure 30 shows that the set of major minerals formed are different, with hematite taking the place of the Fe hydroxide ($Fe(OH)_3$), Cr-ferrihydrite and some of the trevorite ($NiFe_2O_4$) formed in Case 2. Nontronites, gibbsite ($Al(OH)_3$) and pyrolusite (MnO_2) also form during Case 4. Information

about the minor minerals predicted to form during Case 4 is available in the "*.min_info.txt" files in the output DTN: MO0201SPAGIN07.001.
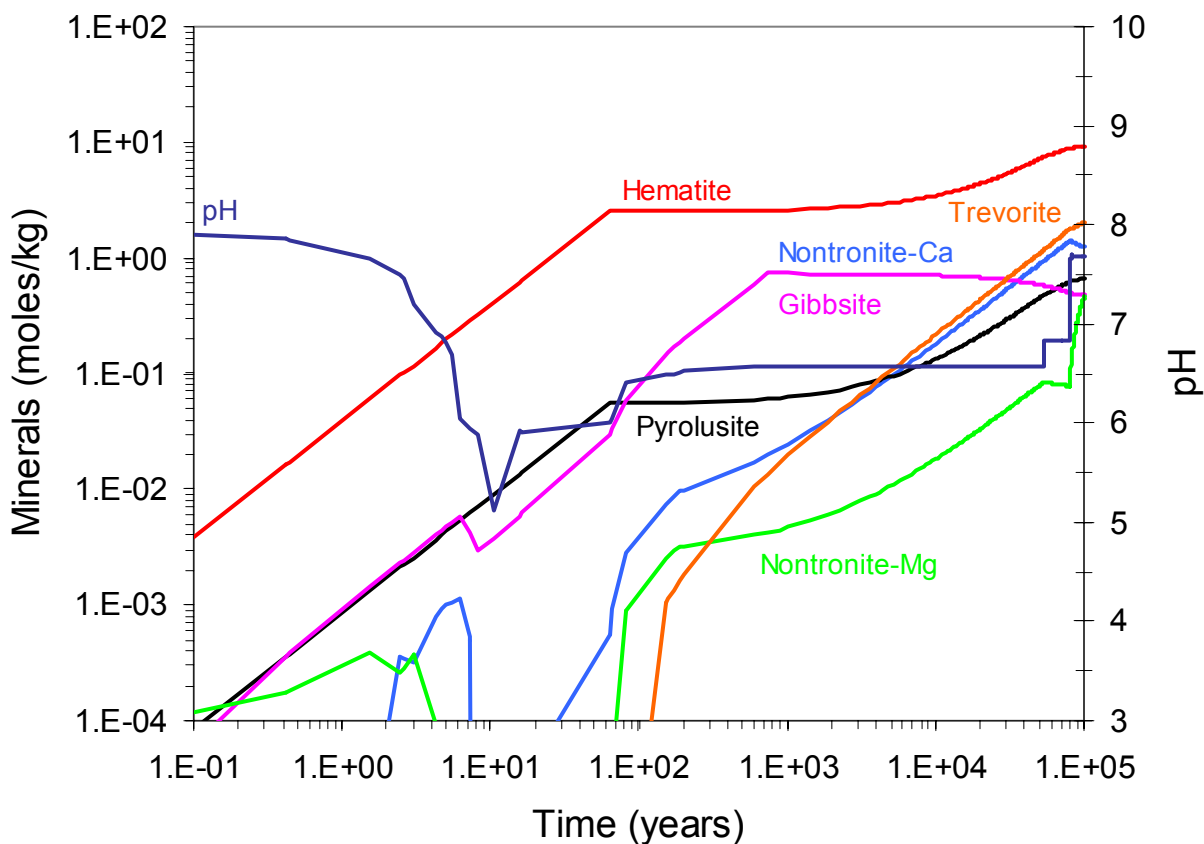
Output DTN: MO0201SPAGIN07.001

Figure 30. Major Mineral Formation During N Reactor SNF Case 4

Figure 31 presents the radionuclide minerals precipitating in Case 4, that control the aqueous solubility of the radionuclides of interest (Figures 19 to 23) and pH versus time from WP breach. The most insoluble Pu mineral (PuO_2) was suppressed (see Assumption 5.4). Since no I or Tc minerals are predicted to form, the WP solution concentrations of these two radionuclides are not solubility limited, but rather are controlled by the pH-dependent degradation rate of the HLW glass and the constant degradation rate of N Reactor SNF (Figures 19 and 22). Since all of the I and Tc in the N Reactor SNF is released into the WP solution at very early times in Case 4, most of the loss of these radionuclides occurs before 1000 years after WP breach (Figures 19 and 22). The HLW glass rate is pH-dependent, thus the aqueous concentrations of elements found in the HLW glass vary with pH. The dominant U mineral is schoepite ($UO_3 \cdot 2H_2O$), with smaller amounts of uranyl phosphate hydrate ($(UO_2)_3(PO_4)_2 \cdot 6H_2O$) and α-uranophane ($Ca(UO_2SiO_3OH)_2 \cdot 5H_2O$) also forming. Since the U WP solution concentration is pH dependent, decreasing when pH decreases, it is notably lower in Case 4 than in Case 2 from ~100 to ~80,000 years after WP breach (Figures 18 and 23). The WP solution concentration of Pu is slightly higher and Np concentration is more than an order of magnitude higher in Case 4

than in Case 2 from ~100 to ~80,000 years after WP breach (Figures 20 and 21). $PuO_2(OH)_2$ forms early during the rapid degradation of the N Reactor SNF and persists in the WP so that only 26% of the initial Pu is lost (Table 15). Formation of NpO_2 also occurs during the rapid degradation of the N Reactor SNF but, it does not remain stable and is lost from the WP before 20,000 years. Instability of NpO_2 leads to a loss of ~98.5% of the Np from the WP (Table 15).
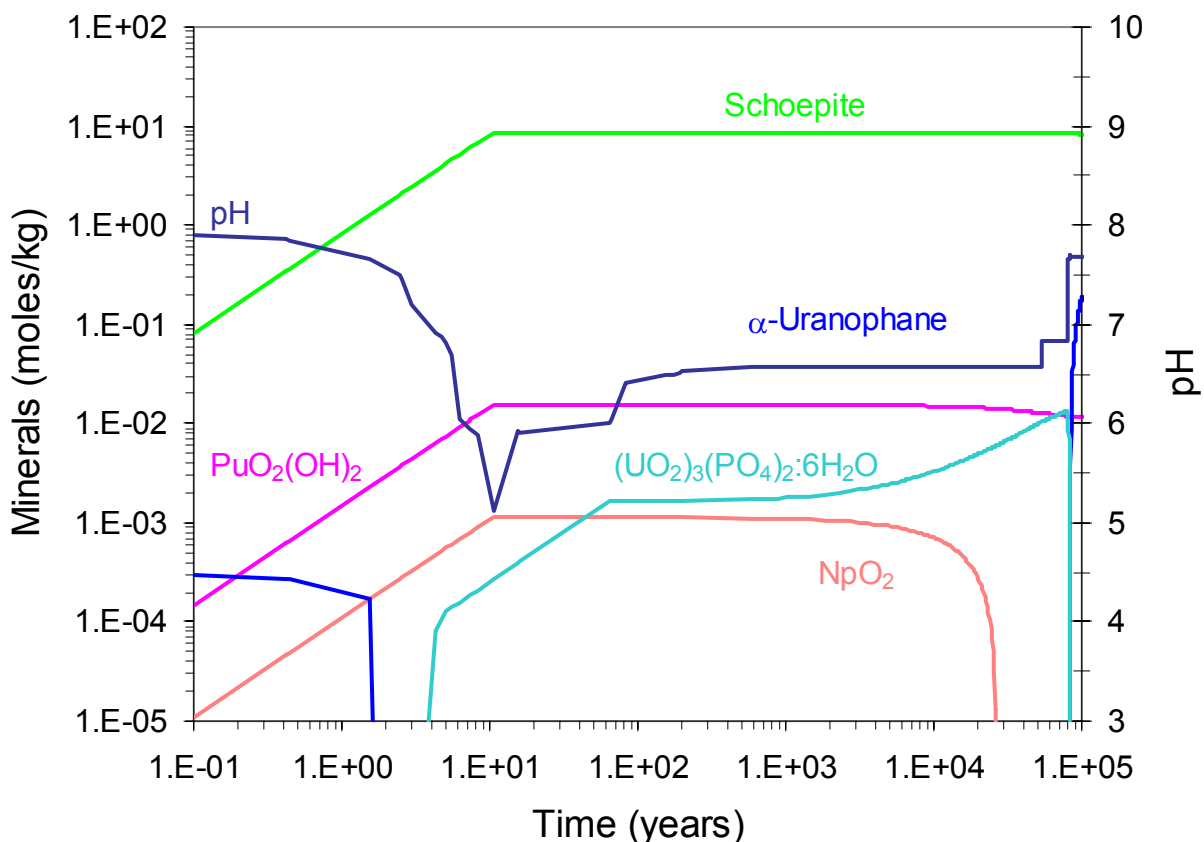
Output DTN: MO0201SPAGIN07.001

Figure 31. Radionuclide Mineral Formation and pH During N Reactor SNF Case 4

6.4.4 Sensitivity to Four MCOs and No HLW GPCs in the WP (Case 0)

Case 0 examines the effect of the average composition and mass (~17,694 kg) of N Reactor SNF in the DOE SNF inventory (DOE 2001a, Attached Electronic File) contained in four MCOs per WP (no HLW GPCs) with the same degradation and drip rate conditions as Case 2. Table 15 shows that slightly more U and Pu were retained in the WP under these conditions than for Case 2, while 45% more of the Np and all of the I and Tc were lost from the WP during Case 0. The minimum pH was more extreme (4.2) and the ionic strength was slightly higher for Case 0 than for Case 2.

Figure 32 shows the degradation of WP components and pH versus time from WP breach during the Case 0 simulation. Minimum pH values are caused by the degradation of N Reactor SNF,

the corrosion of the A516 carbon steel and the 304L Main MCO. Since there is twice as much fuel and larger amounts of A516 carbon steel and 304L stainless steel but no HLW glass in the WP for Case 0, the early period of low pH lasts longer and the pH minimum near 60,000 to 80,000 years is lower for Case 0 than for Case 2 (Figure 18).
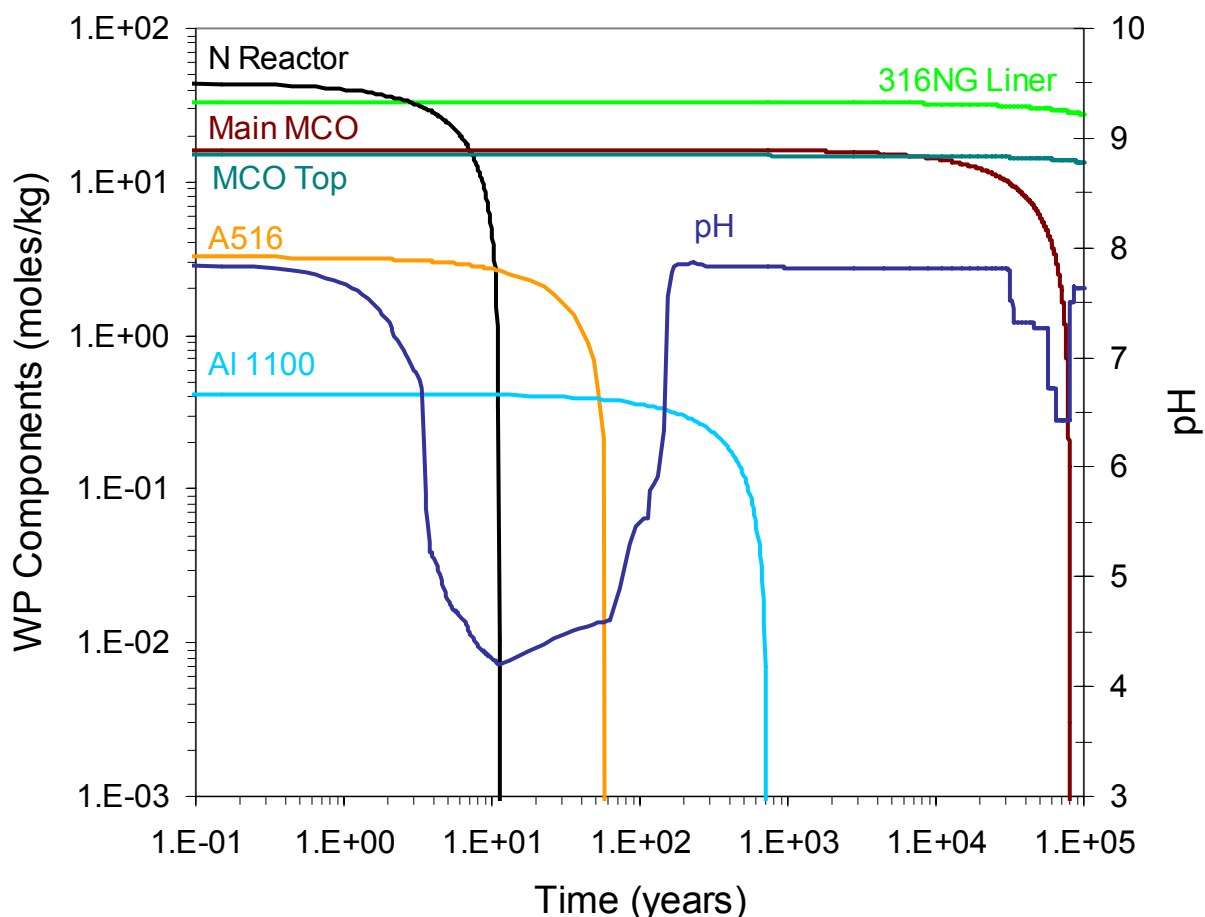
Output DTN: MO0201SPAGIN07.001

Figure 32. WP Components for N Reactor SNF During Case 0

Figure 33 presents the radionuclide minerals precipitating in this simulation. This figure is very similar to Figure 25 for Case 2, except that all the minerals are much more abundant, reflecting the larger amount of N Reactor SNF degrading. The most insoluble Pu mineral (PuO_2) was suppressed (see Assumption 5.4). The dominant U mineral is schoepite ($UO_3 \cdot 2H_2O$), with smaller amounts of uranyl phosphate hydrate (($UO_2)_3(PO_4)_2 \cdot 6H_2O$), and $CaUO_4$ also forming. Uranium solution concentration is dependent on the degradation rate of N Reactor SNF during the first 100 years after WP breach and then appears to be controlled by the solubilites of schoepite, uranyl phosphate hydrate and $CaUO_4$ (Figures 18 and 23). Plutonium solubility increases during the early period of low pH and then is controlled by formation of $PuO_2(OH)_2$ (Figures 18 and 21). Neptunium solubility also increases during the pH low at early times and then is controlled by formation of NpO_2 (Figures 18 and 20). The second pH minimum at about

60,000 to 80,000 years apparently causes partial dissolution of NpO_2, resulting in greater Np loss (~80%) in Case 0 compared to Case 2 (~35%) (Table 15, Figures 18 and 20). Since no I or Tc minerals are predicted to form, the WP solution concentrations of these two radionuclides are not solubility limited, but rather are controlled by the constant degradation rate of N Reactor SNF (Figures 19 and 22). Since all of the I and Tc in the N Reactor SNF is released into the WP solution at very early times in Case 0, the total loss of these radionuclides occurs before 1000 years after WP breach (Table 15, Figures 19 and 22).
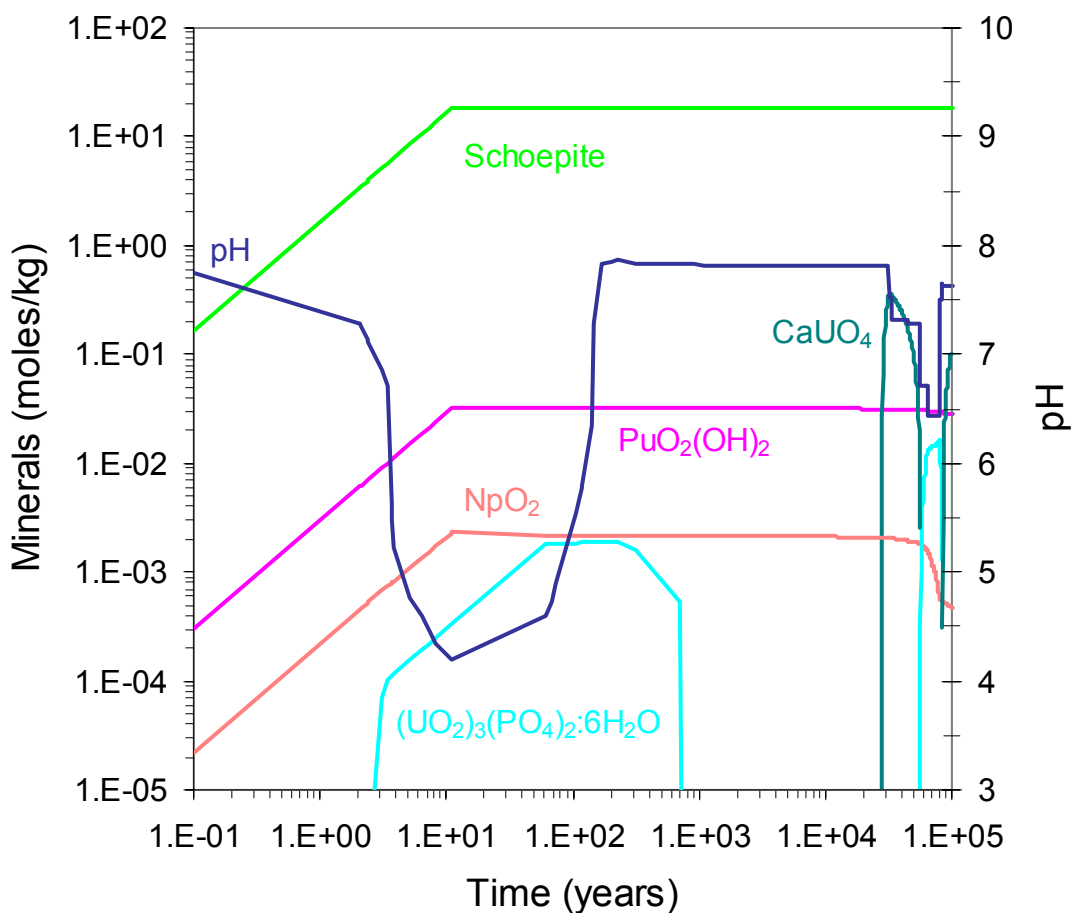
Output DTN: MO0201SPAGIN07.001

Figure 33. Radionuclide Mineral Formation and pH During N Reactor SNF Case 0

Figure 34 presents the results of Case 0, showing the major minerals and pH versus time after WP breach. Information about the minor minerals predicted to form during Case 0 is available in the "*.min_info.txt" files in the output DTN: MO0201SPAGIN07.001. The corrosion products of the steels and Al 1100 are the minerals $Fe(OH)_3$, Cr-ferrihydrite, trevorite ($NiFe_2O_4$), pyrolusite (MnO_2), gibbsite ($Al(OH)_3$) and the Fe-rich smectite, nontronite. Since the WP for Case 0 contains no HLW glass, the amount of nontronite forming is much smaller during Case 0 than during Case 2.
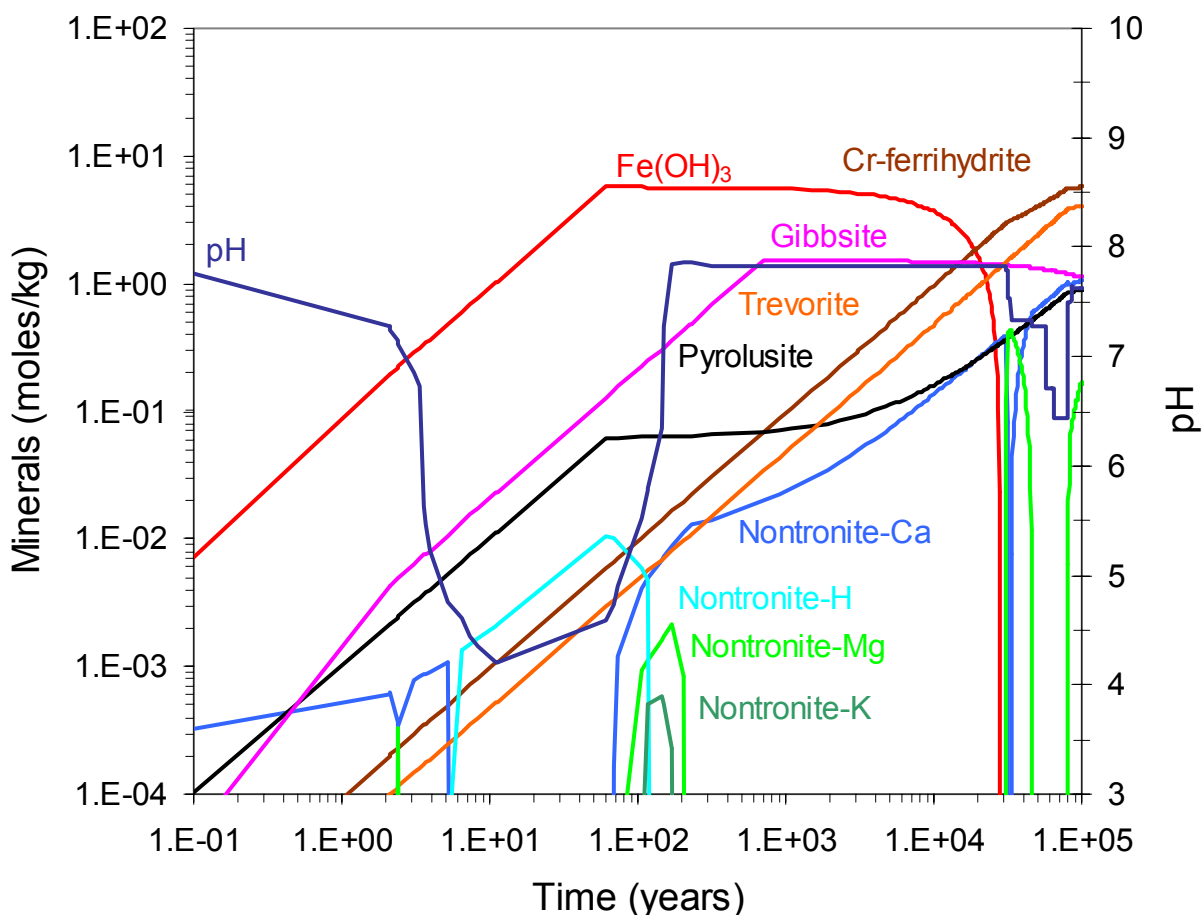
Output DTN: MO0201SPAGIN07.001

Figure 34. Major Mineral Formation During N Reactor SNF Case 0

6.4.5   Internal Criticality Case (Case 1)

In Case 2, the SNF is assumed (see Assumption 5.14) to consist of the average composition and
mass (~8847 kg) of N Reactor SNF in the DOE SNF inventory (DOE 2001a, Attached Electronic
File; modified for EQ6 input in workbook "Rn Fix 05.xls", sheet "DOE_SNF99 (Cat. 7)(2)",
output DTN: MO0201SPAGIN07.001) with 2 MCOs per WP. Case 1 evaluates a more
conservative loading, from a criticality perspective. The case of two MCOs, each containing five
304L baskets (each with 54 fresh Mark IA fuel elements, ~9609 kg), which is similar to some of
the internal criticality cases in CRWMS M&O (2001a, Attachment III). Table 15 indicates that
this case has a similar pH range and maximum ionic strength as the Base Case (Case 2). Case 1
retains more U, Np, I and Tc than Case 2, but less Pu. Since the fresh N Reactor fuel
composition is used for Case 1, the only source for I, Np, Pu and Tc is degradation of the HLW
glass. Table 15 indicates the same percentage of retention for these elements, probably an
indication that these elements are contained in the remaining HLW glass. Figures 19 through 22,
show that the concentrations of these elements are well below those of Case 2 for the first 100
years after WP breach. These radionuclides all have a short-term increase in concentration when

the pH drops increasing the HLW glass degradation rate. Beyond 100 years, I and Tc concentrations are similar to Case 2, while Np and Pu concentrations remain below those of Case 2 until the end of Case 1. The *min_info.txt files for Case 1 indicate that no precipitation of I, Tc, Np or Pu minerals occurred.

6.4.6   Two-Stage Simulation (Case 5)

Case 5 is a two-stage simulation that exposes the HLW glass, the A516 plates and MCO stands, the 304L HLW GPCs and the outer half of the 304L MCOs to degradation before the contents of the MCOs are exposed to J-13 water. Relatively high rates of degradation are used initially to remove all HLW glass before exposing the MCO contents; once the HLW glass is removed, moderate degradation rates are used for the remaining reactants. Table 15 shows that this case results in a higher ionic strength, slightly lower minimum pH and more retention of the U, Pu, and Np (compared to the Base Case), with complete loss of I and Tc from the WP.

Figure 18 shows that the early pH low is above pH 6 for Case 5 since there is no N Reactor SNF degrading during the first stage. This pH low lasts until the A516 steel components and the 304L GPCs are degraded and then rises as the degrading HLW glass has more influence on pH. The pH minimum for Case 5 occurs during complete degradation of the main MCO canisters and then rises to about 6.5 until the MCO top is completely degraded. This is similar to the pH profile of Case 3 except that the pH minimum is delayed and not as extreme since only half of the surface area of the MCO components is allowed to degrade during the first stage of Case 5. This effectively halves the degradation rate of the MCOs. The pH rises again to a plateau at ~7.6 until the 316NG liner is completely degraded. During the complete degradation of the remaining HLW glass, the pH spikes to the maximum value of 8.14 and then drops to ~7.8 as the first stage ends at 34,000 years.

The aqueous concentrations of all of the radionuclides are lower during the first stage of Case 5 than during the first part of Case 3, reflecting the degradation of only HLW glass (Figures 19 to 23). The concentration profiles of I, Np, Pu, and Tc are very similar during the first stage and are controlled solely by the HLW glass degradation rate (Figures 19 to 22). Since no minerals containing these elements form during the first stage (*.min_info.txt files for Case 5 in output DTN: MO0201SPAGIN07.001), all of the I, Np, Pu and Tc in the HLW glass are lost from the WP. Uranium solubility is controlled by the HLW glass degradation rate only at very early times (Figure 23). After ~10 years after WP breach, U solubility is controlled by the precipitation/dissolution of a series of U minerals including uranyl phosphate hydrate $((UO_2)_3(PO_4)_2 \cdot 6H_2O)$, Na-boltwoodite and α-uranophane (*.min_info.txt files for Case 5 in output DTN: MO0201SPAGIN07.001).

During the second stage, the pH is driven down to about 5.7 by the complete degradation of N Reactor SNF and Al 1100 and then rises to ~7.8 by the end of the simulation (Figure 18). The aqueous concentrations of all of the radionuclides increase at the beginning of the second stage of Case 5 reflecting the rapid degradation of N Reactor SNF (Figures 19 to 23). Uranium solubility during the second stage is controlled by the precipitation of schoepite and a small amount of $CaUO_4$ and dissolution of the U minerals that formed during the first stage of Case 5 (*.min_info.txt files for Case 5 in output DTN: MO0201SPAGIN07.001). After the initial concentration spike of Np and Pu concentration, the WP solution concentrations of these

elements in the second stage of Case 5 are controlled by formation of NpO_2 and $PuO_2(OH)_2$, respectively (Figures 20 and 21; *.min_info.txt files for Case 5 in output DTN: MO0201SPAGIN07.001). Since no minerals containing I and Tc form during the second stage (*.min_info.txt files for Case 5 in output DTN: MO0201SPAGIN07.001), they are completely lost from the WP (Table 15, Figures 19 and 22).

6.4.7 Sensitivity to O_2 Fugacity (Case 6)

The Base Case simulation assumed a fixed value for log O_2 fugacity as –0.7 (see Assumption 5.3). Case 6 evaluates the sensitivity of the simulations to reducing the log O_2 fugacity slightly to -10.0, such as might result from the chemical O_2 demand of steel corroding in a closed environment. Table 15 presents the effects of this change, more Np and Pu are retained in the WP during Case 6 than during Case 2. Figures 19 through 23 show that the predicted concentrations of I, Tc and U during Case 6 are very similar to those predicted for Case 2. Plutonium solution concentration is about an order of magnitude lower during most of Case 6 than during Case 2 (Figure 21). Neptunium concentration is at least 2 orders of magnitude lower in the WP solution during Case 6 than predicted for Case 2 (Figure 20). The change in the O_2 concentration allows NpO_2 and $PuO_2 \cdot 2H_2O$ to form early during Case 6, retaining the majority of the Np and Pu in the WP ("*.min_info.txt" files for Case 6 in output DTN: MO0201SPAGIN07.001). The change in the O_2 concentration also increases the pH minimum to 4.99, otherwise Case 6 is similar to the Base Case.

6.4.8 Effects of High Rates of Degradation with Average Flow (Case 7)

The Base Case assumed low rates of steel corrosion, glass dissolution and N Reactor SNF dissolution, while Case 3 evaluates the effects of high rates of dissolution and corrosion combined with low flow-through rates. Case 7 evaluates the effects of high rates of dissolution and corrosion combined with moderate flow-through rates. The results of this case are similar to those of Case 3, with a wide range of pH variation, high ionic strength and complete degradation of WP contents (Table 15 and Figure 26). After the SNF and HLW glass are exhausted, all of the radionuclides except U are flushed out of the WP (Figures 19 to 23; Table 15). Figure 18 shows that the faster drip rate during Case 7 causes the pH to rise to ~7.8 after the degradation of the 316NG liner is complete compared to a pH of only ~5.8 at the end of Case 3. Radionuclide mineral formation during Case 7 is similar to Case 3 (Figure 27 and "*.min_info.txt" files for Case 7 in output DTN: MO0201SPAGIN07.001) except that the higher pH at late times causes $(UO_2)_3(PO_4)_2 \cdot 6H_2O$ to be replaced with $CaUO_4$.

6.5 MELT AND DILUTE WASTE FORM

Table 17 presents a summary of the results for the M&D waste form, including the pH range, the maximum ionic strength, and the percentages of key radionuclides retained in the WP at the end of the simulation (100,000 years after WP breach). The complete output tables (aqueous, mineral, and total moles) for all the cases are included in the files associated with this analysis (output DTN: MO0201SPAGIN07.001).

Table 17. Results Summary for the M&D Waste Form (Group 9)

Case and Objective	EQ6 File Name(*.6I)	Percent of initial moles retained in WP					pH Range		Max Log Ionic Strength
		U	Pu	Np	I	Tc	Min	Max	
Case 0: Base Case + Ingot surface area X 10[a]	M01a1113 M01b1113	54.47	65.60	47.52	37.64	52.71	5.60	8.09	-2.08
Case 1: Criticality case[a]	M11a1113	76.21	70.39	70.39	70.39	70.39	5.76	8.09	-2.10
Case 2: Base Case[a]	M21a1113	54.51	65.65	47.56	37.67	52.76	5.75	8.09	-2.11
Case 3: Worst case: High rates, low flow[a]	M31a2222	0.00	0.00	0.00	0.00	0.00	5.00	9.58	-0.34
Case 4: Base Case with hematite and goethite not suppressed[b]	M41a1113	77.93	68.50	49.63	39.31	55.05	5.26	8.09	-1.91
Case 5: Base Case as two-stage[a] (DOE Canister contents untouched until HLW gone)[c]	M51a2204 M51b1012	22.51	0.00	0.00	0.00	0.00	6.53	8.45	-2.02
Case 6: Base Case[a] + low fO$_2$	M61a1113	53.82	67.10	97.87	37.20	52.09	5.68	8.17	-2.13
Case 7: Base Case[a] + High rates, avg. flow	M71a2223	0.00	0.00	0.00	0.00	0.00	5.48	8.94	-1.49

NOTES: [a]Suppresses: hematite, goethite, soddyite and PuO$_2$; includes added chromate and molybdate phases
[b]Suppresses the minerals soddyite and PuO$_2$; but not hematite or goethite which effectively excludes added chromate and molybdate phases.

For some of the M&D waste form cases examined in this analysis, the volume of remaining WP components and of corrosion products precipitated in the WP nearly reaches the volume of the WP before 100,000 years after WP breach. Table 18 presents the years after WP breach when the volume of the WP would be at least 2/3 full of solids and also the percentage of the WP volume filled with solids at the end of each M&D waste form case. For the portions of these cases after the time when the WP is about 2/3 full of solids Assumptions 5.8 and 5.9 may no longer be reasonable. On the other hand, the degradation rates of WP components would probably decrease if a thick layer of WP corrosion products separates them from the WP solution (See discussion in Assumptions 5.8 and 5.9) and this would slow the production of corrosion products.

Table 18 shows that the WP is not predicted to be totally filled with solids for any of the M&D cases by ~100,000 years after WP breach. For the cases with high degradation rates (Cases 3, 5 and 7) the WP is predicted to be nearly full of solids by ~100,000 years after WP breach. For all of the cases except Cases 4 and 6, the WP is predicted to be at least 2/3 full of solids before 200 years after WP breach. In Case 4, the WP volume is only slightly more than 2/3 filled at the end of the run. This is probably due mostly to the formation of hematite in this run instead of the Cr-ferrihydrite and Fe(OH)$_3$ which are allowed to form in all the other cases. The molar volume of hematite is smaller (30.274 cm^3/mole) than that of Cr-ferrihydrite (129 cm^3/mole) or Fe(OH)$_3$ (34.36 cm^3/mole) (file data0.trc in output DTN: MO0201SPAGIN07.001). The lower pH values predicted to occur during Case 4 (Figure 3) may also destabilize some of the corrosion product

solids that would otherwise form in the WP. The less rapid filling of the WP during Case 6 is probably due to the instability of some of the corrosion product solids in the slightly reducing environment caused by the lower $O_2(g)$ concentration used throughout this run.

Table 18. WP Volume Summary for the M&D Waste Form (Group 9)

Case	% WP Volume Filled with Solids	Years After WP Breach	% WP Volume Filled with Solids	Years After WP Breach
Case 0	76.7	136	85.2	100010
Case 1	66.3	55	85.6	100010
Case 2	65.7	60	85.2	100000
Case 3	67.3	52	96.4	100000
Case 4	66.0	25014	70.9	100000
Case 5	68.6	65	97.2	100020
Case 6	66.0	10741	80.9	100010
Case 7	76.5	99	98.1	100010

Figures 35 to 40 show the predicted variation of pH and WP solution concentrations of I, Np, Pu, Tc, and U during all of the M&D cases. Differences in radionuclide concentrations in the WP solution between the cases are dependent on several variables, some of which are: the degradation rates of the WP components; the J-13 drip rate; the solubilities of solid corrosion products; and the pH of the WP solution. These differences will be discussed on a case by case basis in the following sections.
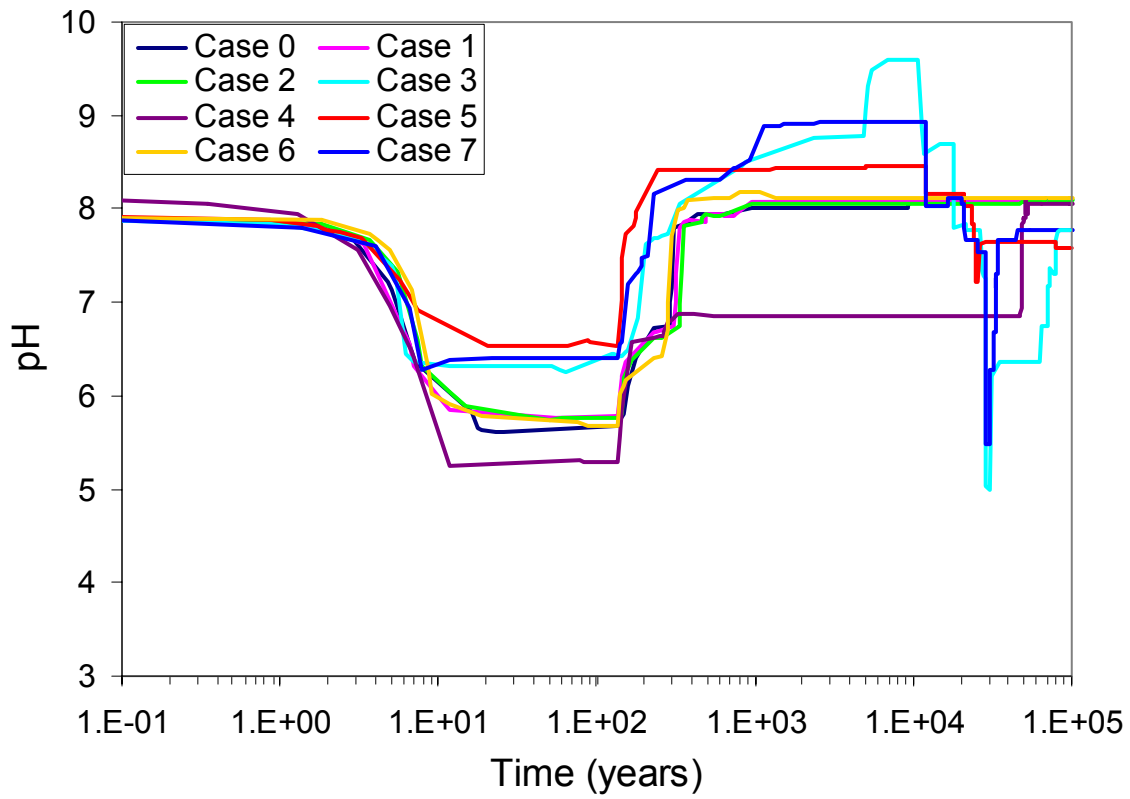
Output DTN: MO0201SPAGIN07.001

Figure 35. pH During M&D Cases
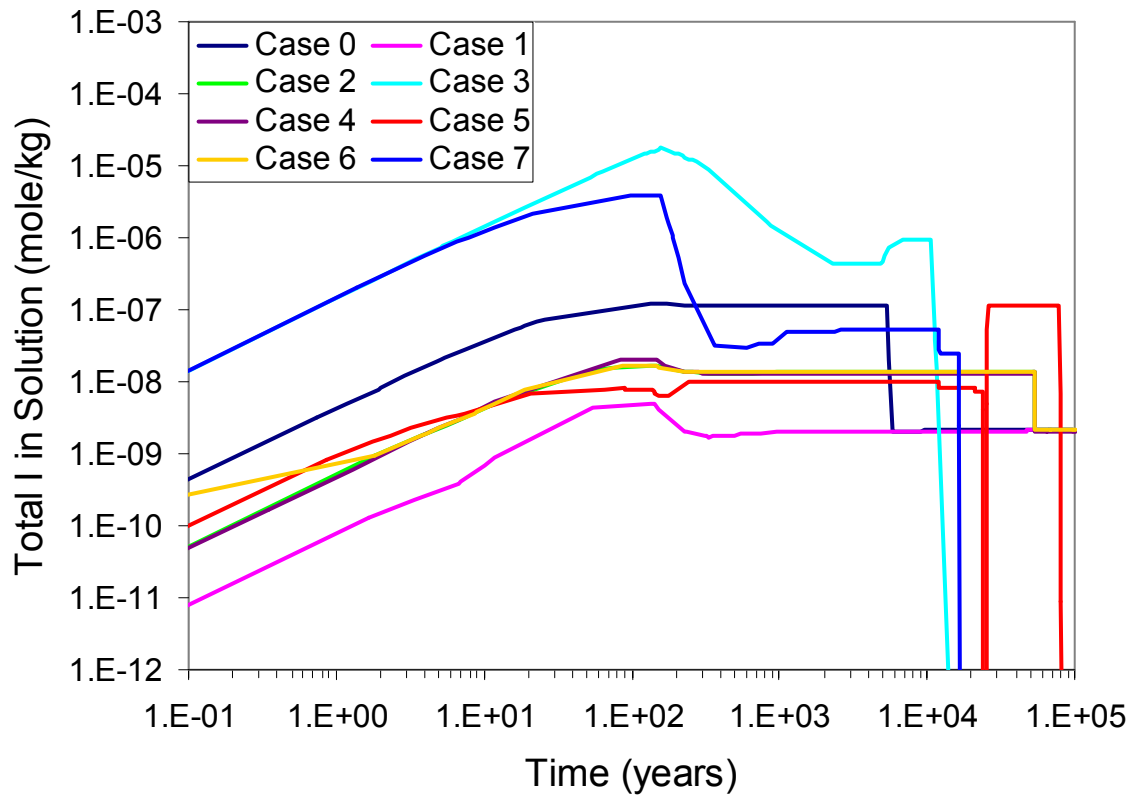
Output DTN: MO0201SPAGIN07.001

Figure 36. Total I in Solution During M&D Cases
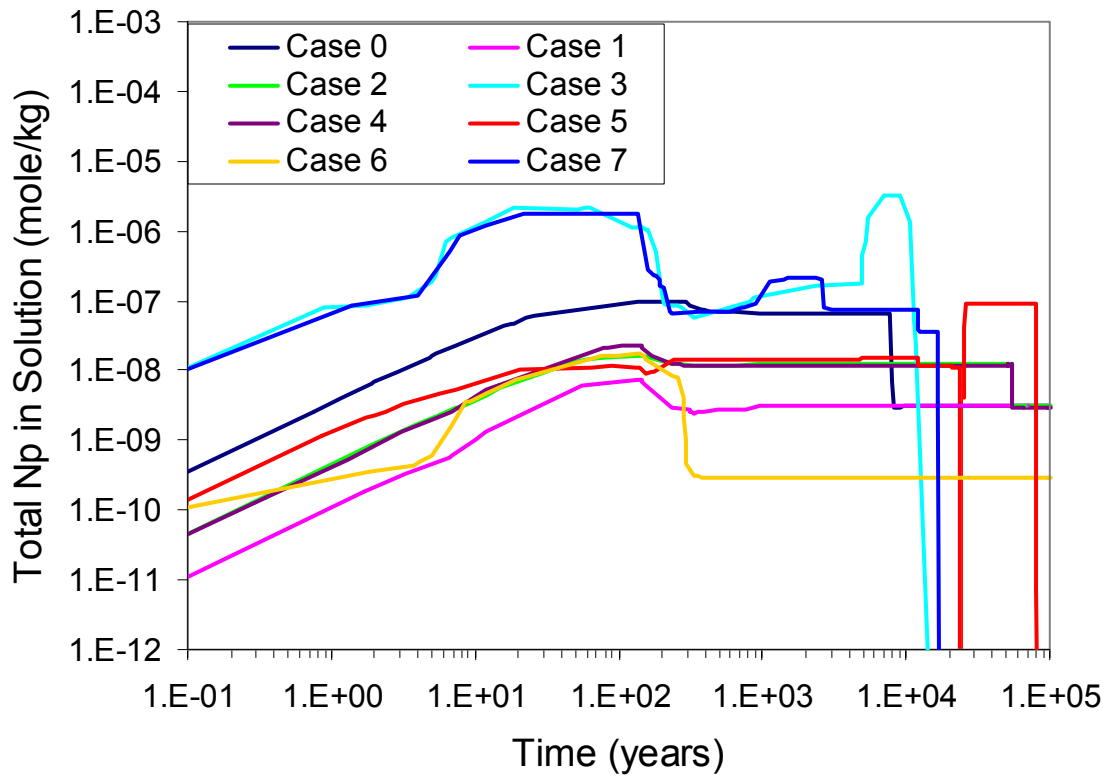
Output DTN: MO0201SPAGIN07.001

Figure 37. Total Np in Solution During M&D Cases
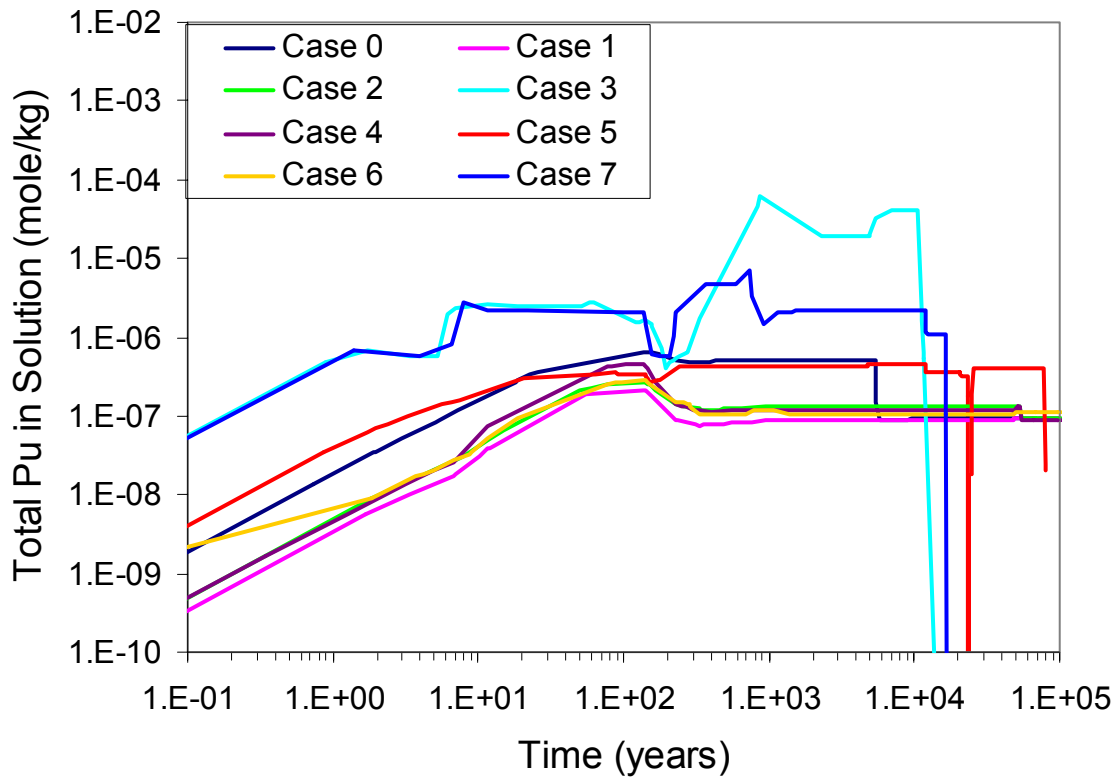
Output DTN: MO0201SPAGIN07.001

Figure 38. Total Pu in Solution During M&D Cases
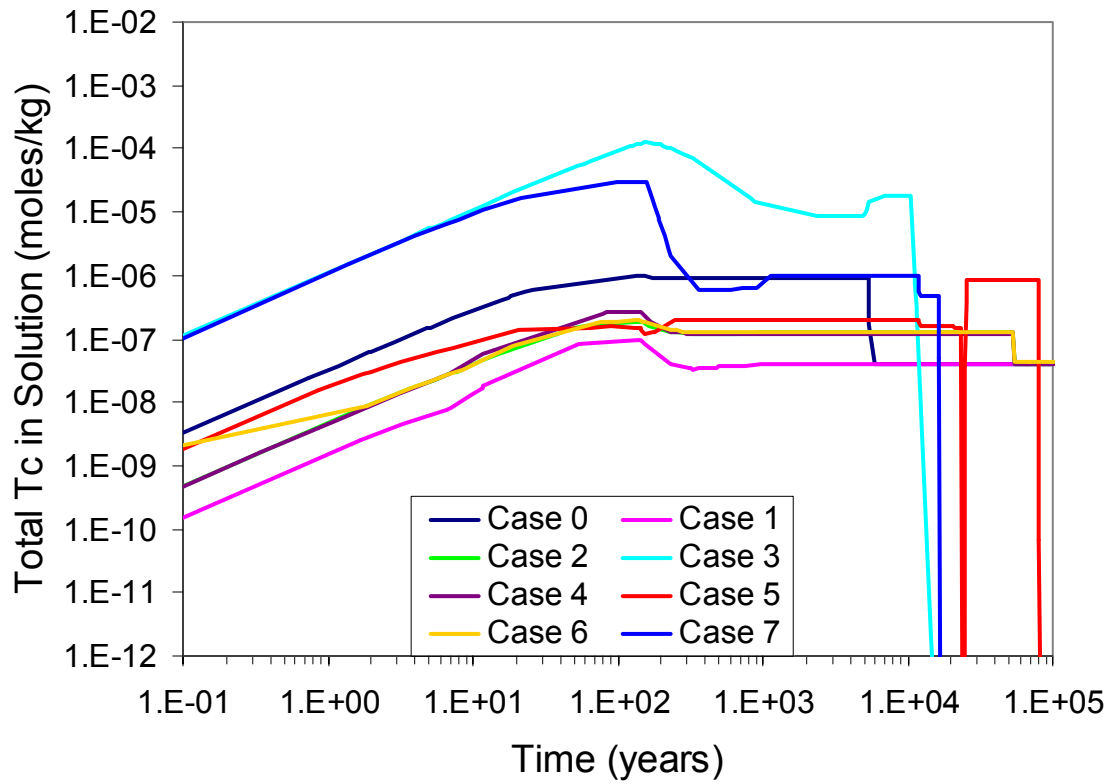
Output DTN: MO0201SPAGIN07.001

Figure 39. Total Tc in Solution During M&D Cases
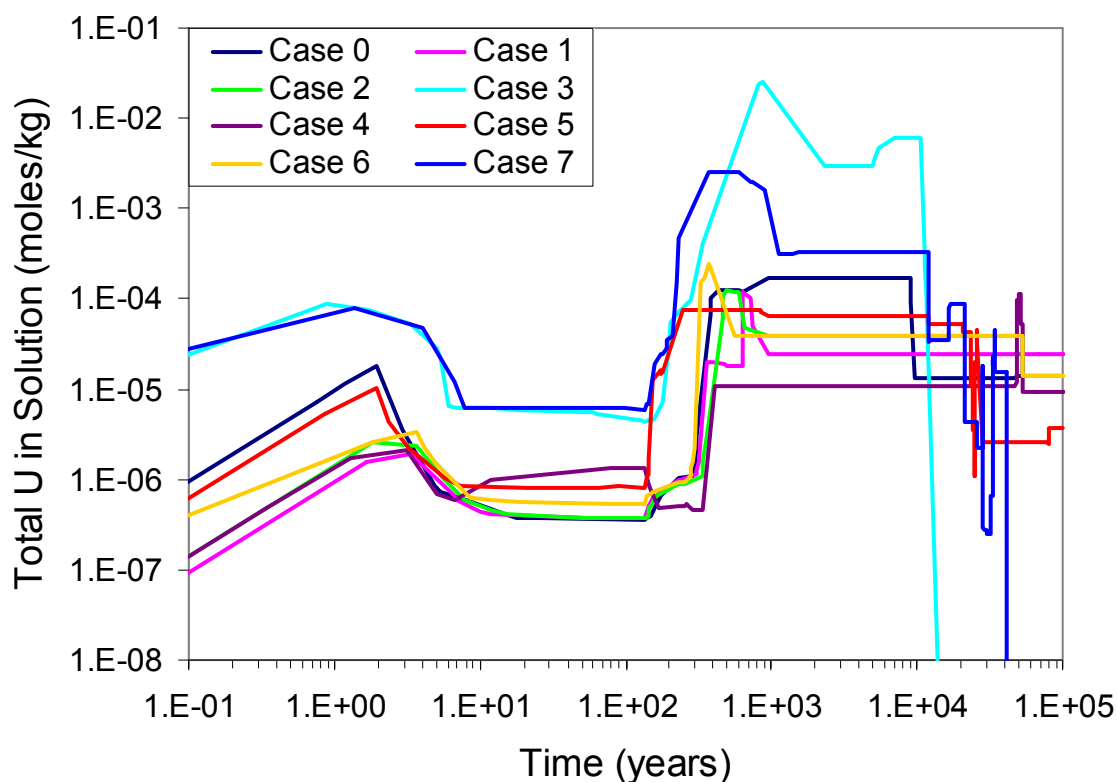
Figure 40. Total U in Solution During M&D Cases

6.5.1 Base Case (Case 2)

The Base Case is a single-stage simulation that examines WP chemistry under moderate rates of corrosion and dissolution, with the expected CO_2 and O_2 fugacities and an 80 mm/year infiltration rate. In this case the WP is assumed to be loaded with one M&D ingot having the average composition taken from the DOE SNF inventory for SNF Group 9 (DOE 2001a, Attached electronic file; see Assumption 5.14) and reduced to a form usable by EQ6 in workbook "Rn Fix 05.xls", sheet "DOE_SNF99 (Cat. 9)" (output DTN: MO0201SPAGIN07.001). Table 17 shows that losses from the M&D WP vary from ~35 to 60% of the initial moles of the radionuclides present during Case 2.

Figure 41 shows the degradation of WP components and pH versus time from WP breach of the Base Case simulation. The pH response at early times is dominated by the corrosion of A516 carbon steel, dropping to a minimum of 5.75 during complete degradation of the M&D ingot coating and remaining below 6 until the outer web is exhausted. After the A516 impact plates are exhausted, the pH rises and reaches a plateau just above 8. The maximum pH value of 8.09 is not reached until about 50,000 years after WP breach, when the DOE canister, the GPCs and M&D fuel are completely degraded.
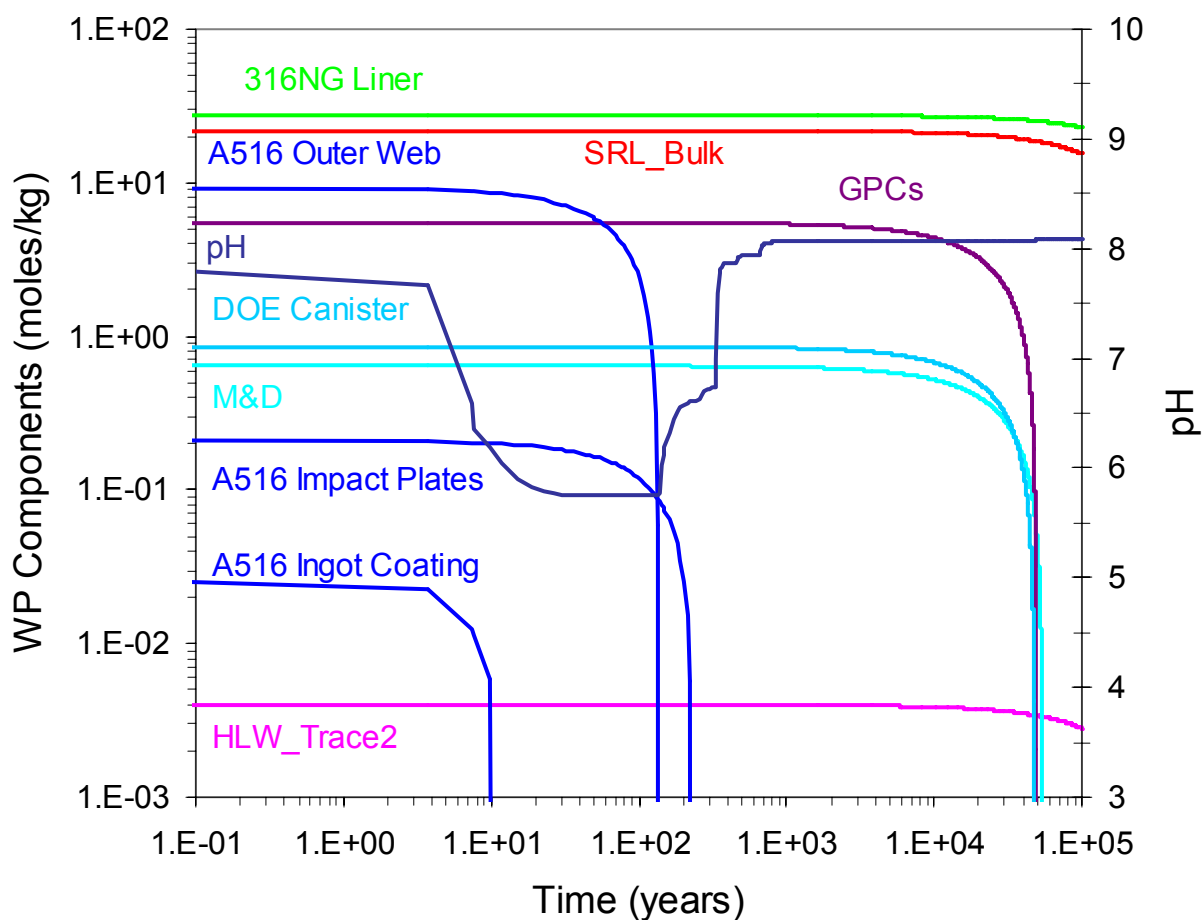
Output DTN: MO0201SPAGIN07.001

Figure 41. WP Components and pH for the M&D Waste Form During Case 2

Figure 42 presents the radionuclide and Gd minerals precipitating in this simulation that control the aqueous solubility of the radionuclides of interest. The most insoluble Pu mineral (PuO_2) was suppressed (see Assumption 5.4). Note that no Pu, Np, I, or Tc minerals form, thus these elements are not solubility limited and their aqueous concentrations are controlled by the degradation rates of the HLW glass and the SNF. The HLW glass degradation rates are pH-dependent, thus the aqueous concentrations of elements found in the HLW vary with pH (Figures 35 to 40). The dominant U minerals are uranyl phosphate hydrate ((UO_2)$_3$(PO_4)$_2$: $6H_2O$), and schoepite, but both of these minerals are unstable and dissolve before 1,000 years after WP breach when the pH rises above 8. Since no radionuclide minerals remain in the WP at the end of Case 2, the radionuclides retained in the WP must be contained in the remaining HLW glass (Table 17 and Figure 41).
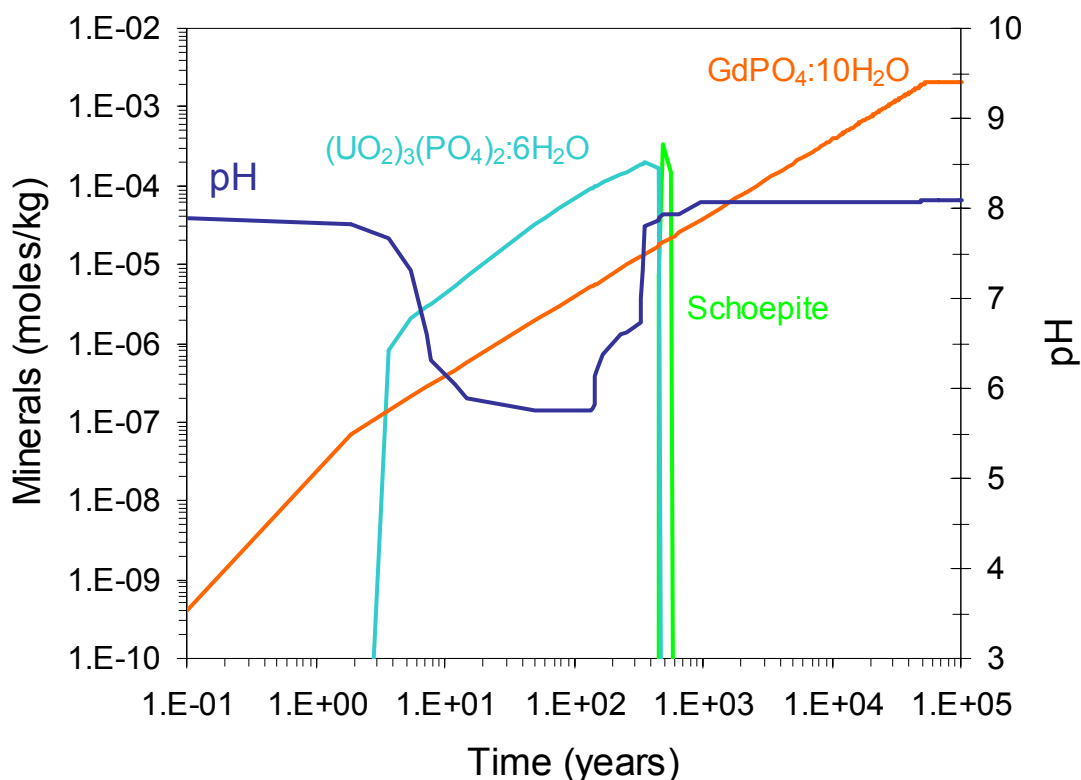
Output DTN: MO0201SPAGIN07.001

Figure 42. Radionuclide and Gd Mineral Formation and pH During M&D Case 2

Figure 43 presents additional results of this Base Case simulation, showing the major minerals and pH versus time from WP breach. Information about the minor minerals predicted to form during Case 2 is available in the "*.min_info.txt" files in the output DTN: MO0201SPAGIN07.001). The corrosion products of the steels and HLW glass are the minerals $Fe(OH)_3$, Cr-ferrihydrite, trevorite ($NiFe_2O_4$), pyrolusite (MnO_2), gibbsite ($Al(OH)_3$), and the Fe-rich smectites of the nontronite family (e.g., nontronite-Ca: $Ca_{0.165} Fe_2Al_{0.33}Si_{3.67}H_2O_{12}$).
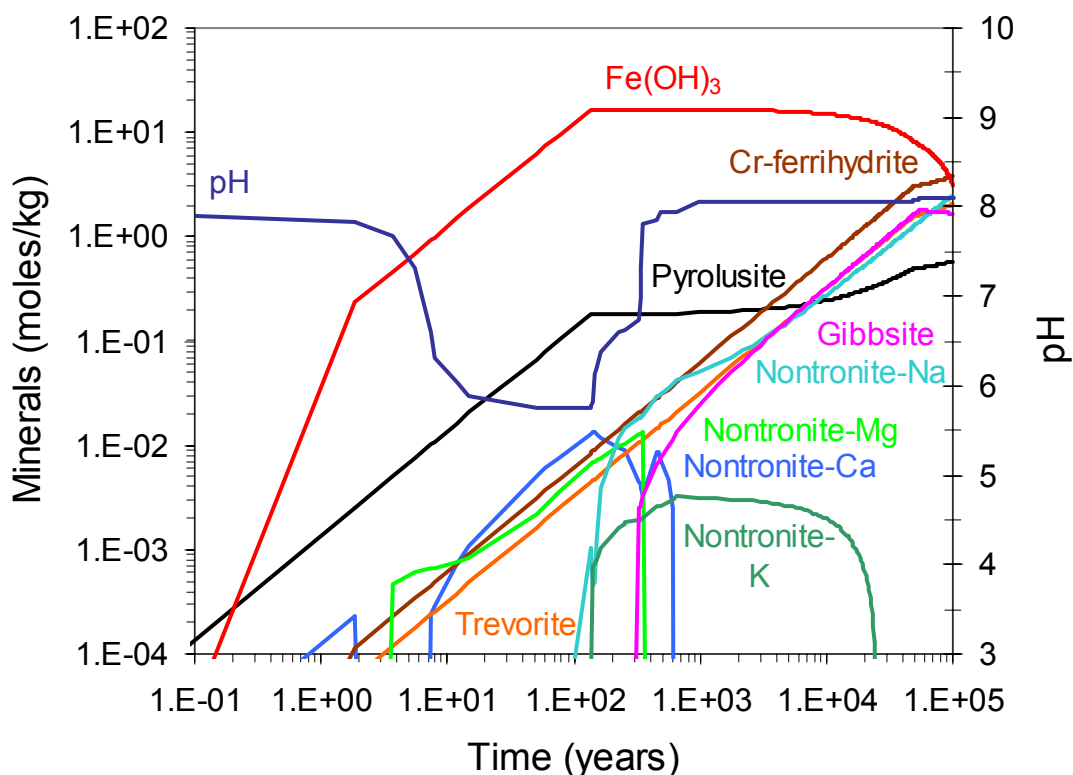
Figure 43. Major Mineral Formation During M&D Case 2

6.5.2 Effects of Increased M&D Ingot Surface Area (Case 0)

Case 0 is a closely related simulation that evaluates the impact of increasing the M&D ingot
surface area ten times under the same conditions as the Base Case (Case 2). This has the effect
of increasing the degradation rate of the M&D ingots tenfold, so that the waste form is
completely degraded by ~5,000 rather than ~50,000 years after WP breach (Figure 41). Table 17
shows that the loss of radionuclides of concern, the pH range and the ionic strength of Case 0 are
very similar to those of the Base Case. Figure 35 shows that the pH profile of Case 0 is also very
similar to that of Case 2. Figures 36 through 39, however, show that the aqueous concentrations
predicted for I, Np, Pu and Tc are about one order of magnitude higher than those for Case 2
until shortly after the M&D ingots are completely degraded. Uranium solution concentrations
are only higher than Case 2 at very early times and between ~1,000 and ~10,000 years after WP
package breach when U minerals are not stable (Figures 40 and 42). So, even though the results
in Table 17 are very similar for Case 2 and Case 0, radionuclide losses from the M&D WP
probably occur much earlier during Case 0.

6.5.3 Effects of High Rates of Degradation with Low Flow (Case 3)

The Base Case assumed average rates of steel corrosion, glass dissolution and M&D waste form
degradation. Case 3 evaluates the effects of high rates of dissolution and corrosion combined

with low flow rates, such as might occur at higher temperatures. The consequences of these rapid degradation rates are a wider range of pH variation (the highest and lowest pH simulated for the M&D waste form), the highest ionic strength, and complete loss of radionuclides from the WP (Table 17).

Figure 44 shows the degradation of WP components and pH versus time from WP breach during the Case 3 simulation. The degradation of the M&D ingots and corrosion of the A516 carbon steel, the 304L GPCs and the 316NG liner cause minimum pH values. There is complete degradation of all WP components by 30,000 years after WP breach.
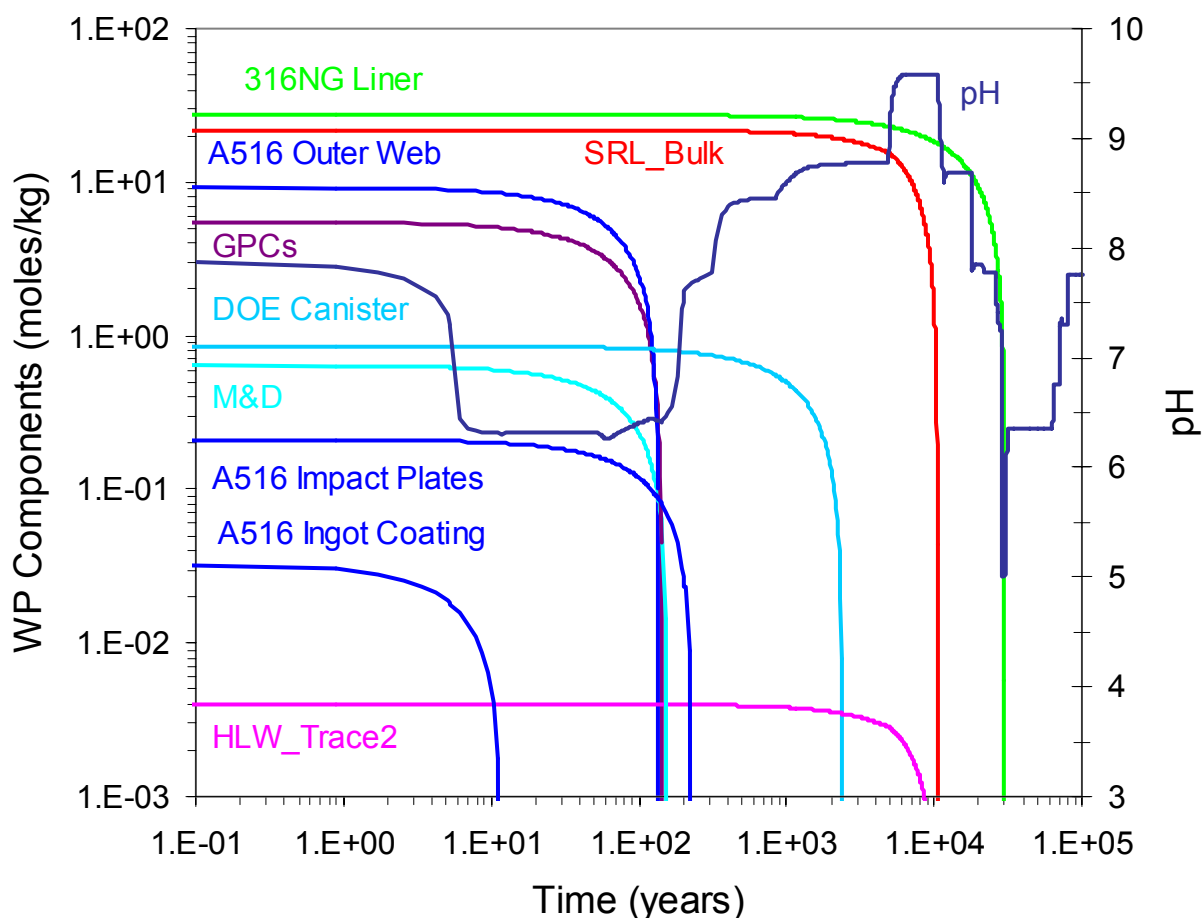
Output DTN: MO0201SPAGIN07.001

Figure 44. WP Components During M&D Case 3

Figure 45 presents the radionuclide and Gd minerals precipitating in this simulation. The dominant U minerals at early times in Case 3 are schoepite ($UO_3 \cdot 2H_2O$) and uranyl phosphate hydrate ((UO_2)$_3$(PO_4)$_2 \cdot 6H_2O$), which are replaced by $Na_2U_2O_7$ when the pH rises above 8. Uranium solution concentration is pH dependent, increasing when pH increases (Figures 35 and 40). No U minerals remain in the WP after 1000 years leading to complete loss of U from the WP after the HLW glass is completely degraded at 10,000 years (Figure 43). The most insoluble Pu mineral (PuO_2) was suppressed (see Assumption 5.4). Plutonium solubility increases during

the early period of low pH and is partially controlled by formation of $PuO_2(OH)_2$ (Figures 35 and 38). $PuO_2(OH)_2$ becomes unstable as the pH rises above 8 and dissolves completely before 1000 years after WP breach. Total loss of Pu from the WP occurs after the HLW glass is completely degraded at 10,000 years (Figures 38 and 43). Neptunium solubility also increases during the early pH low and is partially controlled by formation of NpO_2 (Figures 35 and 37). NpO_2 becomes unstable during the period of extremely high pH between 5,000 and 10,000 years after WP breach and is replaced with $KNpO_2CO_3$, which is stable as long as the level of dissolved carbonate is high and while sufficient Np is available from HLW glass dissolution (Figure 43). Since no I or Tc minerals are predicted to form, the WP solution concentrations of these two radionuclides are not solubility limited, but rather are controlled by the pH-dependent degradation rate of the HLW glass and the constant degradation rate of the M&D ingots (Figures 36 and 39). Since all of the I and Tc in the M&D ingots is released into the WP solution before 200 years after WP breach in Case 3, most of the loss of these radionuclides occurs before 1000 years after WP breach and total loss of I and Tc occurs after complete degradation of the HLW glass (Table 17, Figures 36, 39 and 43).
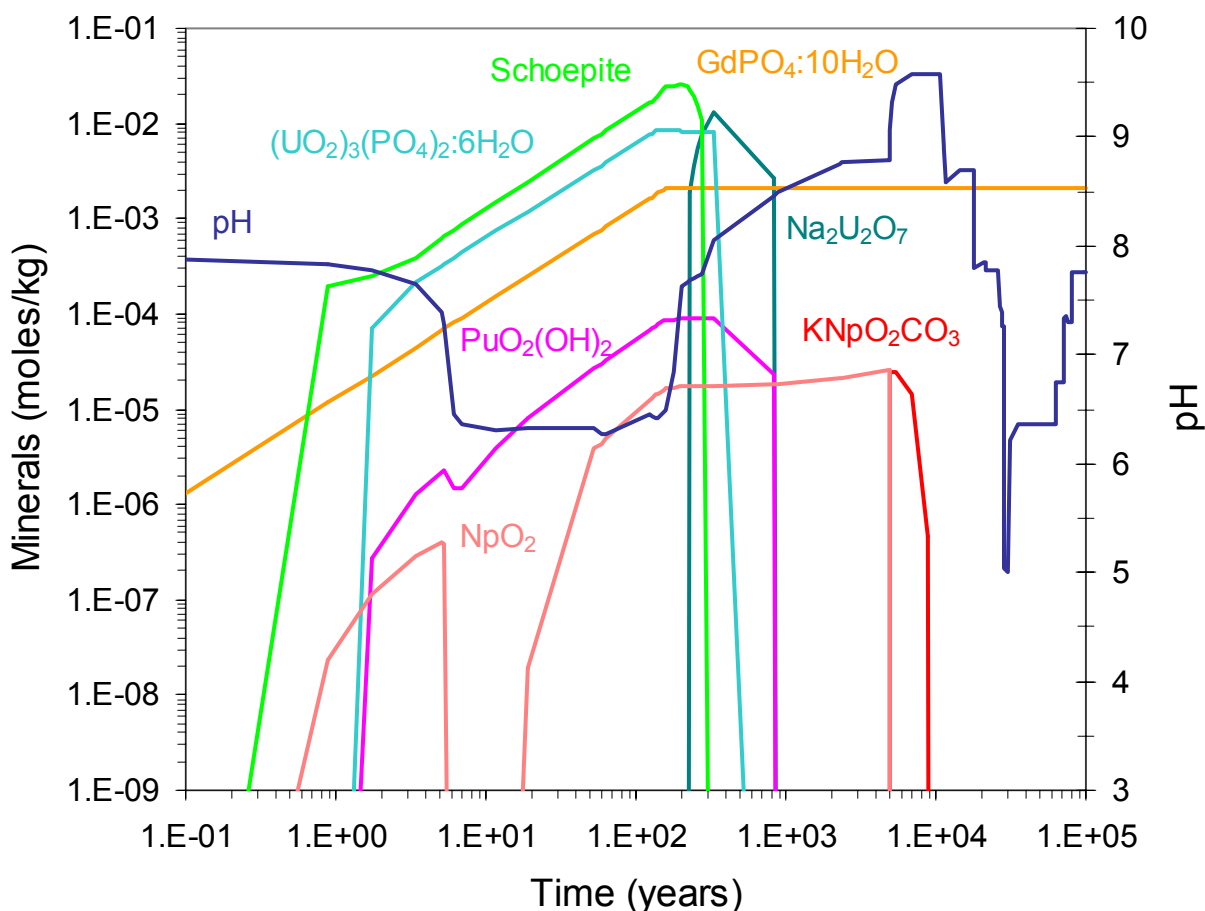
Output DTN: MO0201SPAGIN07.001

Figure 45. Radionuclide and Gd Minerals and pH During M&D Case 3

Figure 46 presents additional results of Case 3, showing the major minerals and pH versus time after WP breach. Information about the minor minerals predicted to form during Case 3 is available in the "*.min_info.txt" files in the output DTN: MO0201SPAGIN07.001. The corrosion products of the steels and HLW glass are the minerals $Fe(OH)_3$, Cr-ferrihydrite, trevorite ($NiFe_2O_4$), pyrolusite (MnO_2), gibbsite ($Al(OH)_3$), and the Fe-rich smectites of the nontronite family (e.g., nontronite-Ca: $Ca_{0.165} Fe_2Al_{0.33}Si_{3.67}H_2O_{12}$). During the period of high pH between 5,000 and 10,000 years after WP breach, gibbsite is replaced by dawsonite ($NaAlCO_3(OH)_2$).
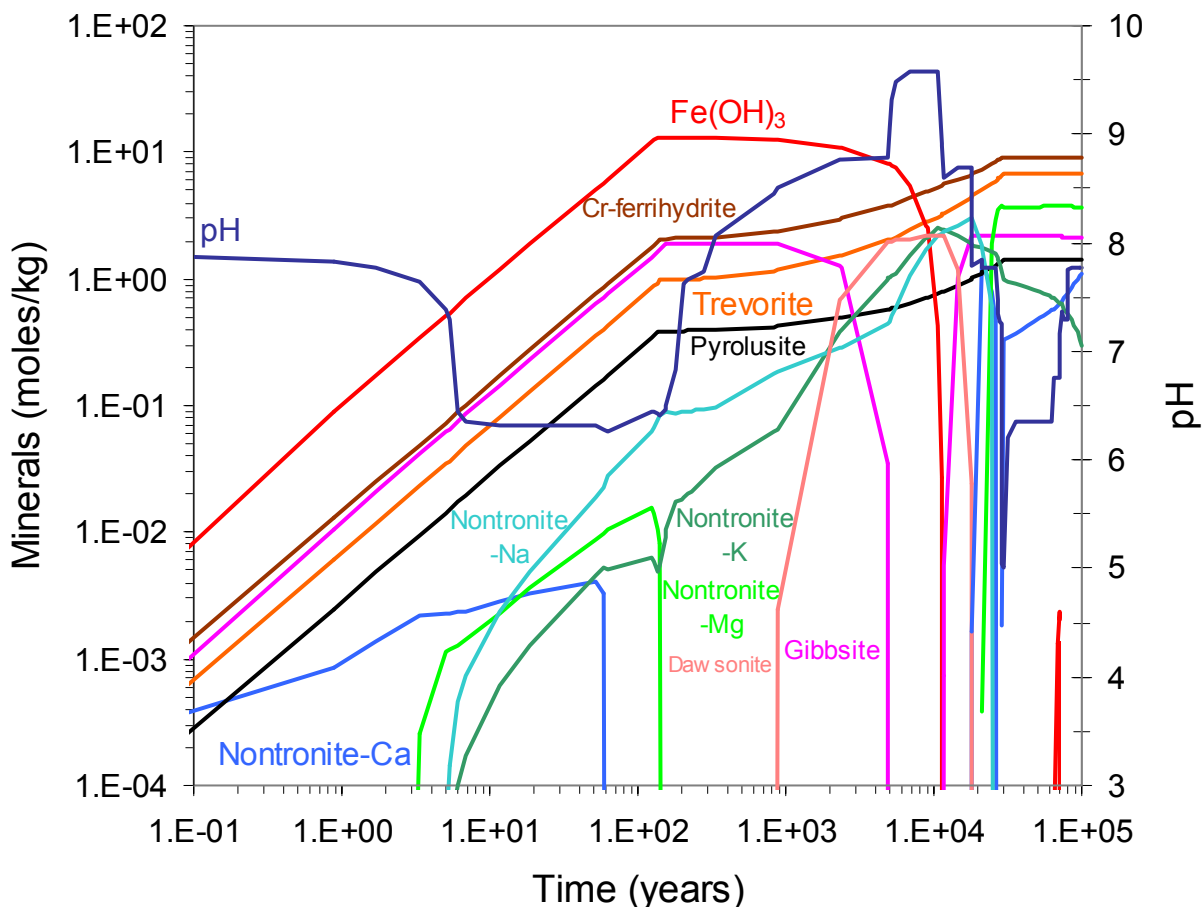
Output DTN: MO0201SPAGIN07.001

Figure 46. Major Mineral Formation During M&D Case 3

6.5.4 Sensitivity to Hematite Formation (Case 4)

The rapid glass dissolution and steel corrosion combined with low flow rates of Case 3 required redefining the data0.ymp database to include a series of Cr-rich minerals and the suppression of hematite and goethite. Case 4 evaluates the effects of not suppressing hematite and goethite (essentially allowing hematite to form) under the same conditions as the Base Case (i.e., as in Case 2, with moderate rates of degradation for HLW glass and steels). Table 17 shows that the

minimum pH is lower than the Base Case and that the percentages of initial moles of I, Np, Pu and Tc retained are slightly higher and that much more U is retained during Case 4.

Figure 47 shows that the major minerals are different as a result of these changes, with hematite replacing Fe hydroxide ($Fe(OH)_3$) and Cr-ferrihydrite. Trevorite ($NiFe_2O_4$), pyrolusite (MnO_2), gibbsite ($Al(OH)_3$), mesolite ($Na_{0.676}Ca_{0.657}Al_{1.99}Si_{3.01}O_{10} \cdot 2.647H_2O$), and the Fe-rich smectites of the nontronite family (e.g., nontronite-Ca: $Ca_{0.165}Fe_2Al_{0.33}Si_{3.67}H_2O_{12}$) also form during Case 4. Information about the minor minerals predicted to form during Case 4 is available in the "*.min_info.txt" files in the output DTN: MO0201SPAGIN07.001.
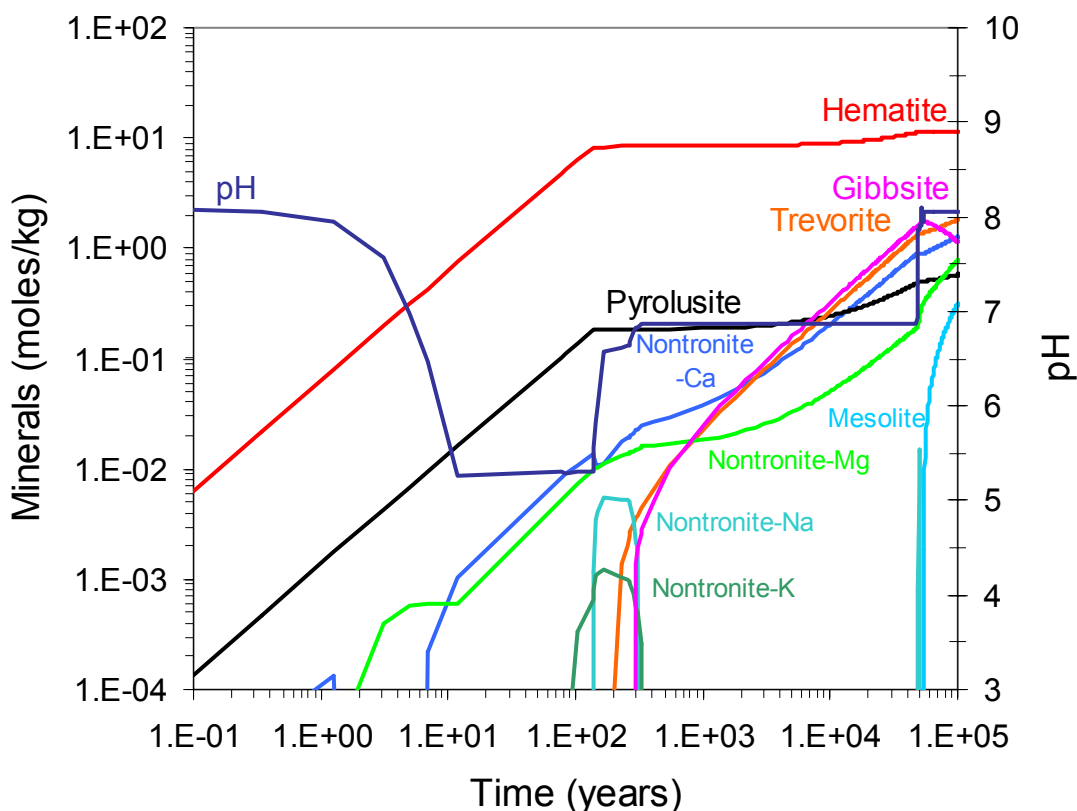
Output DTN: MO0201SPAGIN07.001
Figure 47. Major Mineral Formation During M&D Case 4

Figure 48 presents the radionuclide and Gd minerals precipitating in this simulation that control the aqueous solubility of the radionuclides of interest. The most insoluble Pu mineral (PuO_2) was suppressed (see Assumption 5.4). Note that no Pu, Np, I, or Tc minerals form, thus these elements are not solubility limited and their aqueous concentrations are controlled by the degradation rates of the HLW glass and the SNF. The HLW glass degradation rates are pH-dependent, thus the aqueous concentrations of elements found in the HLW vary with pH (Figures 35 to 40). Figure 35 shows that during the early pH low and from ~300 to ~50,000 years after WP breach, that the pH during Case 4 is at least 0.5 to 1 pH unit lower than during Case 2. The main result of the lower pH is that the total amount of U minerals that form is larger and the

duration of U mineral stability increases. The dominant U minerals are uranyl phosphate hydrate ($(UO_2)_3(PO_4)_2$: $6H_2O$) and schoepite, these minerals are stable until ~50,000 years after WP breach when the pH rises above 8 and they are replaced with $CaUO_4$. Since more uranyl phosphate hydrate ($(UO_2)_3(PO_4)_2$: $6H_2O$) and schoepite form and $CaUO_4$ remains in the WP at the end of Case 4, more U is retained in the WP than during Case 2 (Table 17).
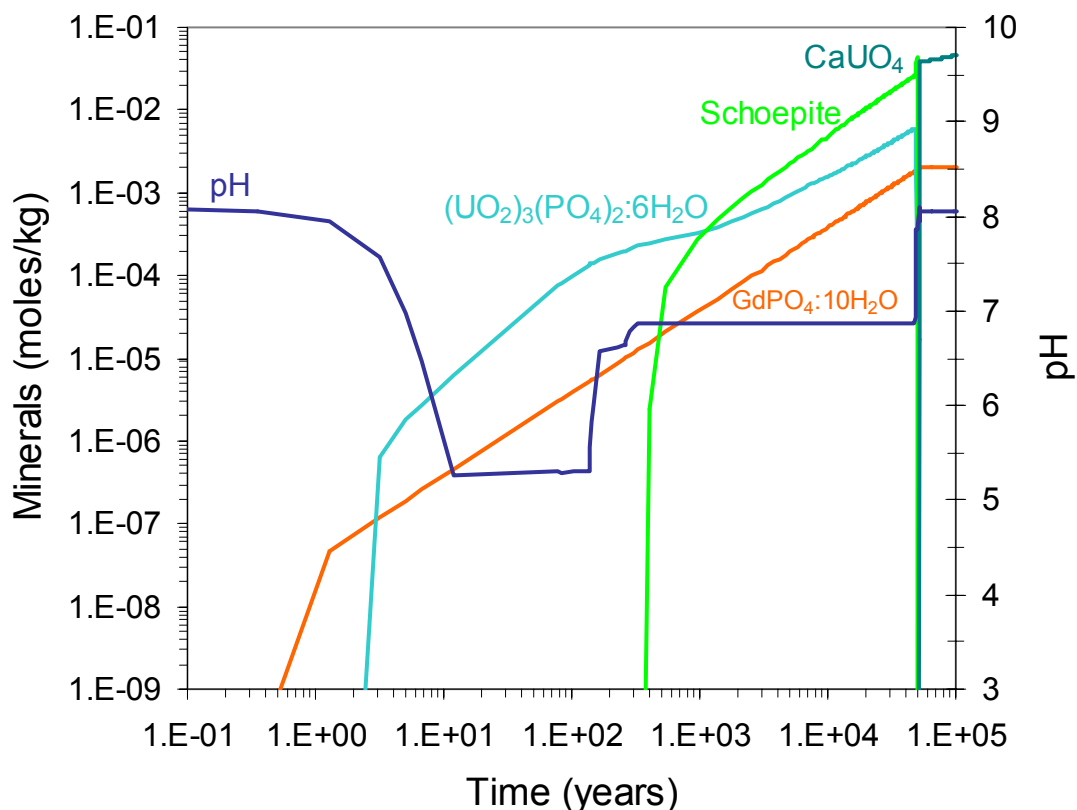
Output DTN: MO0201SPAGIN07.001

Figure 48. Radionuclide and Gd Mineral Formation and pH During M&D Case 4

6.5.5 Internal Criticality Case (Case 1)

The expected loading scenario assumes (see Assumptions 5.14) the average composition of one M&D ingot taken from the DOE SNF inventory for SNF Group 9 (DOE 2001a, Attached electronic file) and reduced to a form usable by EQ6 in workbook "Rn Fix 05.xls", sheet "DOE_SNF99 (Cat. 9)" (output DTN: MO0201SPAGIN07.001). Case 1 evaluates the in-WP chemistry for a more conservative loading from a criticality perspective, a WP with 5 M&D ingots (BSC 2001b, Tables 3 and 11). Table 17 indicates that this case has a similar pH range and maximum ionic strength as the Base Case (Case 2). Figure 35 shows that the pH profile during Case 1 is also very similar to that of Case 2. All of the radionuclides are retained in the WP to a greater extent during Case 1 than during Case 2 (Table 17) which is conservative for internal WP criticality. The change in fuel composition decreases the amounts of soluble I, Np, Pu, Tc, and U available for loss from the WP, compared to Case 2. Similar to Case 2, no

radionuclide minerals remain in the WP by 100,000 years after WP breach (output DTN: MO0201SPAGIN07.001 "m11a1113.min_info.txt" and Figure 42) so that the radionuclides retained in the WP are in the remaining HLW glass (Figure 41).

6.5.6   Two-Stage Simulation (Case 5)

Case 5 is a two-stage simulation that allows the HLW glass, the outer web, and the stainless steel GPCs to degrade completely before the contents of the DOE SNF canister are exposed to J-13 water. Relatively high rates of degradation are used initially to remove all HLW glass before exposing the DOE SNF canister contents. Once the HLW glass is removed, moderate degradation rates are used for the remaining reactants. Table 17 shows that this case results in a more alkaline pH range than Case 2 with increased loss of U and the complete loss of I, Np, Pu, and Tc from the WP.

The aqueous concentrations of all of the radionuclides are lower during the first stage of Case 5 than during the first part of Case 3, reflecting the degradation of only HLW glass (Figures 36 to 40). The concentration profiles of I, Np, Pu, and Tc are very similar during the first stage and are controlled solely by the HLW glass degradation rate (Figures 36 to 39). Since no minerals containing these elements form during the first stage ("m51a2204.min_info.txt" file in output DTN: MO0201SPAGIN07.001), all of the I, Np, Pu and Tc in the HLW glass are lost from the WP. Uranium solubility is controlled by the HLW glass degradation rate only at very early times (Figure 40).   After ~10 years after WP breach, U solubility is controlled by the precipitation/dissolution of a series of U minerals including uranyl phosphate hydrate $((UO_2)_3(PO_4)_2 \cdot 6H_2O)$, Na-boltwoodite, $CaUO_4$ and α-uranophane ("m51a2204.min_info.txt" file in output DTN: MO0201SPAGIN07.001).

The aqueous concentrations of all of the radionuclides, except U, increase at the beginning of the second stage of Case 5 reflecting the degradation of the M&D ingots (Figures 36 to 40). Uranium solubility during the second stage is controlled by the precipitation of small amounts of schoepite and $CaUO_4$ and dissolution of the U minerals that formed during the first stage of Case 5 ("m51b1012.min_info.txt" file in output DTN: MO0201SPAGIN07.001). Since no minerals containing I, Np, Pu, and Tc form during the second stage ("m51b1012.min_info.txt" file in output DTN: MO0201SPAGIN07.001), they are completely lost from the WP (Table 17, Figures 36 through 39).

6.5.7   Sensitivity to O_2 Fugacity (Case 6)

The Base Case simulation assumed a fixed value for log O_2 fugacity as –0.7 (see Assumption 5.3). Case 6 evaluates the sensitivity of the simulations to reducing the log O_2 fugacity to -10.0, such as might result from the chemical O_2 demand of steel corroding in a closed environment. Table 17 presents the effects of this change. In comparison to the Base Case, the pH range is similar and similar percentages of radionuclides are retained, except for Np and Pu. Figures 35 through 40 show that the predicted pH and the concentrations of I, Pu, Tc and U during Case 6 are very similar to those predicted for Case 2. Neptunium concentration is one to two orders of magnitude lower in the WP solution after ~300 years during Case 6 than predicted for Case 2 (Figure 37). The change in the O_2 concentration allows NpO_2 and $PuO_2 \cdot 2H_2O$ to form early

during Case 6, retaining the majority of the Np and slightly more Pu (compared to Case 2) in the WP (output DTN: MO0201SPAGIN07.001 "m61a1113.min_info.txt" and Table 17).

6.5.8   Effects of High Rates of Degradation with Average Flow (Case 7)

The Base Case assumed low rates of steel corrosion, glass dissolution and M&D waste form dissolution, while Case 3 evaluates the effects of high rates of dissolution and corrosion combined with a low flow-through rate. Case 7 evaluates the effects of high rates of dissolution and corrosion combined with the same flow rate as in Case 2. The results of Case 7 are similar to Case 3, but with a slightly narrower range of pH variation, lower ionic strength and complete degradation of WP contents (Table 17 and Figure 35). Radionuclide mineral formation during Case 7 is similar to Case 3 (Figure 45 and "m71a2223.min_info.txt" file in output DTN: MO0201SPAGIN07.001) except that the pH does not rise high enough to form $KNpO_2CO_3$ and $Na_2U_2O_7$ is replaced with $CaUO_4$. After the HLW glass and SNF are exhausted, the radionuclides are flushed out, and no radionuclide minerals remain in the WP at late times (Table 17 and "m71a2223.min_info.txt" file in output DTN: MO0201SPAGIN07.001).

7. CONCLUSIONS

7.1 SUMMARY OF SCIENTIFIC ANALYSIS

This analysis evaluated various cases that explore the chemical interactions of J-13 well water with three DOE SNF groups inside co-disposal DOE SNF WPs with HLW glass . The simulation of the interaction of water with SNF was conducted using EQ3/6 and an associated thermodynamic database. The software was used within its approved limits and without modification. Minor additions to the database data0.ymp.R0 permitted defining pH-dependent rate laws for certain WP components and allowed the precipitation of Cr- and Mo-bearing minerals in the WP. All input and output is included in the files associated with this analysis (output DTN: MO0201SPAGIN07.001).

The dominating controls on the system are the input degradation and drip rates, as well as the assigned fugacities of atmospheric gases (CO_2 and O_2). Note that uncertainty in the drip rates and dissolution rates of the various WP materials is dealt with by using a range of high and low values. Steel degradation generates protons that decrease the system pH, while degradation of HLW glass increases alkalinity, which produces high pH conditions. At high J-13 water drip rates, the duration of these pH changes is decreased, so that near neutral (~7) pH values are more dominant over long time periods. Fixing the O_2 fugacity to atmospheric levels insures that the environment inside the WP is consistently oxidizing. Decreasing the O_2 fugacity tends to moderate and raise the system pH and allows NpO_2 to precipitate (thus helping to retain Np in the WP). In general, the predicted pH is initially low while the steels corrode, and then later elevated as the HLW glass adds alkalinity, increasing the late-time pH.

The predicted WP degradation product mineralogy is dominated by metal oxides (chiefly of Fe) and smectite-type clay minerals. The dominant mineral precipitate is $Fe(OH)_3$ or Cr-ferrihydrite in most of the simulated cases, followed by trevorite, nontronite and pyrolusite. For WPs that contained Al components (Al spacers for N Reactor and Al in the M&D ingots) the precipitation of relatively large amounts of gibbsite was predicted. Chalcedony (SiO_2) formed during cases run with FSV WPs.

The dominant U minerals vary with each DOE SNF group. During cases simulating the degradation of FSV SNF, the precipitation of uranyl phosphate hydrate $((UO_2)_3(PO_4)_2 \cdot 6H_2O)$, Na-boltwoodite, α-uranophane and schoepite was predicted. Schoepite is the major predicted degradation product of N Reactor SNF with smaller amounts of uranyl phosphate hydrate, $CaUO_4$, and α-uranophane also forming. Degradation of the M&D waste form led to precipitation of uranyl phosphate hydrate, schoepite, $CaUO_4$, and $Na_2U_2O_7$. In some cases, the minerals $PuO_2(OH)_2$ (or $PuO_2 \cdot 2H_2O$ for log O_2 fugacity = $^-$10) and NpO_2 were predicted to precipitate, limiting the solubility of Pu and Np. Mineral precipitates containing Tc and I are not predicted to form under these conditions. High or total losses of these two elements were predicted for all the N Reactor SNF cases except Case 1, the criticality case.

Complete loss of radionuclides from the WP before 30,000 years after WP breach was predicted for cases with high degradation rates and 20 or 80 mm/year infiltration rates (Cases 3 and 7). Exceptions were Th, which was mostly retained during degradation of FSV SNF with an 80

mm/year infiltration rate, and U, which was mostly retained during degradation of N Reactor SNF WPs during every case.

The two-stage cases (Case 5) also predicted large losses of all the radionuclides from DOE SNF WPs. Exceptions included Th, which was mostly retained during degradation of FSV SNF WPs, and Np, Pu, and U, which were mostly retained during degradation of N Reactor SNF WPs.

For some of the cases examined in this analysis, the volume of remaining WP components and of corrosion products precipitated in the WP nearly reaches or exceeds the volume of the WP before 100,000 years after WP breach. For the portions of these cases after the time when the WP is about 2/3 full of solids Assumptions 5.8 and 5.9 may no longer be reasonable. On the other hand, the degradation rates of WP components would probably decrease if a thick layer of WP corrosion products separates them from the WP solution (See discussion in Assumptions 5.8 and 5.9). This would slow the production of corrosion products and decrease the amounts of radionuclides lost from the WP.

7.2   CONCLUSIONS OF SCIENTIFIC ANALYSIS

7.2.1   FSV SNF

Factors that increased predicted losses of radionuclides from FSV SNF WPs (relative to the Base Case) included:

- High WP component degradation rates with 20, 80 or 100 mm/year infiltration rate (for I, Np, Pu, and U losses)

- High WP component degradation rates with a 20 mm/year infiltration rate (for Th loss)

- Two-stage case with initial high HLW glass degradation rate with a 100 mm/year infiltration rate followed by a low SNF degradation rate with a 20 mm/year infiltration rate (for I, Np, Pu, Tc and U losses)

Factors that decreased predicted losses of radionuclides from FSV SNF WPs (relative to the Base Case) included:

- Allowing hematite to form in the WP, thus preventing precipitation of alternate Cr and Mo containing Fe(III) minerals.

- Low O_2 fugacity (for Np and Pu)

- High WP component degradation rates with 20, 80 or 100 mm/year infiltration rate (for Th losses)

7.2.2   N Reactor SNF

Factors that increased predicted losses of radionuclides from N Reactor SNF WPs (relative to the Base Case) included:

- High WP component degradation rates with 20 or 80 mm/year infiltration rate (for I, Np, Pu, and Tc losses)

- Two-stage case with initial high HLW glass degradation rate with a 100 mm/year infiltration rate followed by a low SNF degradation rate with a 20 mm/year infiltration rate (for I and Tc losses)

- 4 MCOs and no HLW glass in the WP (for I, Np, and Tc losses)

- Allowing hematite to form in the WP, thus preventing precipitation of alternate Cr and Mo containing Fe(III) minerals (for Np and Pu losses).

Factors that decreased predicted losses of radionuclides from N Reactor SNF WPs (relative to the Base Case) included:

- 4 MCOs and no HLW glass in the WP (for U and Pu losses)

- Allowing hematite to form in the WP, thus preventing precipitation of alternate Cr and Mo containing Fe(III) minerals (for U loss).

- Low O_2 fugacity (for Np and Pu)

- High WP component degradation rates with 20 or 80 mm/year infiltration rate (for U loss)

- Two-stage case with initial high HLW glass degradation rate with a 100 mm/year infiltration rate followed by a low SNF degradation rate with a 20 mm/year infiltration rate (for Np, Pu and U losses)

7.2.3   M&D Waste Form

Factors that increased predicted losses of radionuclides from M&D WPs (relative to the Base Case) included:

- High WP component degradation rates with 20 or 80 mm/year infiltration rate

- Two-stage case with initial high HLW glass degradation rate with a 100 mm/year infiltration rate followed by a low SNF degradation rate with a 20 mm/year infiltration rate

Factors that decreased predicted losses of radionuclides from M&D WPs (relative to the Base Case) included:

- Allowing hematite to form in the WP, thus preventing precipitation of alternate Cr and Mo containing Fe(III) minerals.

- Low O_2 fugacity (for Np and Pu)

8.   INPUTS AND REFERENCES

8.1   DOCUMENTS CITED

Anderson, P.R. and Benjamin, M.M. 1985. "Effects of Silicon on the Crystallization and
Adsorption Properties of Ferric Oxides." *Environmental Science & Technology, 19,* (11), 1048-
1053. [Washington, D.C.]: American Chemical Society. TIC: 247994.

Audi, G. and Wapstra, A.H. 1995. *Atomic Mass Adjustment, Mass List for Analysis.* [Upton,
New York: Brookhaven National Laboratory, National Nuclear Data Center]. TIC: 242718.

BSC (Bechtel SAIC Company) 2001a. *EQ6 Calculation for Chemical Degradation of Fort St.
Vrain (Th/U Carbide) Waste Packages.* CAL-EDC-MD-000011 REV 00. Las Vegas, Nevada:
Bechtel SAIC Company. ACC: MOL.20010831.0300.

BSC (Bechtel SAIC Company) 2001b. *EQ6 Calculations for Chemical Degradation of Melt and
Dilute Waste Packages.* CAL-EDC-MD-000012 REV 00. Las Vegas, Nevada: Bechtel SAIC
Company. ACC: MOL.20010719.0064.

BSC (Bechtel SAIC Company) 2001c. Statement of Work for DOE—Office of Civilian
Radioactive Waste Management, Technical Assistance on Melt-Dilute Criticality and Shielding
Analyses, Revision 2, May 30, 2001. Las Vegas, Nevada: Bechtel SAIC Company. ACC:
MOL.20010619.0626.

BSC (Bechtel SAIC Company) 2001d. *In-Package Chemistry for Waste Forms.* ANL-EBS-MD-
000056 REV 00. Las Vegas, Nevada: Bechtel SAIC Company. ACC: MOL.20010322.0490.

BSC (Bechtel SAIC Company) 2001e. *Geochemical Interactions in a Failed Co-Disposal
Package for Selected U.S. Department of Energy Spent Fuels.* CAL-EBS-PA-000005 REV 00.
Las Vegas, Nevada: Bechtel SAIC Company. ACC: MOL.20011023.0096.

BSC (Bechtel SAIC Company) 2001f. *Defense High Level Waste Glass Degradation.* ANL-
EBS-MD-000016 REV 00 ICN 02. Las Vegas, Nevada: Bechtel SAIC Company. ACC:
MOL.20011015.0502.

BSC (Bechtel SAIC Company) 2001g. *DSNF and Other Waste Form Degradation Abstraction.*
ANL-WIS-MD-000004 REV 01 ICN 01. Las Vegas, Nevada: Bechtel SAIC Company. ACC:
MOL.20010316.0002.

BSC (Bechtel SAIC Company) 2001h. *Performance Assessment of U. S. Department of Energy
Spent Fuels in Support of Site Recommendation.* CAL-WIS-PA-000002 REV 00. Las Vegas,
Nevada: Bechtel SAIC Company. ACC: MOL.20010627.0026.

BSC (Bechtel SAIC Company) 2001i. *Microbial Transport Sensitivity Calculations.* CAL-EBS-PA-000011 REV 00. Las Vegas, Nevada: Bechtel SAIC Company. ACC: MOL.20011015.0024.

BSC (Bechtel SAIC Company) 2001j. *Inventory Abstraction.* ANL-WIS-MD-000006 REV 00 ICN 02. Las Vegas, Nevada: Bechtel SAIC Company. ACC: MOL.20010416.0088.

BSC (Bechtel SAIC Company) 2001k. *Inventory Abstraction.* ANL-WIS-MD-000006 REV 00 ICN 03. Las Vegas, Nevada: Bechtel SAIC Company. ACC: MOL.20020123.0278.

BSC (Bechtel SAIC Company) 2002. *Technical Work Plan for: Department of Energy Spent Nuclear Fuel and Plutonium Disposition Work Packages.* TWP-MGR-MD-000010 REV 01. Las Vegas, Nevada: Bechtel SAIC Company. ACC: MOL.20020402.0441.

Carlson, L. and Schwertmann, U. 1981. "Natural Ferrihydrites in Surface Deposits from Finland and Their Association with Silica." *Geochimica et Cosmochimica Acta, 45,* (3), 421-429. [New York, New York]: Pergamon Press. TIC: 247999.

Cornell, R.M.; Giovanoli, R.; and Schindler, P.W. 1987. "Effect of Silicate Species on the Transformation of Ferrihydrite into Goethite and Hematite in Alkaline Media." *Clays and Clay Minerals, 35,* (1), 21-28. [Long Island City, New York: Pergamon Press]. TIC: 248208.

CRWMS M&O 1996. *Second Waste Package Probabilistic Criticality Analysis: Generation and Evaluation of Internal Criticality Configurations.* BBA000000-01717-2200-00005 REV 00. Las Vegas, Nevada: CRWMS M&O. ACC: MOL.19960924.0193.

CRWMS M&O 1997. *Criticality Evaluation of Degraded Internal Configurations for the PWR AUCF WP Designs.* BBA000000-01717-0200-00056 REV 00. Las Vegas, Nevada: CRWMS M&O. ACC: MOL.19971231.0251.

CRWMS M&O 1998. *EQ3/6 Software Installation and Testing Report for Pentium Based Personal Computers (PCs).* CSCI: LLYMP9602100. Las Vegas, Nevada: CRWMS M&O. ACC: MOL.19980813.0191.

CRWMS M&O 1999a. *DOE SRS HLW Glass Chemical Composition.* BBA000000-01717-0210-00038 REV 00. Las Vegas, Nevada: CRWMS M&O. ACC: MOL.19990215.0397.

CRWMS M&O 1999b. *EQ6 Calculation for Chemical Degradation of Pu-Ceramic Waste Packages: Effects of Updated Materials Composition and Rates.* CAL-EDC-MD-000003 REV 00. Las Vegas, Nevada: CRWMS M&O. ACC: MOL.19990928.0235.

CRWMS M&O 2000a. *Design Analysis for the Defense High-Level Waste Disposal Container.* ANL-DDC-ME-000001 REV 00. Las Vegas, Nevada: CRWMS M&O. ACC: MOL.20000627.0254.

CRWMS M&O 2000b. *Total System Performance Assessment for the Site Recommendation.*
TDR-WIS-PA-000001 REV 00 ICN 01. Las Vegas, Nevada: CRWMS M&O. ACC:
MOL.20001220.0045.

CRWMS M&O 2000c. *Waste Package Degradation Process Model Report.* TDR-WIS-MD-
000002 REV 00 ICN 02. Las Vegas, Nevada: CRWMS M&O. ACC: MOL.20001228.0229.

CRWMS M&O 2000d. *Waste Form Degradation Process Model Report.* TDR-WIS-MD-
000001 REV 00 ICN 01. Las Vegas, Nevada: CRWMS M&O. ACC: MOL.20000713.0362.

CRWMS M&O 2000e. *Inventory Abstraction.* ANL-WIS-MD-000006 REV 00 ICN 01. Las
Vegas, Nevada: CRWMS M&O. ACC: MOL.20001130.0002.

CRWMS M&O 2000f. *In-Drift Accumulation of Fissile Material from Waste Package
Containing Plutonium Disposition Waste Forms.* CAL-EDC-GS-000001 REV 00. Las Vegas,
Nevada: CRWMS M&O. ACC: MOL.20001016.0008.

CRWMS M&O 2001a. *EQ6 Calculations for Chemical Degradation of N Reactor (U-metal)
Spent Nuclear Fuel Waste Packages.* CAL-EDC-MD-000010 REV 00. Las Vegas, Nevada:
CRWMS M&O. ACC: MOL.20010227.0017.

CRWMS M&O 2001b. *Performance Assessment and Sensitivity Analysis of Disposal of
Plutonium as Can-in-Canister Ceramic.* ANL-WIS-PA-000003 REV 00. Las Vegas, Nevada:
CRWMS M&O. ACC: MOL.20010205.0015.

Daveler, S.A. and Wolery, T.J. 1992. *EQPT, A Data File Preprocessor for the EQ3/6 Software
Package: User's Guide and Related Documentation (Version 7.0).* UCRL-MA-110662 PT II.
Livermore, California: Lawrence Livermore National Laboratory. TIC: 205240.

DOE (U.S. Department of Energy) 1998. *Total System Performance Assessment.* Volume 3 of
Viability Assessment of a Repository at Yucca Mountain. DOE/RW-0508. Washington, D.C.:
U.S. Department of Energy, Office of Civilian Radioactive Waste Management. ACC:
MOL.19981007.0030.

DOE (U.S. Department of Energy) 1999. *DOE Spent Nuclear Fuel Information in Support of
TSPA-SR.* DOE/SNF/REP-0047, Rev. 0. [Washington, D.C.]: U.S. Department of Energy, Office
of Environmental Management. TIC: 245482.

DOE (U.S. Department of Energy) 2000a. *Review of Oxidation Rates of DOE Spent Nuclear
Fuel, Part 1: Metallic Fuel.* DOE/SNF/REP-054, Rev. 0. Washington, D.C.: U.S. Department of
Energy. TIC: 248978.

DOE (U.S. Department of Energy) 2000b. *N Reactor (U-Metal) Fuel Characteristics for
Disposal Criticality Analysis.* DOE/SNF/REP-056, Rev. 0. [Washington, D.C.]: U.S. Department
of Energy, Office of Environmental Management. TIC: 247956.

DOE (U.S. Department of Energy) 2001a. *DOE Spent Nuclear Fuel Information in Support of TSPA-SR.* DOE/SNF/REP-047, Rev. 1. Idaho Falls, Idaho: U.S. Department of Energy, Idaho Operations Office. TIC: 250808.

DOE (U.S. Department of Energy) 2001b. *Yucca Mountain Science and Engineering Report.* DOE/RW-0539. [Washington, D.C.]: U.S. Department of Energy, Office of Civilian Radioactive Waste Management. ACC: MOL.20010524.0272.

Estill, J.C. 1998. "Long-Term Corrosion Studies." 2.2 of *Engineered Materials Characterization Report.* McCright, R.D., ed.. UCRL-ID-119564 Volume 3 Rev.1.1. Livermore, California: Lawrence Livermore National Laboratory. ACC: MOL.19981222.0137.

Furet, N.R.; Haces, C.; Corvo, F.; Diaz, C.; and Gomez, J. 1990. "Corrosion Rate Determination Using Fe-57 Mössbauer Spectra of Corrosion Products of Steel." *Hyperfine Interactions, 57,* 1833-1838. Basel, Switzerland: J.C. Baltzer, A.G. Scientific Publishing Company. TIC: 240940.

Goldberg, S.; Forster, H.S.; and Godfrey, C.L. 1996. "Molybdenum Adsorption on Oxides, Clay Minerals, and Soils." *Soil Science Society of America Journal, 60,* 425-432. [Madison, Wisconsin]: Soil Science Society of America. TIC: 252573.

Hillner, E.; Franklin, D.G.; and Smee, J.D. 1998. *The Corrosion of Zircaloy-Clad Fuel Assemblies in a Geologic Repository Environment.* WAPD-T-3173. West Mifflin, Pennsylvania: Bettis Atomic Power Laboratory. TIC: 237127.

Hollingsworth, E.H. and Hunsicker, H.Y 1987. "Corrosion of Aluminum and Aluminum Alloys." Volume 13 of *Metals Handbook.* 9th Edition. Pages 583-609. Metals Park, Ohio: ASM International. TIC: 209807.

Lindsay W.L. 2001. *Chemical Equilibria in Soils.* 1st Edition. Caldwell, New Jersey: Blackburn Press. TIC: 5873.

McCright, R.D. 1998. *Corrosion Data and Modeling, Update for Viability Assessment.* Volume 3 of *Engineered Materials Characterization Report.* UCRL-ID-119564, Rev. 1.1. Livermore, California: Lawrence Livermore National Laboratory. ACC: MOL.19980806.0177.

Parrington, J.R.; Knox, H.D.; Breneman, S.L.; Baum, E.M.; and Feiner, F. 1996. *Nuclides and Isotopes, Chart of the Nuclides.* 15th Edition. San Jose, California: General Electric Company and KAPL, Inc. TIC: 233705.

Propp, W.A. 1998. *Graphite Oxidation Thermodynamics/Reactions.* DOE/SNF/REP-018, Rev. 0. Idaho Falls, Idaho: U. S. Department of Energy. TIC: 247663.

Rai, D. and Ryan, J.L. 1982. "Crystallinity and Solubility of Pu(IV) Oxide and Hydrous Oxide in Aged Aqueous Suspensions." *Radiochimica Acta, 30,* 213-216. Munchen, Germany: R. Oldenbourg Verlag. TIC: 219107.

Runde, W. 1999. "Letter Report on Plutonium Thermodynamic Database." Letter from W. Runde (LANL) to P. Dixon (LANL), August 1, 1999, with attachments. ACC: MOL.19991214.0624.

Schwertmann, U. and Cornell, R.M. 1991. *Iron Oxides in the Laboratory: Preparation and Characterization.* New York, New York: VCH Publishers. TIC: 237942.

Schwertmann, U. and Taylor, R.M. 1989. "Iron Oxides." Chapter 8 of *Minerals in Soil Environments.* Dixon, J.B. and Weed, S.B., eds. SSSA Book Series: 1. 2nd Edition. Madison, Wisconsin: Soil Science Society of America. TIC: 237222.

Spahiu, K. and Bruno, J. 1995. *A Selected Thermodynamic Database for REE to be Used in HLNW Performance Assessment Exercises.* SKB Technical Report 95-35. Stockholm, Sweden: Swedish Nuclear Fuel and Waste Management Company. TIC: 225493.

Stout, R.B. and Leider, H.R., eds. 1991. *Preliminary Waste Form Characteristics Report.* Version 1.0. Livermore, California: Lawrence Livermore National Laboratory. ACC: MOL.19940726.0118.

Taylor, L.L. 2001. *Fort Saint Vrain HTGR (Th/U Carbide) Fuel Characteristics for Disposal Criticality Analysis.* DOE/SNF/REP-060, Rev. 0. [Washington, D.C.]: U.S. Department of Energy, Office of Environmental Management. TIC: 249783.

Titley, S.R. 1963. "Some Behavioral Aspects of Molybdenum in the Supergene Environment." *Transactions of the Society of Mining Engineers, 226,* 199-204. New York, New York: Society of Mining Engineers of AIME. TIC: 249114.

Wilson, C.N. and Bruton, C.J. 1989. *Studies on Spent Fuel Dissolution Behavior Under Yucca Mountain Repository Conditions.* PNL-SA-16832. Richland, Washington: Pacific Northwest Laboratory. ACC: HQX.19890918.0047.

Wolery, T.J. 1992a. *EQ3/6, A Software Package for Geochemical Modeling of Aqueous Systems: Package Overview and Installation Guide (Version 7.0).* UCRL-MA-110662 PT I. Livermore, California: Lawrence Livermore National Laboratory. TIC: 205087.

Wolery, T.J. 1992b. *EQ3NR, A Computer Program for Geochemical Aqueous Speciation-Solubility Calculations: Theoretical Manual, User's Guide, and Related Documentation (Version 7.0).* UCRL-MA-110662 PT III. Livermore, California: Lawrence Livermore National Laboratory. ACC: MOL.19980717.0626.

Wolery, T.J. and Daveler, S.A. 1992. *EQ6, A Computer Program for Reaction Path Modeling of Aqueous Geochemical Systems: Theoretical Manual, User's Guide, and Related Documentation (Version 7.0).* UCRL-MA-110662 PT IV. Livermore, California: Lawrence Livermore National Laboratory. ACC: MOL.19980701.0459.

Yang, I.C.; Rattray, G.W.; and Yu, P. 1996. *Interpretation of Chemical and Isotopic Data from Boreholes in the Unsaturated Zone at Yucca Mountain, Nevada.* Water-Resources Investigations Report 96-4058. Denver, Colorado: U.S. Geological Survey. ACC: MOL.19980528.0216.

8.2   CODES, STANDARDS, REGULATIONS, AND PROCEDURES

AP-2.21Q, Rev. 1, BSCN1. *Quality Determinations and Planning for Scientific, Engineering, and Regulatory Compliance Activities*. Washington, D.C.: U.S. Department of Energy, Office of Civilian Radioactive Waste Management. ACC: MOL.20010212.0018.

AP-SI.1Q, Rev. 3, ICN 4. *Software Management*. Washington, D.C.: U.S. Department of Energy, Office of Civilian Radioactive Waste Management. ACC: MOL.20020520.0283.

ASM International 1987. *Corrosion.* Volume 13 of *Metals Handbook.* 9th Edition. Metals Park, Ohio: ASM International. TIC: 209807.

ASTM A 20/A 20M-95a. 1995. *Standard Specification for General Requirements for Steel Plates for Pressure Vessels.* West Conshohocken, Pennsylvania: American Society for Testing and Materials. TIC: 240026.

ASTM A 240/A 240M-94b. 1994. *Standard Specification for Heat-Resisting Chromium and Chromium-Nickel Stainless Steel Plate, Sheet, and Strip for Pressure Vessels.* Philadelphia, Pennsylvania: American Society for Testing and Materials. TIC: 240020.

ASTM A 276-91a. 1991. *Standard Specification for Stainless and Heat-Resisting Steel Bars and Shapes.* Philadelphia, Pennsylvania: American Society for Testing and Materials. TIC: 240022.

ASTM A 516/A 516M-90. 1991. *Standard Specification for Pressure Vessel Plates, Carbon Steel, for Moderate- and Lower-Temperature Service.* West Conshohocken, Pennsylvania: American Society for Testing and Materials. TIC: 240032.

ASTM B 209–96. 1996. *Standard Specification for Aluminum and Aluminum-Alloy Sheet and Plate.* West Conshohocken, Pennsylvania: American Society for Testing Materials. TIC: 247078.

ASTM G 1-90 (Reapproved 1999). 1990. *Standard Practice for Preparing, Cleaning, and Evaluating Corrosion Test Specimens.* West Conshohocken, Pennsylvania: American Society for Testing and Materials. TIC: 238771.

8.3   SOURCE DATA, LISTED BY DATA-TRACKING NUMBER

8.3.1   Input Data

MO0006J13WTRCM.000. Recommended Mean Values of Major Constituents in J-13 Well
Water. Submittal date: 06/07/2000.

MO0009THRMODYN.001. Input Transmittal for Thermodynamic Data Input Files for
Geochemical Calculations. Submittal date: 09/20/2000.

8.3.2   Output Data

MO0201SPAGIN07.001. Input and Output for Geochemical Interactions in Failed Co-Disposal
Waste Packages for N Reactor and Ft. St. Vrain Spent Fuel and the Melt and Dilute Waste Form.
Submittal date: 01/28/2002.

8.4   SOFTWARE

CRWMS M&O 1999c. *Software Code: EQ3/6.* V7.2b. UCRL-MA-110662 (LSCR198).

CRWMS M&O 1999d. *Software Code: EQ6, Version 7.2bLV.* V7.2bLV. 10075-7.2bLV-00.

9. ATTACHMENT

Attachment   **Title**

    I   Acronyms and Abbreviations

ATTACHMENT I

ACRONYMS AND ABBREVIATIONS

ACRONYMS AND ABBREVIATIONS

ANL   Analysis

BOL   Beginning of Life

CAL   Calculation
CFR   Code of Federal Regulations
CRWMS   Civilian Radioactive Waste Management System
CSCI   Computer Software Configuration Item

DOE   U.S. Department of Energy

EBS   Engineered Barrier System
EOL   End of Life
EPA   U.S. Environmental Protection Agency
EQLIB   Library component of EQ3/6
EQPT   Data file processor component of EQ3/6
EQ3/6   Geochemical model
EQ3NR   Speciation and solubility component of EQ3/6
EQ6   Reaction path component of EQ3/6

FERMI   Enrico Fermi Reactor
FFTF   Fast Flux Test Facility

GPC   Glass Pour Canister

HLW   High Level Waste

LA   License Application
LLNL   Lawrence Livermore National Laboratory
LWBR   Light Water Breeder Reactor

MCO   Multi-Canister Overpack
MTHM   Metric Tons Heavy Metal
M&O   Management and Operating Contractor

NRC   U. S. Nuclear Regulatory Commission

OCRWM   Office of Civilian Radioactive Waste Management

PA   Performance Assessment

QA   Quality Assurance

ACRONYMS AND ABBREVIATIONS (Continued)

SCFT	Solid Centered Flow-Through
SNF	Spent Nuclear Fuel
SR	Site Recommendation
SZ	Saturated Zone
TSPA	Total System Performance Assessment
TRIGA	Training, Research, and Isotope General Atomics
UZ	Unsaturated Zone
VA	Viability Assessment
WP	Waste Package
WIS	Waste Isolation System